Missouri State University

BearWorks

MSU Graduate Theses

Summer 2022

Role of Cyclophilin A and TRIM5α in HIV-1 Infection and Capsid Uncoating

Emma LK Wise
Missouri State University, EmmaWise@MissouriState.edu

As with any intellectual project, the content and views expressed in this thesis may be considered objectionable by some readers. However, this student-scholar's work has been judged to have academic value by the student's thesis committee members trained in the discipline. The content and views expressed in this thesis are those of the student-scholar and are not endorsed by Missouri State University, its Graduate College, or its employees.

Follow this and additional works at: https://bearworks.missouristate.edu/theses

 Part of the Virus Diseases Commons

Recommended Citation

Wise, Emma LK, "Role of Cyclophilin A and TRIM5α in HIV-1 Infection and Capsid Uncoating" (2022). *MSU Graduate Theses*. 3787.
https://bearworks.missouristate.edu/theses/3787

This article or document was made available through BearWorks, the institutional repository of Missouri State University. The work contained in it may be protected by copyright and require permission of the copyright holder for reuse or redistribution.
For more information, please contact BearWorks@library.missouristate.edu.

ROLE OF CYCLOPHILIN A AND TRIM5α IN HIV-1 INFECTION AND CAPSID UNCOATING

A Master's Thesis

Presented to

The Graduate College of

Missouri State University

In Partial Fulfillment

Of the Requirements for the Degree

Master of Science, Cell and Molecular Biology

By

Emma Wise

August 2022

ROLE OF CYCLOPHILIN A AND TRIM5α IN HIV-1 INFECTION AND CAPSID UNCOATING

Biomedical Sciences

Missouri State University, August 2022

Master of Science

Emma Wise

ABSTRACT

Microglial cells are immune cells that protect the central nervous system and are subject to HIV-1 infection. HIV-1 infection of these cells can lead to HIV Associated Neurocognitive Disorders (HAND). Since HIV-1 only codes for 15 different proteins, the virus also uses cellular factors, like Cyclophilin A (CypA), to assist in viral replication. The cell also has antiretroviral restriction factors, like tripartite motif-containing protein 5 (TRIM5α), to protect against infection. The goal of this project is to investigate the role of CypA in the early steps of HIV-1 replication and TRIM5α restriction in microglial cells. I hypothesize that CypA facilitates HIV-1 infection and assists in normal capsid uncoating kinetics. I also predict that blocking CypA interaction will allow for TRIM5α restriction to decrease HIV-1 infection. To study how the interaction between CypA and the capsid affects uncoating, the *in situ* uncoating assay was performed in the presence and absence of the drug Cyclosporin A which blocks this interaction. Lower amounts of CA were found in conditions with CypA binding compared to the absence of CypA. This result suggests that CypA assists with uncoating in CHME3 cells. To research the interplay between CypA and TRIM5α in microglial cells, TRIM5α expression was knocked down using siRNAs and CsA treatment was used to block CypA binding to the capsid. A decrease in TRIM5α expression resulted in an increase of HIV-1 infectivity. This effect was greater when CypA interactions were inhibited. This data indicates that TRIM5α restriction occurs in CHME3 microglial cells when CypA is inhibited. It is likely that CypA plays more than one role in HIV-1 infectivity and replication. Here, I have characterized the effect of CypA on HIV-1 uncoating and the connection between CypA and TRIM5α in microglial cells.

KEYWORDS: HIV-1, uncoating, cyclophilin A, TRIM5α, microglial cells

ROLE OF CYCLOPHILIN A AND TRIM5α IN HIV-1 INFECTION AND CAPSID UNCOATING

By

Emma Wise

Master of Science, Cell Molecular Biology

A Master's Thesis
Submitted to the Graduate College
Of Missouri State University
In Partial Fulfillment of the Requirements
For the Degree of Master of Science, Cell and Molecular Biology

August 2022

Approved:

Amy E. Hulme, Ph.D., Thesis Committee Chair

Randi Ulbricht, Ph.D., Committee Member

Joshua Smith, Ph.D., Committee Member

Julie Masterson, Ph.D., Dean of the Graduate College

In the interest of academic freedom and the principle of free speech, approval of this thesis indicates the format is acceptable and meets the academic criteria for the discipline as determined by the faculty that constitute the thesis committee. The content and views expressed in this thesis are those of the student-scholar and are not endorsed by Missouri State University, its Graduate College, or its employees.

ACKNOWLEDGEMENTS

I would like to thank my family and friends for all of their encouragement and support throughout my academic career. I would also like to thank my committee members, Dr. Ulbricht and Dr. Smith, and the BMS department faculty for their guidance and advising during my graduate and undergraduate journey. Lastly, thank you to Dr. Hulme, who has helped me grow as a scientist and as a person.

TABLE OF CONTENTS

TABLE OF CONTENTS, CONTINUED

LIST OF TABLES

LIST OF FIGURES

INTRODUCTION

Human immunodeficiency virus (HIV) infection causes acquired immunodeficiency syndrome (AIDS). HIV has two main groups: HIV-1 and HIV-2 and within these groups there are more than ten different strains. For HIV-1, M is the most common strain, making up close to 90% of infected individuals (1). HIV-1 can only infect and replicate in cells that have the cluster of differentiation 4 (CD4) receptor, and a majority of these cells are involved in the immune system (2). Viral infection of CD4+ T cells damages immunity and leads to the onset of AIDS (2). Once the immune system is critically damaged, the body is susceptible to opportunistic infections (2). For HIV infection and replication to occur, virions use both viral and cellular factors. Throughout early and late replication, HIV-1 commandeers cellular proteins, such as cyclophilin A (CypA), to aid in the infection process. There are also cellular factors, like tripartite motif-containing protein 5 (TRIM5α) that restrict viral infection. The goal of this project is to investigate the effect of CypA on HIV-1 capsid uncoating kinetics and the relationship between TRIM5α and CypA in relation to HIV-1 infection and uncoating.

LITERATURE REVIEW

HIV-1 Associated Neurocognitive Disorders and Microglia

HIV is transmitted through bodily fluids. This includes direct blood to blood contact, seminal, anal, and vaginal fluids, and breast milk (3). Common modes of transmission include unprotected sex, sharing needles, and transmission from mother to child. HIV cannot be transmitted by shaking hands, coughing, or other everyday interactions (3). As infection takes hold throughout the body, the infected individual's immune system is extremely damaged. Once HIV infection has reached the most severe stage, stage 3, it is classified as AIDS (4). This leaves the body susceptible to opportunistic infections. The conditions associated with AIDS come in a wide range and include a variety of cancers, tuberculosis, pneumonia, and neurocognitive disorders (4).

As infected individuals are able to live longer lifespans, they discover the long-term effects of HIV-1 infection. Neural immune cells contain the CD4 receptor and are susceptible to HIV-1 infection. To access the brain, HIV must cross the blood brain barrier (BBB). This barrier protects the brain from pathogens and toxins circulating in the blood (5). HIV can migrate across the BBB inside infected cells and as free virus (6). HIV-1 can infect the epithelial cells of the brain and the choroid plexus that make up the BBB. The virus can also infect macrophages locate in the central nervous system (CNS). Macrophages in the CNS are also called microglial cells (6). Infected, inactivated microglial cells form a viral reservoir stored in the CNS and the reservoir does not produce virus until the cells are activated (6). As for migration of free virus across the BBB, the exact mechanism for transport remains heavily investigated (6).

Once HIV-1 infects the brain, an individual may develop HIV-1 associated neurocognitive diseases (HAND). There are three subcategories under HAND; asymptomatic neurocognitive impairment (ANI), mild neurocognitive disorder (MND), and HIV-associated dementia (HAD). Increasing with each disorder respectively, the individual's neurocognitive impairment interferes with their daily life (7). The qualitative impairment tends to fluctuate from day to day, similar to elderly cognitive impairment (8). Of the HIV positive community, anyone infected with the virus, 20% to 50% are estimated to develop HAND (7). Treatments focus on decreasing the viral load in the brain. Combination antiretroviral treatment (cART) can successfully lower viral counts in the parenchyma and the cerebrospinal fluid (7). Though HIV cannot be fully removed from the body, cART can decrease the effects of infection.

A major barrier in treating HIV-1 infection is the viral reservoir. The reservoir is a group of inactive CD4+ memory immune cells that become infected (9). The cells are extremely difficult to target because they lack any distinct difference from uninfected cells. When the inactive memory cells activate, they begin producing virus and greatly contribute to increasing total viral load (9). Within the central nervous system, microglial cells create a viral reservoir. These cells contribute to the immune defense in the brain and contain the CD4 receptor. They both protect from pathogens and protect injured portions of the brain (10). As most HIV research focuses on T-cells, the specifics of HIV-1 infection in microglial cells continues to be investigated.

HIV-1 Structure

HIV is an enveloped virus that measures about 100 nm in diameter (11). The exterior is made up of a lipid bilayer with imbedded viral proteins (Fig. 1). These proteins are primarily

envelope glycoprotein 120 (gp120) and envelope glycoprotein 41 (gp41). The proteins within the outer membrane assist with anchoring and infection (11). The lipid bilayer is derived from the host cell that produced the virion (12). Underneath the membrane is a matrix shell made up of the HIV matrix protein (MA) that lines the inside of the virion (12). Within the matrix shell is the conical capsid made of capsid protein (CA). The capsid holds the viral genetic material and accessory proteins (12). The accessory proteins include nucleocapsid protein (NC), protease, reverse transcriptase, integrase, Nef, Vif, and Vpr ((12); Fig. 1). The complex structure and contents of the virus allow it to effectively infect cells and replicate.

HIV-1 Replication

Infection begins with fusion of a virion to the cell membrane (Fig. 2). Bringing the two membranes together is not kinetically favorable due to hydration repulsion. Therefore, for this action to occur, viral fusion proteins must change from a high energy to low energy conformation. For entry, HIV-1 gp120 binds to the CD4 receptor found on the extracellular membrane. Interaction between gp120 and the receptor causes a conformational change in gp120 allowing interaction with a CC chemokine receptor 5 (CCR5) coreceptor. For infection to occur, both CD4 and CCR5 must be present on the cell surface. Interaction with CCR5 triggers gp41, an N terminal fusion peptide, to interact with the cell membrane (14, 15). Once gp41 reaches this stage, it triggers a cascade of events to draw the two membranes together. Gp41 has the C terminal end in the viral membrane and the N terminal end in the cellular membrane. The gp41 protein rearranges and refolds to form a hairpin, making a six-helix bundle (16). This bundle, called the postfusion conformation, puts the C terminal and N terminal ends of gp41 next to each other to draw the membranes together. Partial fusion begins with the formation of a

hemifusion stalk followed by a fusion pore. Then, the two membranes become one to complete fusion and deposit the viral capsid into the cell (16).

Once the capsid enters the cell, a series of cytoplasmic events occur. The exact order of each event remains to be determined. A necessary step for HIV replication is reverse transcription (Fig. 2). During reverse transcription the viral RNA is reverse transcribed to viral complementary DNA (cDNA). For reverse transcription to occur, the reverse transcription complex (RTC) must form. The RTC is made up of nucleocapsid protein, viral accessory proteins, reverse transcriptase, and integrase (17). This process begins with binding of a tRNA primer near the 5' end of the RNA template (18). Next, the RTC reverse transcribes single-stranded RNA into double-stranded DNA through a series of elongation and strand switching steps (19). The RTC degrades the RNA template as it completes reverse transcription, so switching strands from the minus DNA strand to the plus DNA strand is necessary for the complex to continue using a template (19). As reverse transcription occurs, the virus travels towards the nucleus using the cytoskeleton (13). At an undetermined part of replication, the RTC becomes a preintegration complex (PIC) in preparation for nuclear entry (20).

Many specifics about HIV-1 nuclear entry have yet to be defined and because of this, there are multiple models of nuclear import. A major difference between the models focuses on whether or not the capsid has uncoated. Uncoating is when CA disassociates from the conical capsid. In theory, if the capsid uncoats in the cytoplasm, viral PICs are expected to enter the nucleus with little resistance (21, 22). If the capsid remains intact and uncoats at the nuclear pore, it will take longer for viral entry because of the bulky capsid. In reality, viral nuclear entry may occur in a combination of these two possible models (23). Once nuclear entry is complete, integration begins. Integration is the process of inserting viral cDNA into the host cell genome.

This process, catalyzed by the viral enzyme integrase, begins with the removal of two nucleotides from the 3' end of viral cDNA. Exposed 3' ends attack host DNA at targeted sites, joining the 3' end of viral cDNA to the 5' end of host DNA (24). Next, nucleotides are removed from the 5' end of viral cDNA, so it may join the 3' end of host DNA (24). Viral genetic material is now inserted into the host genome, forming a provirus.

Using cellular proteins, the integrated cDNA is transcribed and translated (Fig. 2). HIV genomes are made up of gag, pol, env, and accessory genes (25). Within integrated viral DNA, there is an enhancer sequence upstream from transcription factor binding sites (26). This enhancer, known as nuclear factor kappa-light-chain-enhancer of activated B cells (NF-κB), increases expression of the viral accessory protein Tat. Tat interacts with a trans-activation response element to increase the number of full-length viral mRNA transcribed. Tat also forms a positive feedback loop with NF-κB to increase viral transcription and effectively acts as an activator for viral transcripts (26). Viral transcripts undergo RNA editing by cellular factors, such as adenosine deaminases acting on RNA 1 (ADAR1). Editing must occur for proper formation of the p24 viral protein (27). During translation, HIV-1 hijacks the necessary machinery, including ribosomes, tRNAs, and mRNA binding proteins (28). Rev, a viral protein, is an integral part of this process because it recognizes and binds to Rev responsive elements (RRE) on viral transcripts (29). Rev binds to HIV mRNA to increase stability and assist with nuclear export into the cytoplasm. Translation initiation factors can recognize Rev bound RRE and begin assembling the polysome. Without Rev, viral mRNA is unrecognizable, and this lack of recognition is detrimental for HIV replication (29).

Viral proteins and untranslated viral RNA assemble on the intracellular membrane. Gag, a structural protein, is the first to reach the membrane and targets lipid rafts. The remaining viral

proteins follow gag to assemble at the intracellular side of the membrane (31). Gag recruits endosomal sorting complexes required for transport (ESCRT) to the site. ESCRT catalyzes membrane fission and finalizes the budding step of HIV-1 replication (31). However, the released virion is not yet mature, until a viral protease enzyme cleaves the polyprotein GagPol. Protease cleaves gag into four distinct factors: matrix protein (MA), capsid protein (CA), nucleocapsid protein (NC), and p6 protein (Fig. 2). NC and MA are associated directly with the membrane and CA forms the capsid (Fig. 1; (31)). At this point, mature virions can infect more CD4+ host cells.

The HIV-1 Capsid

The HIV-1 capsid is formed during virion maturation when CA assembles to form the conical core of the virus. A complete capsid is made up of approximately 1,500 CA (Fig. 3; (32)). The CA itself is comprised of two main domains: N-terminal domain (CA_{NTD}) and C-terminal domain (CA_{CTD}). CA_{NTD} consists of seven alpha helices known as H1 through H7. Similarly, CA_{CTD} is made up of four alpha helices labeled H8 through H11 (33). Both domains are connected by a linker and together they associate around a central ring to form hexamers and pentamers (34). The hexamers and pentamers then bind together to form a fullerene cone that is capped on both ends. The flexible lattice presents itself as two types of curved surfaces located in the body and ends of the cone. The curves on the capsid ends are structured as twelve pentameric declinations and the body is made up of hexameric lattice curvatures (35).

HIV-1 capsid houses genomic RNA, NC, reverse transcriptase, and other miscellaneous viral components (32). One of the key functions the capsid performs is protecting its contents from detection and degradation. For example, HIV-1 cDNA is susceptible to the DNA sensor

cyclic GMP-AMP sensor (cGAS), yet this sensor does not detect viral cDNA as it travels towards the nucleus within the capsid (36). Similarly, during infection, HIV-1 recruits cleavage and polyadenylation specificity factor subunit 6 (CPSF6) seemingly to protect against DNA sensors and protection against triggering an innate immune response (37). The capsid also functions to assist with the infection process through uncoating kinetics. There have been links to uncoating discovered in reverse transcription, nuclear pore complex recognition, and DNA integration. Studies have found that treatment with the reverse transcription inhibitor nevirapine delayed core uncoating (38). Another study found that CA was necessary for nuclear import, meaning that CA must be present in some form during import (39). It was also found that different capsid mutants integrated at different sites, linking CA to integration (40). Though the exact timing of capsid uncoating remains unknown, the process is intrinsically linked with infection and overall proper uncoating kinetics are crucial for HIV-1 infectivity.

Models of HIV-1 Capsid Uncoating

Regardless of how much is known about the HIV-1 conical capsid, the exact process of uncoating remains a mystery. Because of this, many models are suggested. The first model, rapid core disassembly, suggests CA monomers disassemble directly upon cytoplasmic entry (Fig. 4A). As the capsid immediately releases its contents into the cell, reverse transcription occurs freely within the cytoplasm (13). Evidence for this version of uncoating was based around an experiment that found very little CA and NC present post integration, but both MA and RT were within the cytoplasm (41). Support for this version of uncoating lasted for many years (13). As research on capsid uncoating progressed, rapid core disassembly was disputed. Studies have shown that isolated RTCs, analyzed directly after infection, contain CA (13). Similarly, the

interaction between cellular factors and CA disproves this version of capsid disassembly (42). If the core uncoated immediately upon entry, then cellular factors would not have ample time to bind to CA. It is also known that certain cellular antiretroviral proteins, such as TRIM5α bind to the capsid and disrupt uncoating. This process occurs in the cytoplasm, again contradicting immediate uncoating (43). Though evidence suggests that capsid uncoating does not happen immediately, there are many other viable models for this process.

As the capsid travels towards the nucleus, it is possible that uncoating occurs in the cytosol. Therefore, the next model is biphasic, or cytoplasmic, uncoating, where CA dissociate in the cytoplasm while the capsid is traveling to the nucleus (Fig. 4B). Simultaneously, as CA detaches, RNA undergoes reverse transcription (13). This model is supported by studies using a cyclosporin (CsA) washout assay and an immunofluorescent assay (38). The CsA washout assay measures capsid uncoating kinetics using TRIM-CypA, a restriction factor found in owl monkey kidney (OMK) cells. The half-life of uncoating, about one hour post infection, corresponds with production of early reverse transcription products (38). An immunofluorescent assay revealed a similar outcome within HeLa cells. The fluorescent signal associated with CA significantly decreased by one hour post infection. This suggests that CA begin uncoating within the cytoplasm and release the RTC while traveling towards the nucleus (44). However, if capsid uncoating occurs early in the infection process, then the capsid's function to protect the contents within from host cell antiretroviral attacks may not be possible, leaving viral RNA and RTC susceptible to host cell restriction factors and DNA sensors. If the capsid's intended function is to protect the contents within from host cell antiretroviral attacks, then this protection may not be possible if CA dissociation begins early within the infection process (13). Though there is

evidence that uncoating begins in the cytoplasm, it may not be where a majority of uncoating occurs.

Another model for uncoating is nuclear pore complex (NPC) uncoating where CA disassembly occurs during nuclear entry (Fig. 4C). Here, reverse transcription is modeled to happen while entirely encompassed by the capsid (13). Support for this model comes from the antiretroviral DNA sensor, cGAS. HIV-1 viral cDNA is susceptible to cGAS sensors but can escape when within the capsid. In dendritic cells, cGAS does not recognize cytoplasmic HIV cDNA as it is being transcribed, suggesting that the capsid stays intact to protect cDNA from host cell DNA sensors by staying intact until it reaches the NPC (36). Using cryogenic scanning electron microscopy (cryo SEM), intact conical viral cores were imaged in proximity to nuclear pores. As the capsids remained in their original structure near NPCs, a major uncoating event may not happen until nuclear entry (45). The intact cores were imaged up to 48 hours post infection. However, previous data displays that capsid uncoating, reverse transcription, and nuclear localization is entirely complete by that time (13). Therefore, this model does not support the intrinsic link between uncoating and reverse transcription. Due to the contrasting data on uncoating, it is possible that this process varies in differing cell types, or environments.

The most recently proposed model of capsid dissociation is nuclear uncoating. In this process, the capsid remains intact until after nuclear import. The capsid fully disassociates once within the nucleus (Fig. 5; (46)). Verification for this model came from using a GFP tagged CA and live cell microscopy in HeLa, CEM-ss cells and macrophages. Intact or nearly intact viral cores were imaged within the nucleus 1.5 hours post infection (39). Further support for nuclear uncoating used a destabilizing compound, PF74. When the capsid was exposed to PF74 within

the nucleus, CA remained susceptible, meaning that the conical core remained intact within the nucleus. PF74 destabilizes the bonds between CA and therefore only works on intact capsid.

Presence of intact capsid within the nucleus was observed in THP1 macrophages, MDM cells, Sup T1 T-cells, and CD4+ T-cells. Similarly, when NPC inhibitors were administered to the cells, intact capsid could still be located within the nucleus. It was concluded that it is entirely possible that HIV-1 uses multiple NPC import pathways to access the nucleus (47). As this model becomes predominant within the field of HIV-1 uncoating research, it remains probable that this process occurs in many forms and may differ between cell types.

Viral Factors That Effect Uncoating

To assist in uncoating, there are interactions inside and outside of the capsid. Many studies have found viral factors that affect the capsid. For example, HIV-1 integrase (IN) is a protein responsible for integrating viral cDNA into host cell DNA, yet this is not its only purpose. IN has been found to directly affect capsid uncoating by adding stability to the CA hexamers and pentamers (48). Absence of IN, or mutations in IN, decreased total capsid as well as slowed the rate of CA disassembly. One study concluded that IN assists CA interaction with cellular factors involved in the infection process, such as CypA (48). Another viral factor involved in capsid uncoating is reverse transcriptase. Inhibiting reverse transcription with nevirapine caused a delay in capsid uncoating (38, 49, 50). This finding lends to the possibility of stable DNA-RNA hybrids or double stranded DNA, made by reverse transcriptase, placing stress on the inside of the capsid. This coincides with the theory that the products made during reverse transcription may assist with capsid uncoating. Similarly, mutated capsid cores that increase stability do exhibit defective reverse transcription (13). This goes along with the thought

that core remodeling must happen to accommodate the transition from flexible RNA to ridged double stranded DNA (13). The viral factors involved with HIV-1 uncoating appear to greatly assist in the overall process.

Cellular Factors That Interact With HIV-1

Due to the small number of proteins within HIV-1 virions, the virus has adapted to using cellular factors to assist in infection. CPFS6 interacts directly with CA and assists with viral cDNA integration. Without CPFS6-CA interactions, the PIC is not properly positioned within the nucleus (51). Transportin-SR2 (TNPO3) is a protein that assists in the nuclear import of serine/arginine splicing factors. TNPO3 interacts with IN and therefore assists in PIC nuclear import. In addition, TNPO3 binds to CA and may destabilize the capsid to assist in uncoating. It is also possible TNPO3 interacting with CA facilitates CPFS6-CA interactions (52, 53). Other cellular proteins that interact with HIV-1 capsids are nuclear pore complex proteins, including Nup358 and Nup153. Nup358 has a domain similar to CypA and promotes CA isomerization that may assist with uncoating. Knocking down Nup153 decreases 2-LTR circles. 2-LTR circles are unintegrated viral DNA that contain two long term repeat sequences. These stretches of DNA can be amplified by PCR and are used to mark nuclear import as they only occur in the nucleus (54). Since decreasing expression of Nup153 decreased nuclear import marker, it is concluded that this protein is necessary for effective nuclear import (13). Similarly, CypA interacts directly with the CA. This protein binds specifically to a CypA binding loop on CA and has a variety of effects on capsid uncoating kinetics.

Cyclophilin A

CypA is a cellular protein classified as a peptidyl prolyl isomerase (PPIase). It is made up of 165 amino acids with a weight of 17 kDa (55). Proteins classified as PPIase assist in protein folding catalyzation by altering proline residues between *cis* and *trans* configurations (56). An interaction between CypA and HIV-1 was discovered many years ago, but the results of this interaction remain unspecified. The CA domain of viral Gag binds to a hydrophobic pocket on the surface of CypA (42). Interestingly, the cell is depleted of CypA after new virus buds and leaves the cell (57). Since the exact role of CypA in HIV-1 infection has yet to be defined, further experimentation is necessary.

CypA directly interacts with the capsid protein (CA) and the two proteins form a complex. This interaction is formed on CA residues 85-93, with Glycine-89 and Proline-90 making up the specific CypA binding loop (Fig. 6). The complex is stabilized by van der Waals interactions and nine hydrogen bonds (58). Initially, this interaction was proposed to destabilize the capsid to assist in uncoating by binding between CA, but there is little data that supports this claim (58). Recently, evidence of a non-canonical CypA binding site on CA has been discovered. The proposed function of this non-canonical binding site is to bind two CA together to increase stability of the conical capsid (Fig. 6). It is also suggested that CypA binds to the most curved CA array, promoting curved capsid assembly (59). The exact location of this non-canonical binding site has yet to be identified, with CypA residues A25, K27, P29, and K30 being ruled out as possibilities (Fig. 6). This binding site has been concluded to be weaker compared to the CypA binding loop. Another possibility is that it is physically difficult for CypA to interact with the noncanonical binding site (60). This junction between CypA and CA is significant in understanding the protein's contribution in HIV-1 infectivity in different cell types.

A few HIV-1 capsid mutants are used to study the capsid's interaction with different proteins. These mutants are created by amino acid substitutions and include A92E, G94D, P90A, and G89V (61, 62). The two most common mutants used to study the interaction between CA and CypA are P90A and G89V. P90A is a mutation in the ninetieth amino acid position in the capsid protein where proline is changed to an alanine (43, 62). Similarly, G89V is in the eighty-nineth position and a change from glycine to valine (40). Both mutations are located in the CypA binding loop and disrupt the capsid protein's ability to bind to CypA (37, 40, 43, 62). The capsid can also be mutated to disrupt interaction with other proteins, such as TRIM5α. G94D and A92E mutated CA cannot bind to TRIM5α (62). Changing the 94^{th} residue on the capsid from glycine to aspartic acid or mutating the alanine in the 92^{nd} residue position to a glutamic acid disrupts TRIM5α restriction interactions with the capsid. All capsid mutants are used to study capsid interactions with key proteins. Understanding what happens when the protein cannot bind to the HIV-1 capsid helps to reveal the relationship between the two proteins.

Many CypA research techniques either knockdown CypA within the cell or inhibit binding of the protein to HIV-1. Using RNA interference (RNAi), CypA expression within the cell of interest can be greatly decreased (63). A specific type of RNAi, short interfering RNA (siRNA), can be used to control CypA expression within cells by targeting CypA RNA and cleaving it to decrease expression. Small nuclear RNA (snRNA) can be used to disrupt unspliced pre-mRNA by skipping exons during splicing (64). CypA can also be knocked down via clustered regularly interspaced short palindromic repeats (CRISPR)/Cas9 technology. This method uses guide RNA (gRNA) to locate and cleave target DNA. The cell then repairs the damaged DNA, leading to a loss of function mutation (65). A frequently administered technique to studying CypA in relevance to HIV-1 is to use the drug Cyclosporin A (CsA). This drug binds

to CypA and blocks its interaction with CA (62). When using CsA, CypA is blocked from being incorporated into virions (66). Both CsA and CA bind to the same hydrophobic pocket on CypA. Because they bind in the same place, CsA acts as a competitive inhibitor against CypA (42).

Cyclophilin A and HIV

A perplexing part of studying cyclophilin A is that the protein's effect on HIV-1 infectivity is cell type dependent. Within Jurkat cells and lymphocytes, inhibiting the interaction between CypA and CA decreases infectivity. Yet, in HeLa cells, disrupting this same interaction increases infectivity of HIV-1 (67). A decrease in CypA caused an increase of infectivity in specific Old World Monkey cells: Vero cells and FRhK4 cells (68). Within dendritic cells, presence of CypA appears to assist viral infection (43). The contradictory response of infectivity to CypA suggests that the protein acts in a species-specific and cell-type specific manner (69). Since the effect of CypA is variable depending on the cell type, there is a variety of proposed roles the protein may play in HIV-1 infectivity and replication.

A possible explanation for this differing effect on infectivity in different cell types is a variable effect on capsid stability. In some cell types, CypA appears to increase stability of the capsid. Higher molar ratios of CypA to CA alter CA assembly and increased capsid stiffness. To do so, CypA interacts with a non-canonical binding site to hold two CA together (59). There are higher levels of CypA expression in HeLa cells when compared to expression in Jurkat cells (67). Since infectivity increases in HeLa cells in the absence of CypA binding, it is possible that at lower concentrations of CypA, there is a stabilizing effect. Opposingly, at higher concentrations of CypA, there is a destabilizing effect (67). Therefore, the susceptibility of Jurkat

cells to CypA depletion may be due to higher concentrations of CypA compared to other cell types.

Some data suggest that CypA is involved in modulating cellular restriction factors. For example, CypA plays a role in Tat palmitoylation. Tat is found in high concentrations in T-cells and can be inhibitory to viral infection (57). Palmitoylation, the addition of fatty acids onto polar, uncharged amino acids, controls the amount of Tat present in the cell. Tat can interact with the membrane trafficking protein phosphatidylinositol (4,5) bisphosphate (PI(4,5) P_2) and this interaction becomes much stronger when Tat is palmitoylated (57). In fact, palmitoylated Tat has such a strong attraction to PI(4,5)P_2 that Tat expression is decreased (57). Therefore, the more palmitoylated Tat present, the less Tat is expressed. Further, it prevents secretion, causing Tat to accumulate on a membrane bound protein, greatly affecting membrane traffic. CypA is necessary for Tat palmitoylation, though the exact mechanism is not known. Consequently, HIV-1 controls Tat secretion and retention by depleting the cell of CypA via budding (57). Similarly, CypA influences infection within human cells by blocking restriction factor 1 (Ref-1; (69)). Ref-1 is a restriction factor that targets capsid proteins in retroviruses. Ref-1 is blocked from interacting with the capsid because CypA-CA relations (70). Therefore, HIV-1 may have evolved to use CypA as protection against restriction factors (71).

TRIM5α

Another cellular restriction factor that is presumably influenced by CypA is TRIM5α. This protein acts as an antiretroviral defense against retroviruses in the cell. All members of the TRIM family have the domains really interesting new gene (RING), B-box, and coiled-coil domains (72). The alpha isoform of TRIM5 specifically contains a C-terminal B30.2

(SPRY) domain, which assists in capsid recognition (73). The RING domain interacts with HIV-1 CA through selective binding to ubiquitinate the capsid (72). B-Box domains allow for capsid restriction through higher-order assembly to form trimer-of-dimers configurations (74, 75). Lastly, coiled-coil domains assist with TRIM5α self-association (76). When TRIM5α binds to CA it oligomerizes and forms a hexagonally organized net (Fig. 7; (75)). When TRIM5α forms a higher order assembled trimer of dimers there are two SPRY domains per complex. SPRY domains are the domains that interact directly with the HIV-1 capsid. As one domain binds to the capsid the other SPRY domain will rotate, making it appear as if the protein is walking across the capsid. This movement occurs until the protein connects with another TRIM5α to form the lattice (75).

TRIM5α is a restriction factor targets the HIV-1 capsid immediately upon entry and disrupts reverse transcription. Although the exact mechanism is still unknown, there is evidence of premature or restricted uncoating due to TRIM5α restriction (77). Higher amounts of dissociated CA within the cytoplasm of old-world monkey cells expressing TRIM5α supports the accelerated uncoating model of restriction (78). The restriction factor functions as an E3 ubiquitin ligase to protect the cell from retroviral infection (72). TRIM5α restricts HIV-1 infection by binding to the capsid, accelerating uncoating, and marking the virus for ubiquitination. Disrupting the uncoating kinetics of the capsid exposes the viral genome to proteosome degradation (78). Though this restriction is heavily studied in old world monkey cells, the roll of TRIM5α is less understood in human cell lines.

Similar to CypA and its cell type specificity, TRIM5α restriction is species specific. A study investigated the infectivity of HIV, simian immunodeficiency virus (SIV), and murine leukemia virus (MLV) in nineteen different species' CD4+ immune cells. Humans, owl

monkeys, African green monkeys, rhesus macaque monkeys, cats, and dogs were some of the species included in this test. Of the species tested, TRIM5α in old world monkey cells decreased HIV infection. This was contrary to the higher amounts of infection found in the human cell lines (79). Many studies focused on the difference between TRIM5α in rhesus macaque monkeys ($TRIM5\alpha_{rh}$) and TRIM5α in humans ($TRIM5\alpha_{hu}$) due to the contrasting effect on HIV-1 infection. Replicated studies have shown that $TRIM5\alpha_{rh}$ successfully restricts HIV infection but $TRIM5\alpha_{hu}$ does not (43, 62, 68, 72). The exact reason for the lack of restriction in humans has yet to be defined, but there has been some indication that CypA may stop $TRIM5\alpha_{hu}$ restriction.

TRIM5α and CypA

Recently, a link between TRIM5α and CypA has been revealed in terms of HIV-1 infection. Two studies, conducted in macrophages and lymphocytes, have linked TRIM5α to a decrease in HIV-1 infection (43, 62). In the initial research conducted in macrophages, when CypA-CA interaction was inhibited using P90A capsid mutants or a CypA knock down, infection significantly decreased compared to the control sample. In the same conditions, a TRIM5α knockdown rescued infection (43). A similar study in lymphocytes produced similar results. Infection decreased with P90A inhibiting CypA interaction with the capsid, compared to the wild-type capsid. Again, infectivity remained the same between P90A and wildtype capsids in TRIM5α knockout samples (62). These results suggest that CypA-CA interactions block TRIM5α restriction in human CD4+ immune cells (Fig. 8). This may be the reason for the absence of TRIM5α restriction within human cells. Further studies in different cell types are imperative to understanding this possible interaction between CypA, TRIM5α, and HIV-1 infection.

Hypothesis and Aims

Previous studies from the Hulme lab examined the role of CypA in early steps of HIV-1 replication. Zachary Ingram's Master's thesis investigated the effect of CypA on HIV-1 reverse transcription, nuclear import, and capsid uncoating in CHME3 microglial cells (80). This research indicates that CypA enhances HIV infection in microglial cells. Treatment with CsA decreased overall infectivity of HIV in CHME3 microglial cells (Fig. 9). Specifically, CypA enhanced late HIV-1 reverse transcription. For the uncoating experiment, initial results revealed less uncoating present in infected samples treated with EtOH when compared to samples treated with CsA (80). The results also indicated an overall decrease of HIV-1 uncoating in the presence of CypA (80). As this was a preliminary study, further research is necessary to investigate the effect of CypA on HIV-1 capsid uncoating. There has also been recent speculation concerning TRIM5α restriction and CypA. Multiple studies have found that inhibiting CypA interactions with the capsid rescues TRIM5α_{hu} restriction as mentioned previously. Studies have been conducted in lymphocytes and macrophages so far (43, 62). To further understand the possible connection between the two proteins and capsid uncoating, studies involving other cell types are warranted.

With the results from previous research, there is an indication that CypA and TRIM5α are involved in the early replication steps of HIV-1 infection. Initially it was hypothesized that CypA destabilized the capsid and assisted with uncoating (58). But as research on this topic progressed, it is more likely that the effect of CypA is cell type dependent. For microglial cells, there has been evidence that CypA facilitates normal HIV capsid uncoating kinetics (80). In a similar vein, studies have found a possible link between TRIM5α restriction and CypA. This effect may be cell-type specific as well. The relationship between TRIM5α and CypA has been

previously investigated in lymphocytes and macrophages (43, 62). This project will investigate the relationship between the two proteins in microglial cells. Therefore, the goal of this thesis is to investigate the role of CypA in HIV-1 replication. The *in situ* uncoating assay will be used to analyze the effect CypA has on HIV capsid uncoating. To inhibit CypA, the drug CsA will be used to block CypA interaction with CA. To investigate the relationship between TRIM5α and CypA, a TRIM5α siRNA knockdown will be used in tandem with an infectivity assay. This will allow analysis of TRIM5α restriction in the presence and absence of CypA.

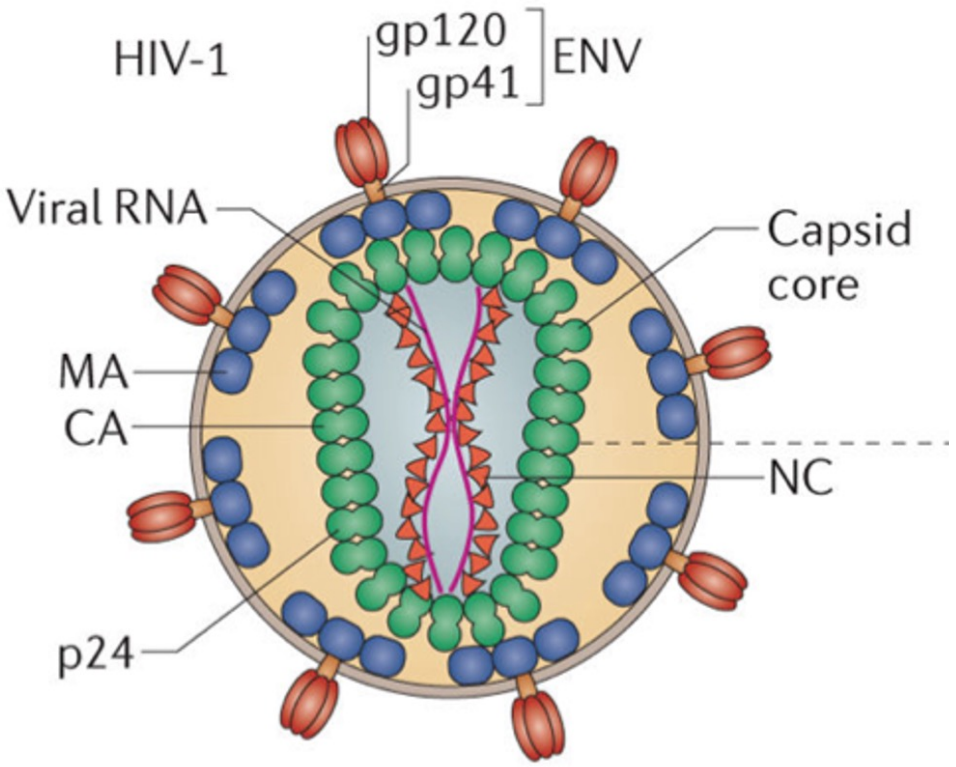

FIG 1 Structure of Mature Virion. Image depicts a mature HIV-1 virion. Gp120 and gp41 are indicated in red. The matrix protein is in dark blue, capsid protein is in green, nucleocapsid is orange triangles, and the viral RNA is pink. Modified from (13).

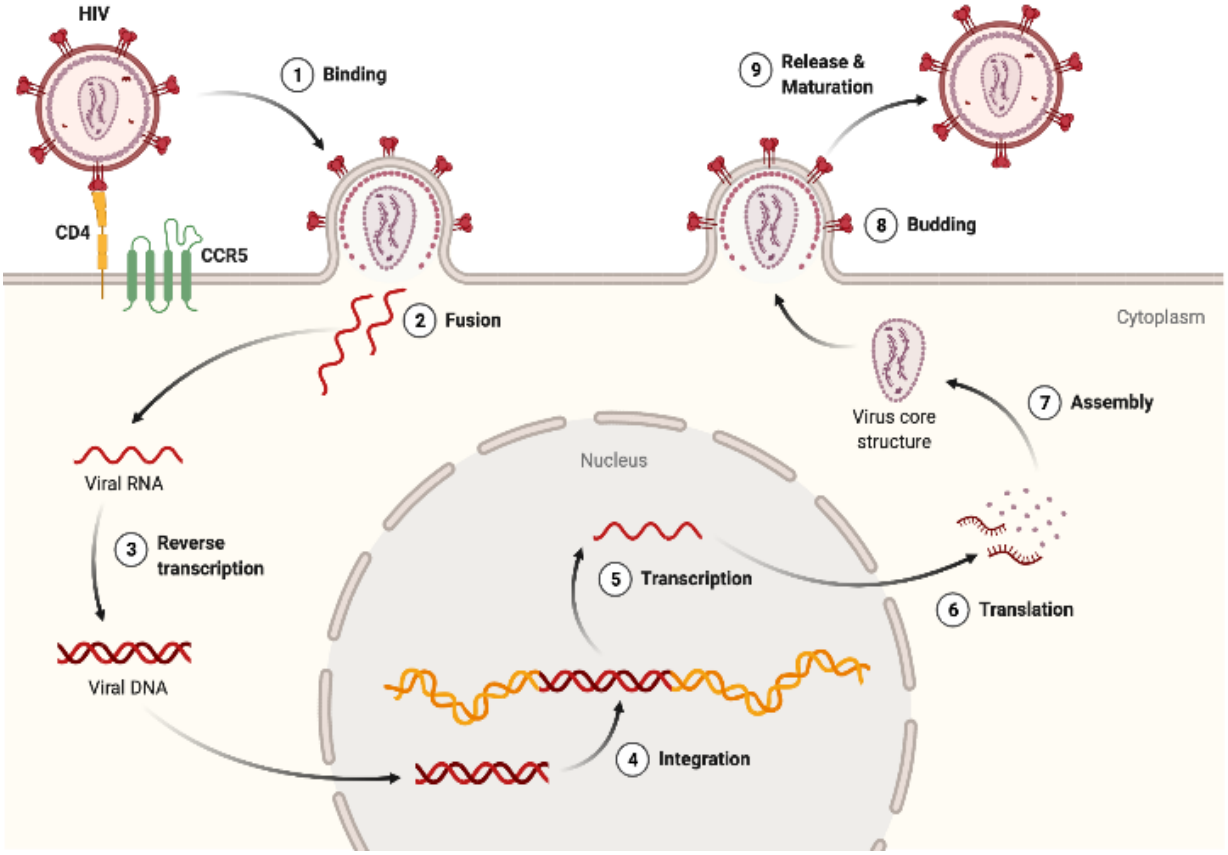

FIG 2 HIV-1 Replication Cycle Schematic. Replication begins with virion binding. Nine steps occur for successful virion replication. This progress infects the cell with HIV-1 and produces viable virus (30).

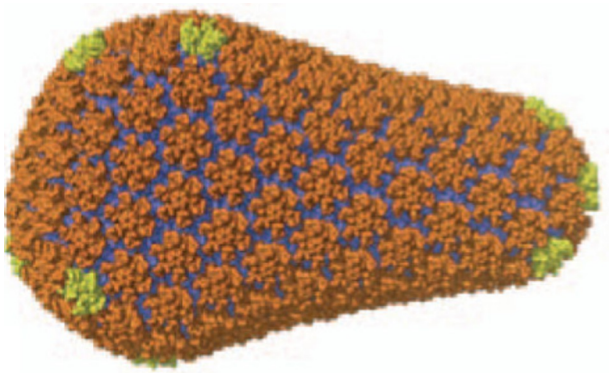

FIG 3 HIV-1 Mature Capsid Structure. The mature capsid is enlarged and shows the hexamers in orange and pentamers in yellow. The hexamers and pentamers are made up of monomers. Modified from (13)

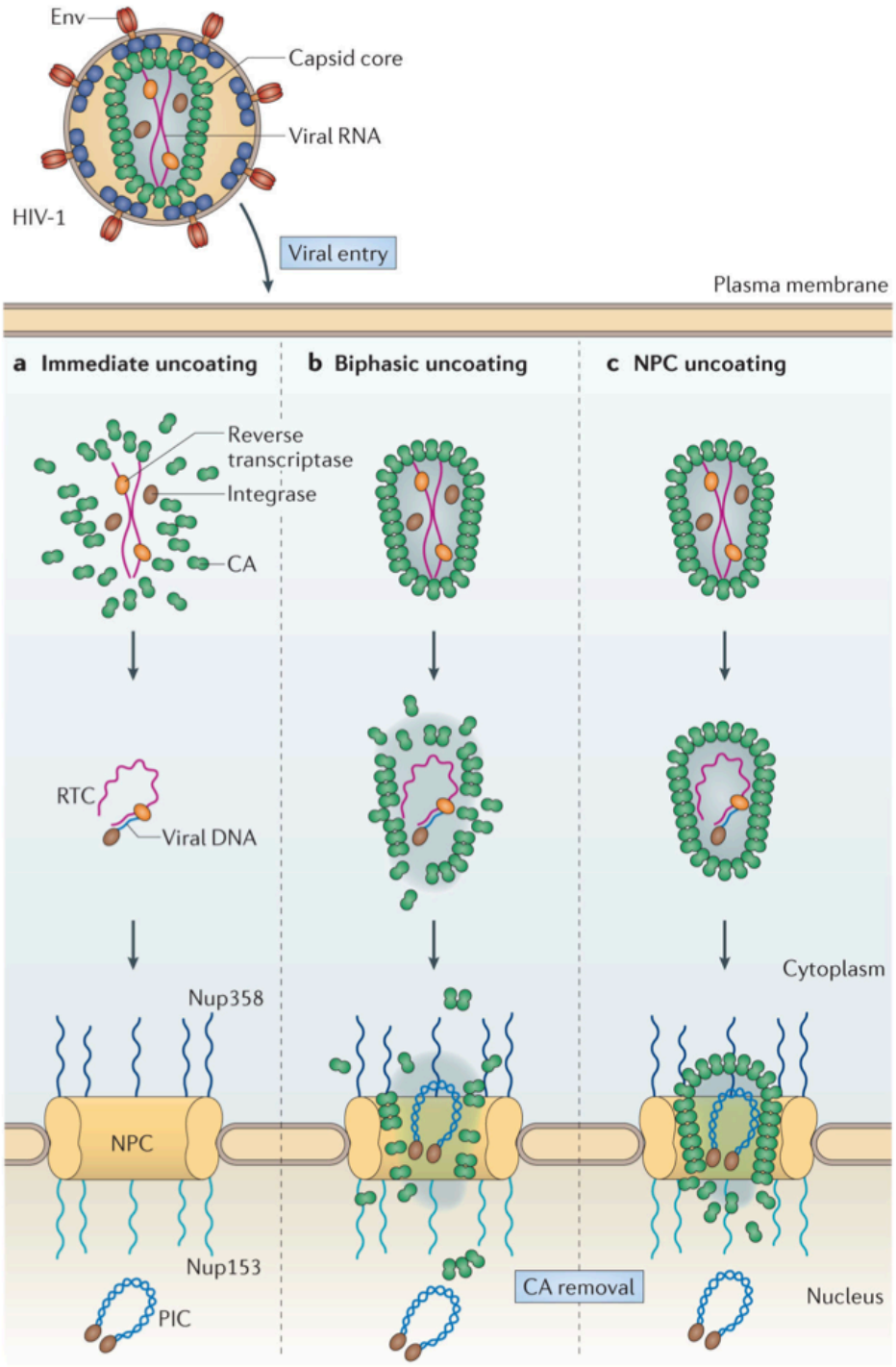

FIG 4 Immediate, Biphasic, and NPC Uncoating Models. (A) In immediate uncoating the capsid disassociates immediately upon entry. (B) Biphasic uncoating models uncoating in the cytosol while the capsid travels towards the nucleus. (C) Nuclear pore complex uncoating shows uncoating occurring at the nuclear pore (13).

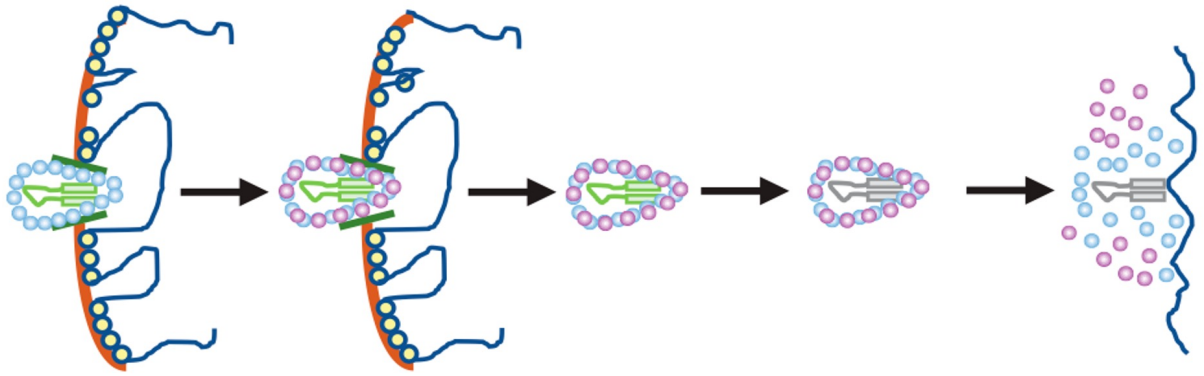

FIG 5 Nuclear Uncoating Model. Image depicts the viral capsid fully uncoating after entering the nucleus (39).

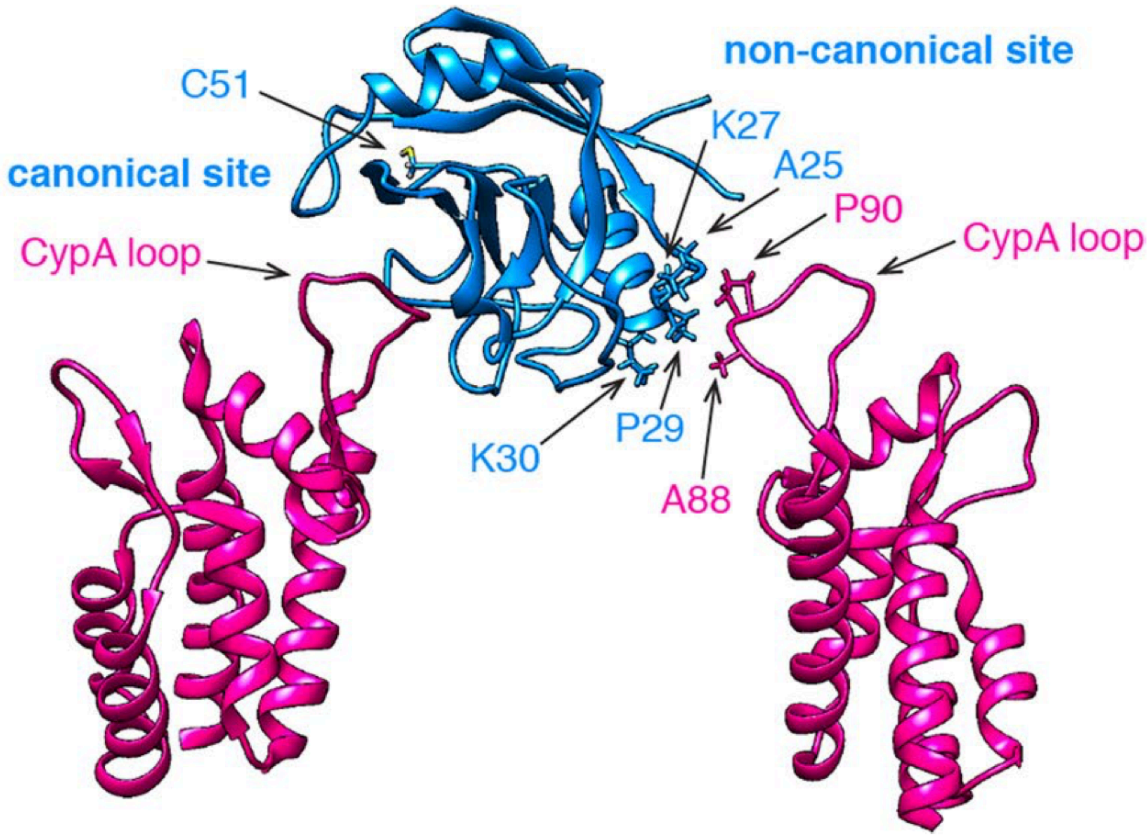

FIG 6 CypA Bound to CA. Structure of CypA (blue) bound to two HIV CA (pink). Proposed noncanonical binding site is bound on the right and the CypA binding loop on the left. Image indicates with arrows the residues involved in the interaction between the proteins. Modified from (60).

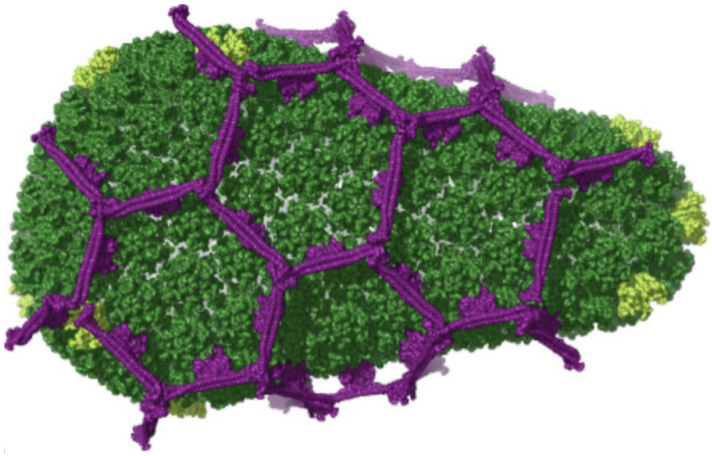

FIG 7 TRIM5α Bound to the HIV-1 capsid. TRIM5α (purple) bound to the viral capsid (green). Image shows the hexamers (dark green) and pentamers (light green) that make up the capsid. Modified from (35).

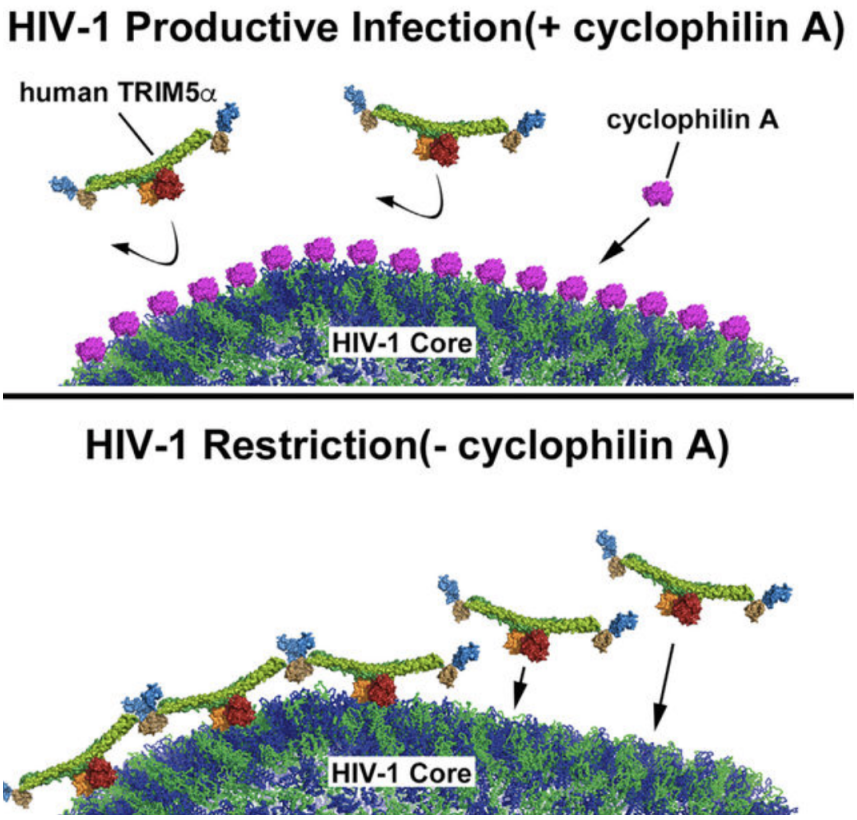

FIG 8 TRIM5α Binding to the Viral Core in Absence of CypA. Proposed model of CypA blocking TRIM5α restriction in human cells. CypA is in pink, TRIM5α depicted as a complex composed of green, red, blue, and yellow portions, the viral core is dark blue and dark green (62).

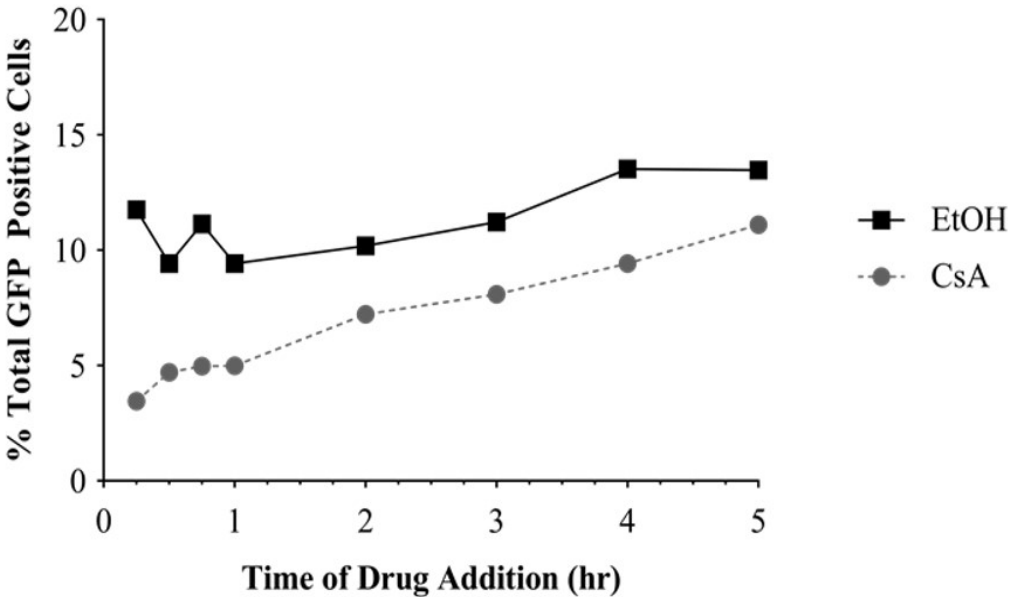

FIG 9 Infectivity Results With Treatment of CsA or EtOH. Black line is CHME3 cells treated with EtOH. Dotted gray line is CHME3 cells treated with CsA. The percent of GFP positive cells indicates the percentage of infected cells (80).

METHODS

Cell Culture and Maintenance

All research was conducted in accordance with continuing IBC protocols 2022-02.3 and 2022-02.4. The most recent update of these protocols were approved on 2/24/2022 (see Appendix A). Institutional Review Board approval was not required for use of the human cell lines used in this research. Cultured cells were kept in a tissue culture incubator at 37°C and 5% CO2. Cells were split once they reached approximately 80% confluence. 293T HEK cells and CHME3 microglial cells were cultured in 100 x 20 mm Falcon culture dishes (Corning). Media for the 293T cells was comprised of 1X Dulbecco's Modified Eagle Medium (DMEM; Corning), and 10% fetal bovine serum (FBS; R&D Systems), with 100 U/mL penicillin, 100 U/mL streptomycin, and 292 μg/mL L-glutamine (1% PSG; Corning). CHME3 media was made of 1X DMEM, 1X PSG, 5% FBS, 1% PSG, and 0.91 mM Sodium Pyruvate (Corning).

The 293T HEK cell line was provided by the Hope lab at Northwestern University. To split 293T HEK cells, media was removed from the dish and 1 mL of trypsin (Corning) was added to the cells. The trypsin was aspirated off and 1 mL of trypsin was added to the dish then removed. The dish was then placed in the incubator and the new plate was labeled and prepped by adding 10 mL of fresh media. Once cells were lifted from the bottom of the plate, the cell plate was treated with 10 mL of fresh media. Cells were gently pipetted to break up clumps. Lastly, 1 mL of the cell solution was added dropwise into the new plate.

The CHME3 cells were provided by the Naghavi lab at Northwestern University (81). To split CHME3 cells, the cells were washed with 5 mL of 1X phosphate buffered saline (PBS; Corning). Next, they were treated with 3 mL of trypsin to remove the cells from the bottom of

the plate. As the cells briefly incubate in trypsin, the new plate was labeled and prepped by adding 10 mL of fresh media. The plate with cells was then treated with 7 mL of media to neutralize the trypsin. Cells were then pipetted to break up any clumps and 1.5 mL of the cell solution was added dropwise to the new plate.

Making Dual Labeled Virus

Cells at 80% to 90% confluency were seeded out into a 10 cm tissue culture dish by adding 1.5 mL cells into the dish. Typically, one confluent plate of cells can yield five plates of transfected cells. The following day, the transfection solution made up of DMEM, HIV-GFP proviral plasmid, CMV-VSV-g plasmid, GFP-Vpr plasmid, S15-tomato plasmid, and 40 μL per reaction of PEI transfection reagent (Polysciences) was mixed. The amount of plasmid used to make the dual labeled virus stocks was varied to optimize labeling (Table 1). The solution was incubated at room temperature for 15 minutes and then added to the plates dropwise. Cells were then stored in the tissue culture incubator for 24 hours. The following day 10 mL of fresh 293T media was added to each plate and allowed to sit for 16 to 18 hours. Last, virus was harvested, and a gown and double gloves were worn to avoid contamination. Media from a transfected plate was transferred to a conical tube. Next, the filtering apparatus was assembled. To do so, the plunger was removed from a 20 mL syringe (BD Biosciences) and a Millex syringe driven filter unit was screwed to the bottom of the syringe. The media was placed into the syringe and slowly forced through the filter into a 50 mL conical tube. This step was performed with caution as to not spill any media containing virus. The filtered virus was aliquoted into labeled cryovials and stored at -80°C. Any material that encountered the virus was thoroughly bleached to kill any virus producing cells or any remaining virus.

Virus on Glass

To test viral labeling, virus was plated onto coverslips to analyze its fluorescence. To begin, glass coverslips soaked in 70% ethanol were plated into 24-well plates. Two coverslips per virus tested was used, one for staining and one for background control. Coverslips were washed with 100μL of 1X PBS three times and then treated with 0.01% poly-L-lysine (Sigma-Aldrich) for fifteen minutes. This treatment gives the coverslips a positively charged surface for the negatively charged virus to adhere to. During the incubation period, a 1:10 virus dilution was made in CHME3 media. Once the incubation time lapsed, coverslips were washed three times with 1X PBS. The washing buffer was removed via aspiration and 400 μL of diluted virus was added to each coverslip. Next, the 24-well plates were spinoculated at 1200 x g for 1 hour at 16°C. Once complete, the virus was removed, and samples were rinsed with 1X PBS. Coverslips were treated with 4% paraformaldehyde for fifteen minutes at room temperature. Samples, again, were rinsed three times with 1X PBS. Finally, 1X PBS was added to each well and samples were covered in aluminum foil and stored at 4°C overnight. On day 2, coverslips were stained with primary antibody, 241-D to target CA, and incubated overnight. Secondary antibody (Jackson ImmunoResearch) that targeted the primary antibody and contained the Cy5 tag followed on the consecutive day. Primary and secondary antibody staining protocol was the same as the *in situ* assay staining, as described below. Similarly, coverslips were mounted onto slides and stored at 4°C until imaging.

***In Situ* Uncoating Assay**

Day 1. The first day began with removing glass coverslips from a 70% Ethanol bath and placing them, one at a time, into individual wells of a 24-well plate (Falcon, Corning). This was

performed in the tissue culture hood. Coverslips were next washed with 500 µL of 1X PBS three times. Following the wash, coverslips were treated with 500 µL of 0.1% Gelatin (Millipore EmbryoMax Specialty Media) and incubated at room temperature for 30 minutes. While the coverslips sat in the gelatin, CHME3 cells were split according to protocol. The remaining cells were counted using a hemocytometer. A diluted cell mix was made to plate 120,000 cells per coverslip. Once the coverslips were done incubating, the gelatin was removed and 500µL of the cell solution was added to the appropriate wells.

Day 2. To continue the *In Situ* assay, the plated cells were infected with virus in the tissue culture hood and the coverslips fixed on a time-course. All steps following were performed in the minimal amount of light to avoid photobleaching. A virus infection solution was made for CsA wells, the BafA well, and EtOH wells according to the well plate template (Fig. 10). Dual labeled virus was used at a 1:10 or 1:5 concentration. To make the solution for CsA samples 2875.20µL of cell media, 3.20µL of 1X DEAE Dextran used at 10 µg/mL, 1.60µL of CsA (EMD Millipore) at a concentration of 2.5 µM, and 320µL of dual labeled virus were combined. The EtOH solution was made up of 2875.20µL of cell media, 3.20µL of Dextran, 1.60µL of EtOH, and 320µL of dual labeled virus. Last, the BafA control virus solution was made of up 718.40µL of media, 0.80µL Dextran, 0.40µL EtOH, 0.80µL BafA at a working concentration of 0.02µM, and 80µL dual labeled virus. To each well, 400 µL of the viral solution was pipetted into the appropriate well. After that, the plates were placed into the centrifuge to spinoculate at 1200 x g and 16°C for 1 hour. This synchronizes infection by bringing all of the virions to the extracellular membrane to begin endocytosis. Fusion does not occur until warm media is added. Next, cells are removed from the centrifuge and rinsed with 500µL 1X PBS. After the spinoculation, 400µL of warm CHME3 media was added to each well.

The BafA coverslip received a 400µL of a media-BafA solution made up of 800µL media and 0.80µL of BafA. No additional EtOH or CsA was added to the remaining coverslips. At this time, the 0-hour coverslips were fixed by adding 4% paraformaldehyde to the wells and incubated at room temperature for 15 minutes. Then, the cells were washed with 500µL of 1X PBS three times. The remaining coverslips were fixed at 1-, 2-, 3-, and 4-hours post infection. The fixed coverslips were covered with 500µL 1X PBS and stored overnight at 4°C.

Day 3. The next day was performed on the lab bench. To begin, the staining box was prepared by wetting strips of paper towel and lining the parameter of the box to keep the coverslips from drying out during the staining process. In a dark room, the 1X PBS was removed from the coverslips and, using tweezers, the coverslips were removed from the 24-well plate and placed into the staining box. All coverslips were immediately covered in 100 µL of 1X PBS. Once all coverslips were transferred, they were incubated in permeabilization solution for 15 minutes at room temperature. This solution was comprised of 0.05% Triton X in 1X PBS. During incubation, the lid to the box was closed to avoid photobleaching. Once finished, coverslips were washed with 100µL 1X PBS four times with a 5-minute incubation on the fourth wash. After that, coverslips were incubated in 100µL of blocking solution, made of 10% FBS, for 30 to 40 minutes. During the incubation time, the primary antibody solution, with the antibody 241-D at a 4000X concentration, was mixed using the equation to achieve a 1X concentration (Fig. 11). This antibody targets CA that makes up the HIV-1 capsid. Finally, post incubation, the antibody solution was added to all coverslips, except the secondary only control. The black staining box was carefully placed into 4°C and stored overnight. ProLong Glass Antifade Mountant (Thermofisher), a gel mount, that is stored at 4°C was brought up to room temperature to use the next day.

Day 4. The last day started with mixing the secondary antibody solution, using anti-human 647 antibody (Jackson ImmunoResearch) at a 400X concentration. This antibody targets the primary human antibody used in Day 3 and contains the Cy5 fluorescent tag that allows for visualization of intact capsid. The equation was used to achieve a 1X concentration. (Fig. 12) The staining box was removed from the refrigerator and placed on the lab bench. Coverslips were washed with 100 μL 1X PBS. Following were three washes in 1X PBS for 5 minutes each. Next, the secondary antibody solution was added to each coverslip. The solution was allowed to incubate for 1 hour at room temperature. After the time passed, coverslips were washed with 1X PBS three times for 5 minutes each. Lastly, gel mount was used to fix the coverslips onto glass slides. The mount used preserves fluorescence to prevent photobleaching. The slides were allowed to dry for 2 to 3 hours and then stored at 4°C for up to two weeks before imaging.

Imaging With Microscope. To image the *in situ* assay coverslips, a Leica SP8 DMI8 confocal microscope was used in tandem with the Leica Application Suite X (LASX) software. To start, the microscope and the computer were turned on. Next, once all hardware is on, the microscope software was opened. Within the software, "Acquire" was selected and 2 sequential scans were added, for a total of 3. Each sequential scan changes the wavelength to analyze the three fluorescent tags. The confocal microscope takes Z stack images at each wavelength. Next, for sequential scan 1, GFP was selected and adjusted from 15 to 30 percent transmission. Scan 2 was the user defined dTomato, and scan 3 was the computer setting Cy5. Once the software was set up, the slides with the coverslips were set under the microscope. A cell was found manually using the light of the microscope, then the topmost Z section of the cell and bottom most Z section were selected. Once complete, "take picture" was selected and the microscope took an image of the cell. Each image was comprised of an average of 30 Z sections. This was repeated

10 times per slide at different locations on each coverslip. Once all images were taken, they were saved onto the computer.

Data Analysis. To begin analysis for each image, the background fluorescence had to be manually removed, in a process called thresholding. The uninfected control sample was used to determine the amount of background GFP and dTomato fluorescence present. The secondary antibody only control was used to find the amount of background caused by the Cy5 signal. Using the thresholds, the background was removed for all experimental samples and samples were saved as TIFF images.

Following download, the images were analyzed using a semiautomatic counting software. Using the ImageJ Overlap Intensity macro plugin, the fluorescence of each image was quantified (82). This software uses colocalization analysis to measure the overlap of two signals. To do this, it locates all GFP signals on the image and labels them as a region of interest (ROI). It then measures the intensity of Cy5 and dTomato signals in each ROI. Images were able to be processed in batches that were organized by sample. The maximum fluorescence for each ROI was saved in a Microsoft Excel sheet for further analysis. Using Excel, the mean maximum fluorescence of Cy5, percent uncoating, and percent fusion were calculated and compared between samples.

siRNA TRIM5α Knockdown

Day 1. To begin the knockdown, CHME3 cells must be 60% to 80% confluent in the culture dish. Two cultures of cells were prepared to ensure there were enough cells. Before starting, all equipment was cleaned using a 70% ethanol solution. Cells were split according to the protocol above. The remaining cells from both dishes were saved in a 50 mL conical tube and

15 μL of the cell solution was used to count using a hemocytometer. Next, the number of cells needed to plate $1.7x10^5$ cells per well in a 6-well plate was calculated. Using the calculated amount, the diluted cell solution was mixed, and 2 mL of the cell solution was aliquoted into each well of two 6-well plates. The plates were incubated overnight.

Day 2. All equipment was treated with RNAase Zap (Fisher Scientific) and placed under an ultraviolet light for 15 minutes prior to the experiment. The following day the cells were transfected with siRNA pools targeting TRIM5α and GAPDH (Horizon). As controls, a nontarget siRNA (Horizon) and a no siRNA transfected were used. Once treatment was finished, each siRNA solution was mixed for each appropriate sample. Two Eppendorf tubes were used for each sample, labeled tubes A and B. To tube A, 50 μL of OPTIMEM media was added. To tube B, 100 μL of OPTIMEM media was added. Next, 4 μL of lipofectamine RNAiMax (Invitrogen) was added to tube A and mixed by tapping. Tube B then received 3 μL of the appropriate siRNA duplex (100pmol/μL) and mixed by tapping. Both tubes were incubated at room temperature for 5 minutes. Next, tube A contents were added to tube B, mixed by pipetting, and incubated at room temperature for 20 minutes. During incubation, the CHME3 media was aspirated from the cells in the two 6-well plates and replaced with 1 mL of OPTIMEM media. Each well was labeled for TRIM5α, GAPDH, NT4, or no siRNA. After the 20 minutes, the siRNA duplex mixtures were added to the appropriate wells in both 6-well plates in a dropwise manner and each plate was rocked back and forth to mix the wells. The plates were placed in the incubator. Next, four hours later, the transfection media was replaced with 1 mL warmed DMEM media that does not have PSG and samples were incubated overnight.

Day 3. The transfected samples from one plate were transferred to two 96-well plates, one for CsA and one for EtOH. One 6-well plate was saved for RNA isolation later. To transfer

samples to a 96 well plate, the media was removed from the cells, and they were washed with 2 mL of 1X PBS. The PBS was removed, and 1 mL of trypsin was added to release cells from the bottom of the plate. Once the cells lifted from the bottom of the plate, 1 mL of warmed CHME3 media was added to each well and the media was pipetted to break any clumped cells. For each sample run, the cells were placed in a separate conical tube and counted using a hemocytometer to determine the number of cells per transfection sample. Using the number of cells in each tube, the amount needed to have 6,000 cells per well was calculated. A solution was mixed for each condition using the appropriate cells and CHME3 media. To the 96-well plate, 100µL of this cell solution was added to the appropriate wells, using the multichannel pipette. Cells were plated according to the schematic (Fig. 13) and the plate incubated overnight.

Day 4. The cells were infected with HIV-GFP reporter virus that fluoresces infected cells. In the 96-well plate, an infectivity dilution was used to analyze infectivity. To start, 1X and 2X media was made for both CsA and EtOH. The 1X media was made up of 6mL of cold CHME3 media, 3µL of 2000X polybrene, and 3µL of either 2000X CsA or EtOH. The 2X media was made up of 1mL of cold media, 1µL of 2000X polybrene, and 1µL of 2000X CsA or EtOH. To the first column of each plate, 100µL of the appropriate 2X media was added using the multichannel. The remaining columns received 100µL of 1X media to the CsA and EtOH 96-well plate. Next, the virus solution was mixed to create the serial dilution. An example for the $1/16^{th}$ serial dilution is a viral mix made up of 1.75 mL of cold CHME3 media and 250µL of HIV-GFP virus. Once mixed, 100µL of the solution was added to the first column for each plate. For the serial dilution, 100µL from column 1 was added to column 2 and mixed by pipetting gently. This process was repeated for all columns except the last one to keep an uninfected control. For last column to receive virus, 100µL was discarded into bleach for the proper

dilution. Once virus was added to the cells, the plate was centrifuged at 1,200xg for 1 hour at 16°C. While the 96 well plates were spinning, RNA was isolated from the cells in the 6-well plate with the transfected cells according to protocol previously described and samples were stored -20°C. When spinoculation was complete, the virus solution was replaced with warm media that contained 3μL CsA or EtOH for all wells and the plate was placed into the incubator overnight.

Day 5. Cells were viewed under a light microscope to ensure they were still healthy and alive. The plate was incubated overnight.

Day 6. On the last day, the cells were harvested. To do this, 100μL of cell fix solution was made up that contained one part paraformaldehyde to one-part 1X PBS mixed in a 15 mL conical tube. Cells were lifted from the bottom of the plate, as before, using trypsin. The samples sat in trypsin longer to naturally release from the bottom of the well because cells were fragile after infection. Cells were resuspended in the trypsin and 100 μL of cell fix was added to each well using the multichannel. The plate was then sealed with parafilm, wrapped in aluminum foil to avoid photobleaching of the virus, and stored at 4°C for a minimum of 4 hours. Once finished, the cells were ready for flow cytometry.

Flow Cytometry

To analyze the cells for infectivity, the Accuri C6 flow cytometer (BD Biosciences) was used. From the 96-well plates with siRNA, 2 wells of the same sample were combined into 1 glass tube for a total of 400μl of sample into each tube. If not performing flow cytometry the same day, samples were stored at 4°C. Next, the flow cytometer and the software were turned on according to machine guidelines. An empty tube was placed on the sip and the machine was

backflushed. The template “Pekic” was used for siRNA analysis. This template has gated graphs that select the amount of living cells and GFP positive cells in each sample analyzed. The software was set to 10,000 events or 120μL and a fast run. After that, the sample was placed on the sip and run was selected. The negative control line on the graph for the uninfected sample was moved to between 0.1% and 0.0% to remove background for each sample. Data in the analysis file from plots 1 and 2 in the template were saved.

TRIM5α Primer Cloning

RNA Isolation From CHME3 Cells. To isolate total RNA from CHME3 cells the Qiagen RNeasy Plus Mini kit was used. The standard protocol was followed for this kit. Before starting, 10μL of B-mercaptoethanol was added to 1 mL of Buffer RLT Plus in the chemical hood. To begin, CHME3 cells were split according to the protocol above. The remaining cells were added to a 15 mL tube and 15 μL used to determine the number of cells via a hemocytometer. Approximately 10,000 cells were transferred to a new 15 mL tube and centrifuged at 300 x g for 5 minutes to pellet the cells. Remaining media in the tube was aspirated for disposal.

Next, the cell pellet was loosened by flicking the tube and 350 μL of Buffer RLT plus was added to lyse the cells and the sample was pipetted to mix the solution. To homogenize the lysate, the total cell solution was added directly to the purple QIAshredder spin column (Qiagen) in a 2 mL collection tube. The sample was centrifuged for 2 minutes at maximum speed and the flow through saved. Following, the flow through was added to a white and purple gDNA Eliminator column and centrifuged for 30 seconds at 8000 x g or until all liquid has passed

entirely through the column. Next, 350 μL of 70% ethanol was added to the flow through and mixed via pipetting.

To a pink RNeasy spin column, 700 μL of this solution was added and centrifuged for 15 seconds at 8000 x g, and the flow through was discarded. To the same pink column, 700 μL of Buffer RW1 was added and centrifuged as before and the flow through was discarded. Again, to the same RNeasy spin column, 500 μL of Buffer RPE was added and centrifuged again for 15 seconds at 8000 x g, and the flow through was discarded. This step was repeated and centrifuged for 2 minutes at 8000 x g or until the pink column was dry. The pink column was placed in a new collection tube and centrifuged at full speed for 1 minute to remove any residual liquid. Next, the column was placed in a 1.5 mL Eppendorf tube for collection and added 50 μL of RNase free water and centrifuged for 1 minute at 8000 x g. The final total CHME3 RNA sample was stored at -20°C. Total RNA concentration was determined using a nanodrop spectrophotometer.

Reverse Transcription Reaction With Total RNA. To start primer development, the RNA was reverse transcribed to cDNA (Fig. 14). For this reaction, the reagents in table 2 were combined and samples were pipetted to mix. A negative reverse transcription control was made up by replacing reverse transcriptase with water. Samples were incubated for 1 hour at 37°C. Next, the cDNA was amplified using PCR.

PCR Amplification. cDNA was amplified using TRIM5α primers A, C, and E. A master mix for PCR products was mixed using SsoFast EvaGreen Supermix (Bio-Rad) protocol or GoTaq Green Master Mix (Promega). Both protocols were used in an attempt to optimize amplification. GoTaq Green was more efficient and used for repeated experiments. PCR products were run on a 3% agarose gel to confirm amplification using a gel electrophoresis rig.

Gel Electrophoresis. The 3% gel was made by combining 75 mL of 1X TAE with 2.25 g of agarose. The solution was heated and 2.25 μL of ethidium bromide was added. The gel was allowed to cool slightly and then poured into the gel rig to form the wells. Once the gel was solid it was properly positioned in the rig and 1X TAE was poured into the gel rig up to the fill line. The samples were pipetted into wells. The gel rig was run at 100V for 45 minutes and imaged on a gel reader.

PCR Clean Up and Ligation Reaction. PCR products were cleaned up using two kits: QIAquick PCR Purification Kit (Qiagen) and Wizard SV Gel and PCR Clean-Up System (Promega). The Wizard kit was used because reagents in the Qiagen kit had expired. The PCR products were purified using the protocol for the appropriate kit. Once purified, the samples for TRIM5α primers A and C underwent pGem Teasy ligation reactions (Promega). The reagents mixed together for the ligation reaction were 5μL of cutsmart buffer (NEB), 1.5μL of nuclease free water, 2μL of purified PCR inserts, 1μL of ligase, and 0.5μL of pGem Teasy vector. The solution was incubated overnight at 4°C.

Transfection of Vector Into HB101. To begin transformation, 100 μL of competent HB101 cells (Promega) were thawed slowly on ice for 15 minutes. Next, 2 μL of the ligation solution was added into the cells and the tube was flicked to combine. After, the cells chilled in ice for 10 minutes. Immediately following, samples were heat shocked in a bead bath set to 42°C for 45-50 seconds then the tube was put back in ice for 2 minutes. To the tube of HB101 cells, 900 μL of LB media was added. The samples were placed on a shaker set to 220 RPM for one hour at 37°C. While shaking, LB-Amp plates were placed in the incubator to warm. After the samples were done shaking, 100 μL of the cell solution were plated onto the LB plate. The

remainder of the solution was stored at 4°C. The plated cells were placed into the incubator at 37°C overnight.

Bacterial Culture. Of the colonies that grew from the transfected HB101 cells, one single colony was selected to grow up in a culture. To culture the cells, 3 mL of 0.1% ampicillin media mix was aliquoted into culture tubes for each sample. An example of master mix was 32 mL of LB media with 32 μL of ampicillin added. Next, near a flame, one colony was put onto the end of a pipette tip and the tip was ejected into the culture. The samples were placed into the shaker set to 220 RPM at 37°C overnight.

Miniprep. The following day, samples were put through a miniprep to isolate the plasmids. The Qiagen Qiaprep miniprep kit and protocol for the kit using a microcentrifuge was used. Lyseblue was not added to the samples, so the protocol followed did not include that reagent's steps. EB buffer was used to elute at the end. Samples were stored at 4°C.

EcoR1 Restriction Digest. After the miniprep, a restriction digest was implemented. The 1X master mix was made up of 3 μL of cutsmart buffer (NEB), 0.5 μL of EcoR1 (NEB), and 16.5 μL of water. Next, 20 μL of master mix was added to an Eppendorf tube labeled per each sample. To each tube, 10 μL of the appropriate miniprep DNA was added to the digest master mix. Samples were incubated for 1 hour at 37°C. While samples incubate, gel electrophoresis was set up as detailed above. After incubation, the digest samples were each mixed with 6 μL of loading dye and 25 μL of each sample was loaded into the gel. The gel was run and imaged using a gel reader.

Primer Efficiency: qPCR. To calculate primer efficiency, a serial dilution of the pGem-Teasy-TRIM plasmid had to be run through qRT-PCR. The serial dilution was made up of 10^7, 10^6, 10^5, 10^4, 10^3, 10^2, 10^1 plasmid DNA with 10^7 being the miniprep DNA stock solution. For

each tube, starting with 10^6, 45µL of water was aliquoted into each tube. Then, 5µL of the previous tube was added. Therefore, 5µL of 10^7 was put into 10^6, then 5µL of 10^6 was put into 10^5 and so on. Next, the master mix was made according to the number of tubes used. For example, for 24 qPCR reactions, 241.92µL of water, 288µL of iTaq master mix (Bio-Rad), 8.64µL of forward primer (Table 3), and 8.64µL of reverse primer (Table 3) were mixed together to make the master mix. Next, 19µL of the master mix was aliquoted into the qPCR tubes. Once complete, 1µL of each serial dilution sample was put into the appropriate tube. Instead of sample in the last tube, 1µL of water was added as a control. Finally, the tubes were run on the qPCR machine using the iTaq protocol. For the cycling conditions, the polymerase activation was set at 95°C for 20-30 seconds, denaturation at 95°C for 2-5 seconds, annealing/ extension at 60°C for 15-30 seconds. This was run for 25-30 cycles. Melt curve analysis was from 65°C to 95°C in 0.5°C increments for 2-5 seconds per step. Results were saved in a Microsoft Excel sheet for later analysis.

TABLE 1 Amount of Plasmid Used for Dual Labeled Virus Stock

Plasmid	3-7-20 Stock 1	3-7-20 Stock 2	3-7-20 Stock 3	2-13-21 Stock A	2-13-21 Stock B	2-13-21 Stock C
HIV-GFP	3.70µg	3.70µg	3.70µg	3.70µg	3.70µg	3.70µg
GFP-Vpr	1.00µg	1.00µg	1.00µg	1.00µg	1.50µg	1.50µg
S15-tomato	5.50µg	5.50µg	5.50µg	5.50µg	5.50µg	2.00µg
VSV-g	1.09µg	1.09µg	1.09µg	2.10µg	2.10µg	2.74µg

TABLE 2 Total RNA Reverse Transcription Reaction

Reagents	Concentration	Amount
AMV Buffer (Promega)	5X	4 μL
$MgCl_2$	50 mM	2 μL
dNTPs (Promega)	10 nM	2 μL
RNasin (Promega)	-	1 μL
AMV reverse transcriptase (Promega)	-	1 μL
Random Hexamers (Promega)	-	2 μL
CHME3 RNA	1.3 μg/μL	0.76 μL
Deionized H2O	-	7.24 μL

TABLE 3 Primer Table

Primer	Sequence
Forward Primer GAPDH	5’-GCACCGTCAAGGCTGAGAAC-3’
Reverse Primer GAPDH	5’-GCCTTCTCCATGGTGAA-3'
Forward Primer TRIM5α-A	5’ -TTCTGTACAGCACCTCTTGTCC-3’
Reverse Primer TRIM5α-A	5’-AAAGAAGGGAGACAGCAAGGAAA-3’
Forward Primer TRIM5α-C	5’-ACCTCTTGTCCAGGTGCAT-3’
Reverse Primer TRIM5α-C	5’-ATTGGGGACAATATGGCACAAG-3’
Forward Primer TRIM5α-E	5’-TCTTGTCCAGGTGCATCTCATA-3’
Reverse Primer TRIM5α-E	5’-ATAGAAAGAAGGGAGACAGCAAGG-3’

A

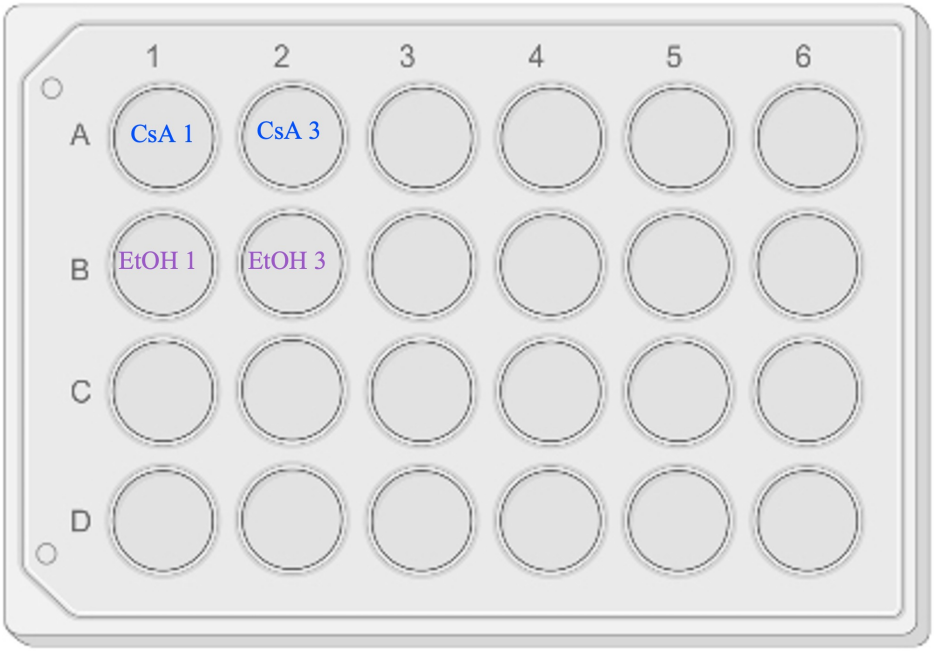

B

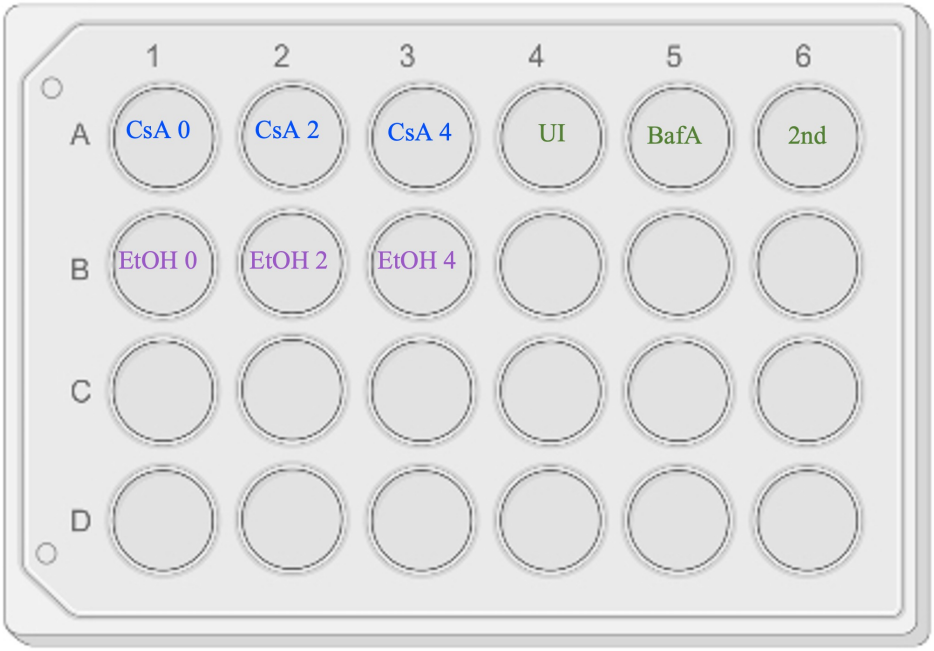

FIG 10 24-Well Plate Schematic For the *In Situ* Uncoating Assay. CsA treated coverslips are depicted in blue, EtOH are in purple, and controls are in green.

C1V1=C2V2

(4000X)(V1)=(1000 µL)(1X)

V1= .25 µL

* V2 was increased to provide a V1 that was at least .2 µL

Total volume = .25 µL of 1° antibody + 999.77 µL antibody solution

FIG 11 Primary Antibody Equation. The amount of primary antibody needed for staining was calculated using the dilution equation C1V1 = C2V2. The starting concentration was 4000X. The ending concentration was 1X. The final volume was 100 µL per coverslip, accounting for one extra coverslip. The final volume was adjusted if necessary to be above 0.2 µL.

C1V1=C2V2

(400X)(V1)=(400 µL)(1X)

V1= 1 µL

Total volume = 1 µL of 2° antibody + 399 µL of antibody solution

FIG 12 Secondary Antibody Equation. Using C1V1 = C2V2, the amount of secondary antibody was calculated. The starting concentration was 400X and the final was 1X. The ending volume was 100 µL per coverslip plus 100 µL.

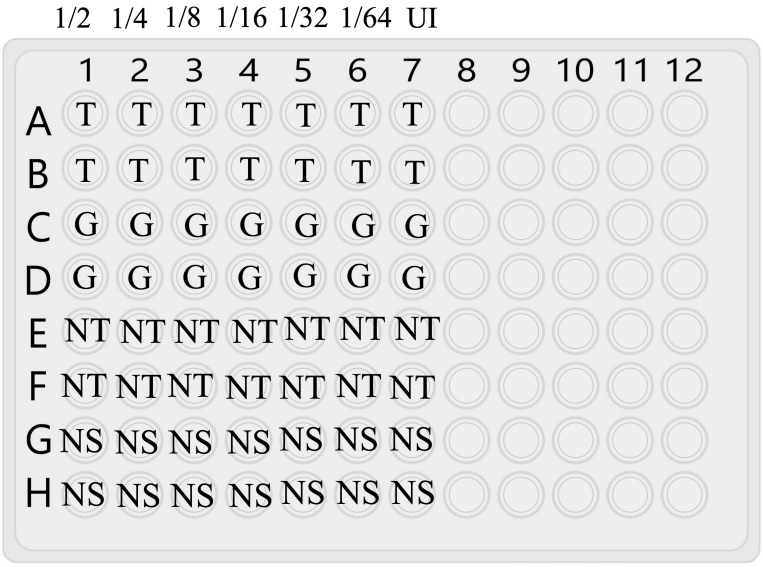

FIG 13 96-Well Plate Schematic. Image depicts the set up for the 96 well plate used in the siRNA knockdown. Two plates were prepared, one for CsA and one for EtOH. This plate shows an example serial dilution. In the plate, T represents TRIM5α siRNA, G is GAPDH knockdown, NT is the NT4 pool siRNA and NS is no siRNA.

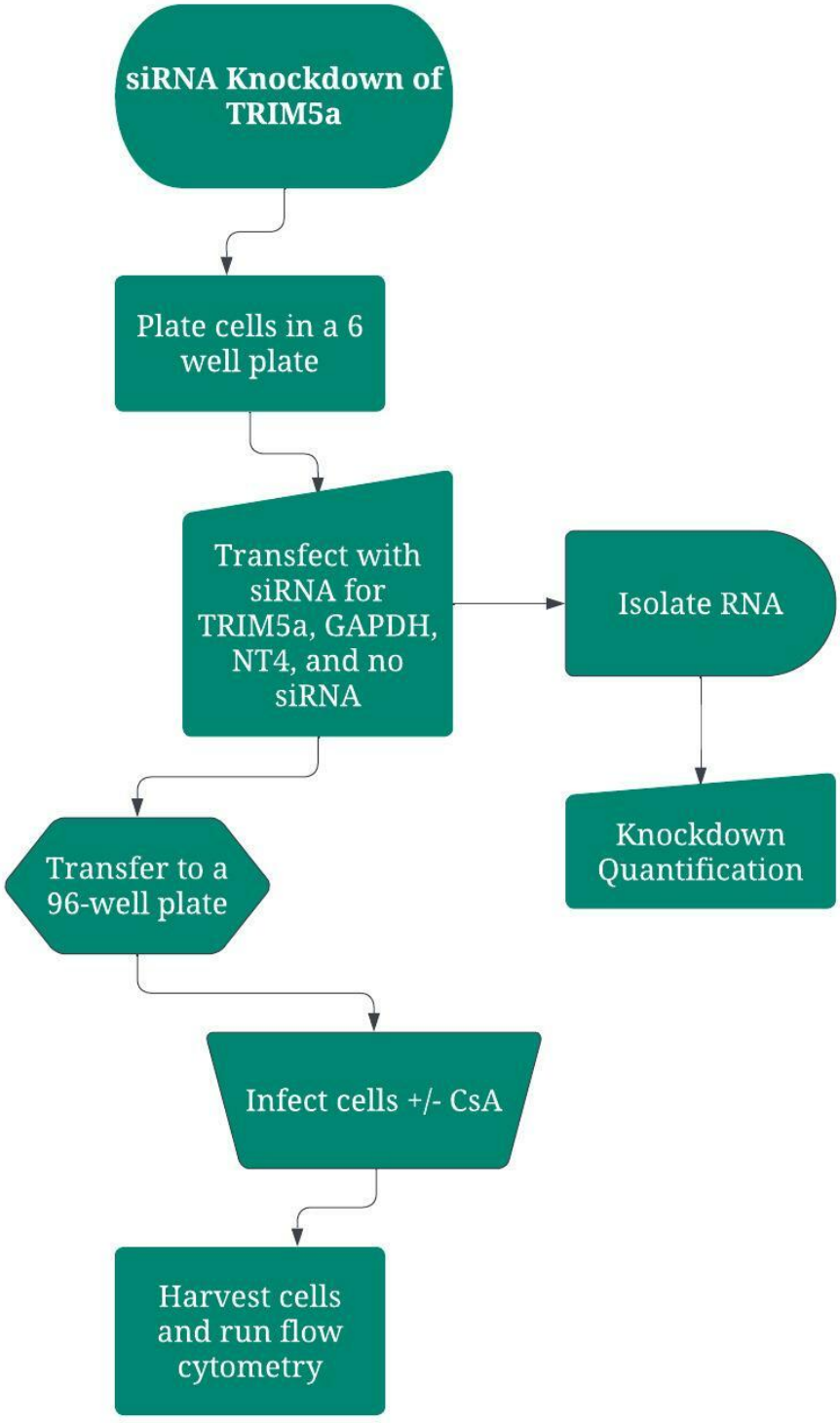

FIG 14 Method Flow Chart for Aim 2. The chart shows the process used to test the effect of CypA and TRIM5α for aim 2.

RESULTS

Effect of CypA on HIV-1 Uncoating

I hypothesize that CypA assists with uncoating. To investigate the effect of CypA on uncoating in microglial cells, the *in situ* uncoating assay was used. To block interaction between CypA and CA, samples were treated with the inhibitor CsA. It is expected that microglial cells treated with CsA will report a higher amount of CA compared to cells treated with EtOH.

Description of the *In Situ* Uncoating Assay. The *in situ* uncoating assay allows uncoating to be analyzed within infected cells. CHME3 cells were fixed on a time course after infection with dual labeled VSV-g pseudotyped virus. To make the dual labeled virus four plasmids are transfected into 293T cells. The HIV-GFP plasmid contains all viral proteins necessary for replication except has a frameshift mutation to disrupt the viral envelope gene and blocks formation of infectious virus. The VSV-g plasmid produces the env protein to allow the virus to infect via endocytosis and produces single use virus (83). Typically, HIV enters the host cell through binding and fusion with the cell membrane, not by endocytosis. Despite this difference in infection, uncoating occurs as it would in wildtype HIV (38). GFP-Vpr labels the viral complex and allows for visualization of the viral particles within cells (Fig. 15). The HIV-1 membrane itself has also been labeled with a s15-dTomato fluorescent protein. (dTomato; Fig. 15) (84).

After fixation, samples undergo primary and secondary antibody staining that targets CA of the HIV-1 capsid. The secondary antibody is Cy5 fluorescent tagged. Samples are imaged using fluorescent microscopy to reveal presence of the viral complex, viral membrane, and CA present during each time point. In the images, the viral complex located within the capsid

appears green, due to GFP-Vpr; viral membranes are red because of dTomato labeling; and CA is blue, due to the Cy5 secondary antibody staining (Fig. 15). Overlap of dTomato and Cy5 indicates virus that has neither fused nor uncoated (Fig. 15). In this assay the amount of CA signal present in the hours following HIV-1 infection is tracked to reveal the effect CypA has on uncoating.

Analyzing Dual Labeled Virus Stocks. To ensure that the virus stocks produced in the lab had the proper labeling, each stock was analyzed. By mounting the virus onto glass slides and imaging each sample, the amount of fluorescence from each tag was calculated as a percentage (Fig. 16). Percent dTomato is the percent of GFP labeled virus that also has the dTomato label. The threshold for viable stock is 80% dTomato, indicating that 80% of GFP labeled virions also contained dTomato labeling. It is important to know the amount of dTomato membrane labeling compared to GFP labeling because it can be taken into consideration when analyzing presence of membrane in experiments that use this virus. When making the virus, some cells received a varied amount of each plasmid in an attempt to optimize labeling. The three viral stocks made on 3-7-2020 all received the same amount of each plasmid. The stocks made on 2-13-2021 received varied concentrations of each plasmid (Table 1). All stocks, except EW 3-7-20 batch 2, meet or exceed the 80% threshold for dTomato labeling (Fig. 16). The EW 3-7-20 batch 2 reached 75% dTomato labeling and the remaining virus stocks met the threshold, so all stocks were determined usable for further experiments.

The virus was also analyzed for the amount of Cy5 staining to determine the amount of CA detectable for each stock. The stocks made on 3-7-20 each had Cy5 staining at 60% to 84% (Fig. 16). This means that at least 60% of virus that contained the GFP label had detectable Cy5 signal from antibody staining. Interestingly, all stocks made on 2-13-21 show considerably lower

Cy5 fluorescence when compared to virus made on 3-7-20 (Fig. 16). For the February stocks, all Cy5 signal detection was below 20%. From this analysis, stocks 3-7-20 batch 2 and 2-13-21 batch A were selected to be used in future experiments.

Assay Development and Controls. For the *in situ* uncoating assay, microglial cells were infected with dual labeled virus in the presence of CsA or ethanol (EtOH) and fixed on a time course from 0 to 4 hours post infection. Samples were then stained with antibody for CA and imaged (Fig. 17). The semi-automatic overlap intensity counter in ImageJ was used for image analysis (82). A total of three *in situ* uncoating assays were conducted and analyzed. Data from these assays were combined to visualize trends. The controls include a Bafilomycin A (BafA) treated sample used as a fusion inhibitor control, a secondary antibody only coverslip, and an uninfected sample. The drug Bafilomycin A is a V-ATPase inhibitor and blocks VSV-g HIV fusion. It achieves this by blocking endosomal fusion of the VSV glycoprotein to the cell membrane (85).

To analyze the *in situ* assay results, the maximum fluorescent intensity of Cy5 was calculated for each virion marked by GFP-Vpr. This number reveals the amount of CA present in each virus and can be used to see how much uncoating has occurred in each condition. To avoid counting capsid from unfused virus, only Cy5 signal from virus without dTomato signal was included in uncoating analysis. The average CA signal, or mean maximum fluorescence intensity, was then calculated for each condition for each time point.

Effect of CypA on Uncoating. To analyze the amount of CA present in each condition, the data was pooled into one scatterplot (Fig. 18). The BafA fusion control had an average CA signal detection of 160, which is relatively similar to the detection of 152.1 and 164.7 for EtOH treated samples at 1- and 2-hours respectively. Combined data from all assays shows a change in

the mean maximum Cy5 signal in the CsA treated samples compared to the EtOH samples. The CA signal is higher in CsA compared to EtOH at the 0-, 1-, 2- and 3-hour time points (Fig. 18 and Table 4). The 1-hour time points are barely dissimilar, with a difference of 2.4 (Table 4). The trend set by the 1-, 2-, and 3-hour time points is switched at 4-hours post infection where there is more CA signal detected in the EtOH condition compared to the CsA condition (Fig. 18). At this final time point, there is more CA signal detected in the EtOH condition compared to the CsA condition. This data indicates that when CypA is able to bind to the HIV-1 capsid, there is less CA present for time points 1-, 2-, and 3-hours post infection.

Of the combined data, the greatest difference between the CsA and EtOH conditions is found in the 3-hour time point (Fig. 18 and Table 4). CsA treated samples reported a Cy5 signal of 157.7 and EtOH samples reported 92.92 (Fig. 18 and Table 4). It is important to mention that for this time point specifically, the CsA data is made up of three experiments, while the EtOH is only made up of data from two assays. Despite this difference, this trend can be trusted because similar results were produced from the two complete experiments for the same time point (Table 4). The 3-hour time point from the June experiment showed a signal of 162.3 for CsA and 91.72 for EtOH. Similarly, the February experiment yielded a signal of 120.9 for CsA and 94.17 for EtOH. Therefore, the result of 157.7 for CsA and 92.92 for EtOH is expected for this time point. Overall, Cy5 levels, that measure the amount of CA present, are consistently greater in CsA conditions compared to EtOH.

When analyzing each *in situ* uncoating assay separately, there are some trends found in all three. The BafA fusion control had similar results for all experiments with Cy5 signal detection of 171.5, 130.9, and 176.9 for June, February, and March respectively (Fig. 19 and Table 4). For the 0-hour time point, there was a higher signal in the CsA condition compared to

the EtOH for the June, February, and March experiments, with March having the largest difference (Fig. 19). Interestingly, the 0-hour time points all reported average signal detection numbers below 100 for all experiments (Fig. 18 and Table 4). The 1-hour time point was not as consistent. The June and March experiments showed more Cy5 signal in CsA compared to EtOH (Fig. 19A and C). On the other hand, the February experiment reported a higher average Cy5 signal in the EtOH condition compared to the CsA 1-hour time point (Fig. 19B). Both the 2- and 3-hour time points had similar results for all assays. There was more Cy5 signal reported in the CsA condition compared to the EtOH sample. The last time point, 4-hour, showed more Cy5 signal in CsA compared to EtOH for the March experiment (Fig. 19C). For both June and February, there was more average CA signal in the EtOH treated sample compared to the CsA 4-hour time point (Fig. 19A and C). Overall, this data indicates that there is more CA present at specific time points.

When comparing the average CA signal for each condition, the number of virions per sample must be considered because if one condition with more virions compared to another then there may be an artificially increased amount of CA. The largest difference in the number of virions when combining all the data is the 3-hour time point for the pooled data. The CsA treated coverslips had a total of 444 virions, while the EtOH coverslips only had 170 (Fig. 18). The June experiment viral counts per coverslip were also inconsistent, ranging from 150 to 15 virions for the 1-hour conditions (Fig. 19A). This is because the 1-hour EtOH coverslip split into four pieces during the experiment, and only a few fragments were saved for imaging. Also, the March experiment 3-hour EtOH sample was lost, so that sample has data from two experiments instead of three.

To ensure that there was no bias occurring from one experiment outweighing another when pooling the data from all three experiments, the average signal was calculated by manually averaging the mean Cy5 signal from the June, February, and March assays. The result was similar to the average that had been produced from the pooled data and verified that no one experiment was shifting the average (Table 4). Some subtle differences were observed, but the average CA intensity did not change dramatically. For example, the EtOH 1 timepoint had a manual calculation of 122.2 and a pooled calculation of 152.1 (Table 4). This difference is most likely due to the June experiment because it only had 15 virions detected for this sample. On the other hand, the EtOH 3 sample was nearly identical with a manual calculation of 92.94 and the pooled average of 92.92 (Table 4). This data confirms that there is no bias present when comparing the combined data time points.

Effect of CypA on CA Maximum and Minimum Signal. It is important to note that the confocal microscope was functioning at the top of its detection capabilities. The maximum signal is 251 and many virions were detected at this maximum signal, clustered at the top of each scatterplot. Because so many virions appeared to be at this signal, the percentage of virions at maximum Cy5 signal was calculated (Fig. 20). For most samples, there was a higher percentage of virions at the maximum signal for CsA samples compared to EtOH samples. For the June experiment, 1-, 2-, and 3- hour CsA samples all had over 30% of virions at the maximum signal (Fig. 20A). The same time points for EtOH all had less than 30%. The February experiment had more variability between samples, but at hours 2 and 3 there was more virions at the maximum signal in CsA samples than EtOH samples (Fig. 20B). Last, the March assay reported more virions at the maximum detection in CsA samples for all time points except 0 hours (Fig. 20C).

This experiment had up to 72% of total virions for the CsA 3-hour time point at the maximum signal detection.

For comparison, the percentage of virions in each sample at the minimum signal of 0 was also calculated (Fig. 21). The general trend for all experiments was more virions at the minimum were detected in the EtOH samples versus the CsA samples. This result was found in the June experiments for all conditions but hour 4 (Fig. 21A). At the last hour the data switches with more CsA samples at the minimum than EtOH. For 0- and 1-hour samples, 67% of virions were at 0 signal detection (Fig. 21B). The February assay had no discernible trend between CsA and EtOH. Although, there were more virions at the minimum signal at the 0 hour time point compared to the remaining samples. The March assay overall had the lowest reported percentage of virions at the minimum Cy5 signal detection across all time points. The outlier in this experiment was hour 1 EtOH, which had 81% (Fig. 21C). The remaining time points all had percentages under 25% with most reporting more EtOH treated virions at 0 compared to CsA (Fig. 21C).

Viral Fusion Analysis. Something to consider is whether or not treatment with CsA or EtOH has an effect on viral fusion and therefore infection. To continue analysis of the *in situ* assays, the percentage of fusion was calculated for each sample (Fig. 22). If the fusion is significantly different between samples, then it is not feasible to compare uncoating between samples. The percentage of viral fusion was calculated by dividing the number of virions that report 0 dTomato fluorescence by the total virions counted per sample. Though fusion is expected to vary between samples, it is not expected to increase as time increases. The BafA control has fusion inhibited for VSVG-HIV, so any fusion in this sample is considered background detection.

For the June experiment, BafA exhibited 31% of background fusion, 33% for the February experiment and 15% for the March experiment (Fig. 19A, 19B, 19C). There was a high percentage of fusion present in the 0-hour time points for all three experiments (Fig. 22). When comparing the percentage of fusion reported for CsA and EtOH, there was not a large enough difference to indicate any change in fusion. Though, in each experiment, there was fusion calculated below the BafA control fusion percentage. In the June *in situ* assay, both CsA and EtOH had the highest fusion percentage at 0 hours post infection. For hours 1, 2, and 3, there was a higher percentage of fusion present in the EtOH samples when compared to the CsA coverslips for experiment 1 (Fig. 22). The 1-, 2-, and 3-, hour CsA samples reported 26%, 19%, and 15% fusion respectively. EtOH fixed at 1-, 2-, and 3-, hours had a higher percentage of fusion, showing 47%, 42%, and 41% accordingly (Fig. 22A). At the 4-hour time point, the percentage of fusion was greater in CsA compared to EtOH. The February experiment reported similar fusion when comparing CsA to EtOH conditions. The difference between each percentage was less that 10% for all timepoints (Fig. 22B). The March experiment did have a large difference between the 0-hour time points, with the EtOH percentage being nearly half the CsA percentage (Fig. 22C). The 1-hour samples were similar in fusion percentages. The 2 and 4 hour time points for the March assay both showed more fusion in the EtOH sample compared to CsA. When considering the fusion data, all percentages were similar enough in all experiments to trust that treatment with CsA did not affect viral function.

Effect of CypA on Human TRIM5α Restriction

In addition to facilitating uncoating, CypA may be involved in blocking TRIM5α restriction in human cell lines (43, 62). To explore this possibility in the CHME3 cell line,

TRIM5α was knocked down using a pool of four siRNAs. The negative controls were knockdown with the nontarget siRNA NT4 and reaction without siRNA. The cells were treated with pools of 4 siRNAs that targeted GAPDH as a control to analyze knockdown. The amount of TRIM5 knockdown was quantified using qRT-PCR. To determine the effect of CypA on TRIM5α restriction, an infectivity assay was performed on the cells in the presence and absence of CsA. It is predicted that CypA blocks TRIM5α restriction and when CypA is inhibited, infection will decrease. It is expected that the percent of GFP positive cells will increase when TRIM5α is knocked down. The results from these experiments will reveal if CypA protects HIV-1 from TRIM5α restriction.

Effect of CsA on HIV Infectivity. Previous data has shown that treating CHME3 cells with CsA decreases HIV-1 infectivity (80). Similar results were found in the siRNA knockdown experiment from May. It was found in the NT4 knockdown condition for both the raw data and normalized data. When comparing infectivity in these cells, treatment with CsA overall decreased infectivity when compared to cells treated with EtOH (Fig. 23A). Yet, a similar increase was found at the dilution with the highest amount of virus in both the raw data and the normalized data (Fig. 23A and B). The TRIM5α knockdown condition showed a decrease of about 20% infectivity with treatment of CsA when compared to EtOH at the 1/64 (0.015625) dilution (Fig. 23C). To compare this data further, it was normalized to the EtOH sample to calculate a fold change. The $1/64^{th}$ (0.015625) dilution in the May experiment showed a decrease of almost 0.6 fold when TRIM5α knockdown cells were treated with CsA compared to EtOH (Fig. 23D). There was a slight increase in the fold change at the dilution with the highest amount of virus (0.0625 dilution), where the CsA sample reached just above the EtOH (Fig. 23D). NT4 siRNA treated cells were chosen over cells that had no siRNA treatment because the

experimental conditions were more similar to the TRIM5α knockdown cells. Therefore, CsA treatment did cause an expected decrease of HIV-1 infectivity in CHME3 microglial cells in both knockdown conditions.

Effect of TRIM5α Knockdown on HIV Infectivity. To determine the effect of TRIM5α in the presence and absence of CsA, infectivity was compared between TRIM5α knockdown and NT4 knockdown cells. Looking at the raw data from the May experiment, the trend shows a higher percentage of cells were infected when TRIM5α was knocked down compared to when the restriction factor is present. This trend was present for both CsA and EtOH treated cells (Fig. 24A and C). The difference between TRIM5α and NT4 knockdown infectivity was greater in the CsA treatment compared to the EtOH treatment. For example, the 1/32 (0.03125) dilution in the CsA treatment had 51% infectivity in the TRIM5α knockdown cells while the NT4 knockdown showed 35% infectivity (Fig. 24A). For comparison, the 1/32 (0.03125) dilution in the EtOH sample had an infectivity of 60% for the TRIM5α siRNA sample compared to 49% in the NT4 pool knockdown (Fig. 24B).

To better compare the effect of TRIM5α knockdown on infection between the CsA and EtOH treatments, the percentage of infected cells was normalized to the equivalent NT4 control was set to 1 to calculate a fold change. For both CsA and EtOH treatments, there was a gradual increase in the difference between the control and experimental treatment as the viral dilution decreased from $1/16^{th}$ to $1/512^{th}$. For EtOH cells, the greatest difference is at $1/256^{th}$ (0.00390625), with infectivity in the TRIM5α knockdown 2-fold higher than that in the NT4 control (Fig. 24B). The difference was even greater between the normalized NT4 and TRIM5α reactions for the CsA sample (Fig. 24D). The largest difference was at $1/512^{th}$ (0.001953125)

dilution, the dilution with the least amount of virus, where the percent of infected cells in the TRIM5α knockdown nearly reaches 3-fold higher than the NT4 control (Fig. 24D).

Effect of CypA on TRIM5α Restriction. Interestingly, CsA was less effective at decreasing infectivity in cells that had a knockdown of TRIM5α. In the May experiment, when comparing the difference of infectivity between CsA and EtOH, CsA decreased infectivity less when TRIM5α was knocked down. The 1/32 (0.03125) dilution showed the percent of GFP positive cells for CsA treated NT4 cells to be 35%. The EtOH infectivity for NT4 knockdown cells was 49% (Fig. 25A). When TRIM5α was knocked down, the CsA treatment yielded an infectivity of 51%. EtOH treatment in TRIM5α knockdown cells had an infectivity of 60% (Fig. 25A). The difference between the two knockdown conditions shows that depleting the amount of TRIM5α present decreases the effectiveness of CsA. The same thing is seen in the normalized data in the dilution with the least amount of virus. To normalize the data, the equivalent EtOH reaction was set to 1 for TRIM5α and NT4 knockdowns to show the fold change in infectivity. The TRIM5α knockdown shows a fold change of just over 0.5, whereas the NT4 knockdown shows a change of 0.3, indicating less infectivity when the restriction factor is present (Fig. 25B).

Trends From Three Independent Experiments. For the second aim, three siRNA knockdown experiments were conducted: March, May, and June. Both May and June had the same viral serial dilution of $1/16^{th}$ to $1/512^{th}$. The remaining experiment, March, had a serial dilution of 1/2 to $1/64^{th}$. For all experiment to be comparable, March data from $1/16^{th}$ to $1/64^{th}$ is represented in the graphs. This allows for trends to be more apparent and makes sure viral overinfection is not skewing the results.

The March siRNA experiment showed an unexpected increase of infected cells treated with CsA for both TRIM5α and NT4 knockdown conditions at the dilution with the highest

amount of virus, 0.0625 dilution (Fig. 26A and C). CsA treated cells in this TRIM5α knockdown condition exhibited a fold change increase of over 1.5 and in the NT4 knockdown condition, an increase of around 1.2 (Fig. 26A and C). The June experiment showed similar results, but to a less severe extent, with the TRIM5α knockdown CsA treatment showing a fold change of just above 1 and the NT4 knockdown CsA treatment having a fold change of around 1.1 (Fig. 26B and D). In the dilutions with a lower amount of virus, treatment with CsA caused a decrease in HIV-1 infectivity in both March and June experiments, similar to the May experiment. At the dilution with the least amount of virus, the CsA condition showed a fold change of near 0.8 for both TRIM5α and NT4 knockdown conditions in the March experiment (Fig. 26A and C). The June experiment showed a fold change of around 0.5 for both knockdown conditions at the dilution with the lowest amount of virus as well. Therefore, CsA treatment decreased infectivity in CHME3 microglial cells treated with lower amounts of virus in both experiments.

The effect of the TRIM5α knockdown was analyzed in the March and June experiments. Both data sets were normalized to NT4 by setting the control to 1 to show a fold change. For the March knockdowns, EtOH treated TRIM5α knockdown cells showed a nearly 1.3 fold change increase compared to NT4 at the dilution with the least amount of virus (Fig. 27A). The TRIM5α knockdown showed a larger 1.45 fold increase compared to the NT4 control when treated with CsA (Fig. 27C). For the June experiment, the greatest difference of infectivity between the knockdown conditions was also at the dilution with the least amount of virus, 1/512 (0.001953125). The EtOH treated knockdown cells showed a fold change of 2.3 in TRIM5α siRNA treated cells compared to the control NT4 knockdown (Fig. 27C). The CsA condition produced a fold change increase of 3 in TRIM5α knockdown cells (Fig. 27D). This trend of more significant increases in infectivity of HIV-1 in microglial cells when TRIM5α is depleted was

found for all other dilutions was found for all other dilutions for both March and June. Similar to the May results, CsA treatment was less effective when TRIM5α expression was decreased within the cell. At the dilution with the least amount of virus, for the March experiment, treatment with CsA in the NT4 knockdown condition reported a fold change decrease of 0.8 compared to the same treatment in the TRIM5α knockdown that produced a fold change of 0.7 (Fig. 28A). In the June experiment, the 1/64 (0.015625) dilution showed a fold change decrease of 0.6 in the CsA treated NT4 condition (Fig. 28B). At the same dilution, the CsA treated TRIM5α knockdown produced a fold change of 0.9 (Fig. 28B). To see if this is an ongoing trend, the fold change for each dilution was averaged for all experiments. The greatest fold change difference was present in the dilution with the highest amount of virus, where the average for CsA treated NT4 knockdown cells was around 1.1 and the average for CsA treated TRIM5α knockdown cells was around 1.3 (Fig. 29). For the other dilutions, there was a slight increase in the fold change between CsA treated NT4 and TRIM5α knockdown conditions. This data indicates that CsA does not function as efficiently when the restriction factor expression is decreased.

Knockdown Quantification. The primer efficiency was not able to be calculated for the TRIM5α, so the amount of TRIM5α knockdown remains to be defined (see Appendix B). Fortunately, the GAPDH knockdown control was able to be quantified for the June experiment. For this quantification, ten RNA samples isolated from various knockdown conditions and controls were run in triplicate: TRIM5α knockdown with and without reverse transcriptase, GAPDH knockdown with and without reverse transcriptase, NT4 knockdown with and without reverse transcriptase, no siRNA control with and without reverse transcriptase, and water with and without reverse transcriptase. The Ct values from qRT-PCR were averaged for the triplicate

runs (Table 5). The -RT reactions and water samples had average Ct values ranging from 29-33, indicating no contamination (Table 5). For the no siRNA, NT4, and TRIM5α samples with reverse transcriptase, average Ct values ranged from 13-15 (Table 5). The GAPDH knockdown average Ct value was 18.88, a 10-fold difference compared to the other samples (Table 5). The average for the GAPDH knockdown was calculated using values from Ct1 and Ct2 because the number from Ct3 was a much later cycle than expected. Since the value for Ct3 for the GAPDH knockdown was 28.62, it is most likely that there was no RNA added to the sample. The Ct3 result for the +RT GAPDH knockdown was more similar to the -RT reactions for the GAPDH sample, with numbers ranging from 28.71 to 29.07. Though the TRIM5α knockdown was not able to be analyzed, the GAPDH qPCR results indicate a knockdown of expression.

TABLE 4 Average Cy5 Signal

Sample	June	Feb	March	Pooled	Average of June, February, March
CsA 0	45.05	91.28	91.75	80.62	76.02
EtOH 0	39.79	73.50	33.12	59.61	48.8
CsA 1	138.3	131.9	191.4	150.5	153.8
EtOH 1	49.87	147.4	169.2	152.1	122.2
CsA 2	134.9	179.7	219.7	174.5	178.1
EtOH 2	106.6	164.7	190.3	164.7	153.86
CsA 3	162.3	120.9	192.0	157.7	158.4
EtOH 3	91.72	94.17	-	92.92	92.94
CsA 4	89.52	151.7	210.5	137.3	150.57
EtOH 4	149.9	181.6	175.9	166.7	169.13
BafA	171.5	130. 9	176.9	160.0	159.76

TABLE 5 GAPDH Knockdown qRT-PCR Results.

Sample	Ct 1	Ct 2	Ct 3	Average
TRIM5α +RT	15.55	15.40	16.16	15.70
TRIM5α -RT	29.55	29.68	29.97	29.73
GAPDH +RT	18.99	18.76	28.62*	18.88
GAPDH -RT	29.02	28.71	28.89	28.87
NT4 +RT	13.24	14.69	15.08	14.34
NT4 -RT	30.07	30.37	30.22	30.22
No siRNA +RT	12.93	13.26	13.66	13.28
No siRNA -RT	29.35	29.20	29.33	29.29
Water +RT	29.64	30.16	29.69	29.83
Water -RT	31.85	32.98	34.81	33.21

*Not included in the average

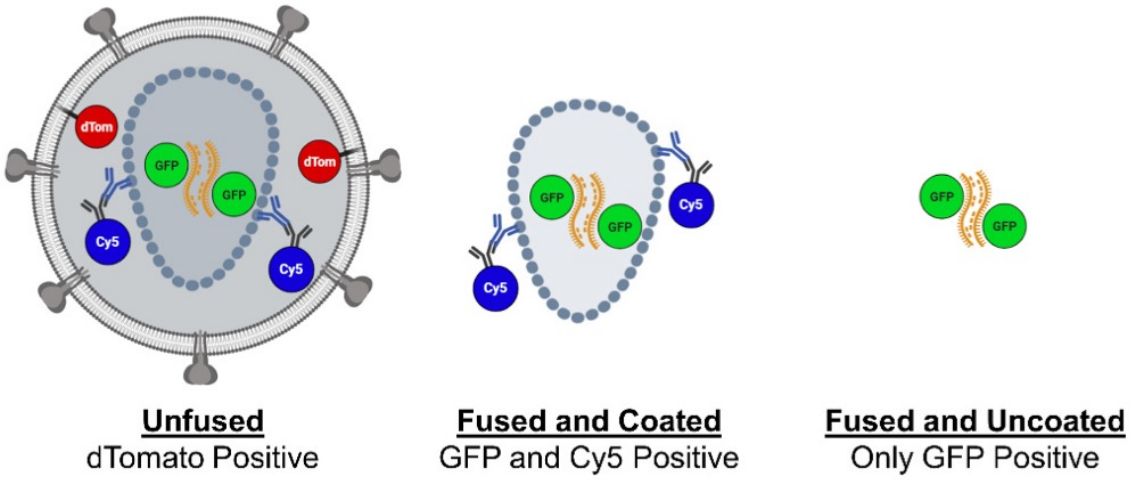

FIG 15 Dual Labeled Virus Schematic. The membrane of each virion is labeled with dTomato, and the viral core has been labeled with GFP. Unfused virus displays dTomato labeling. Fused and coated virus are GFP and Cy5 positive. Cy5 fluorescence is provided by primary and secondary antibody staining. Fused and uncoated virus are only GFP positive (82).

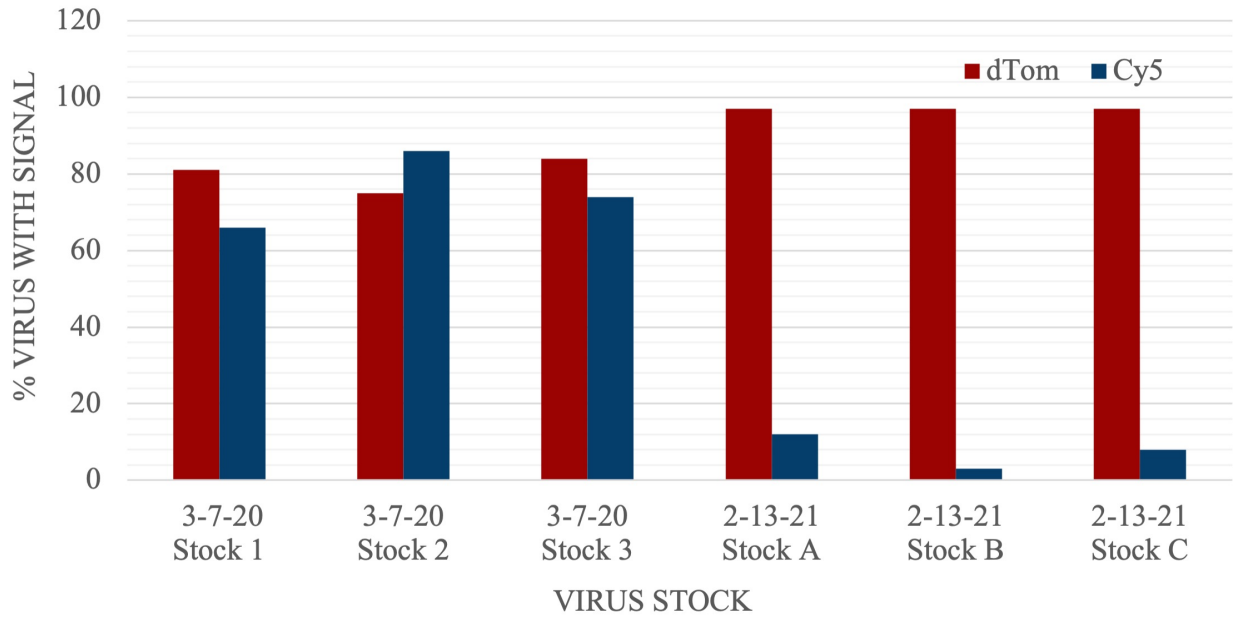

FIG 16 Graph of Virus Validation. Membrane fluorescence and capsid staining was analyzed for each stock of dual labeled virus.

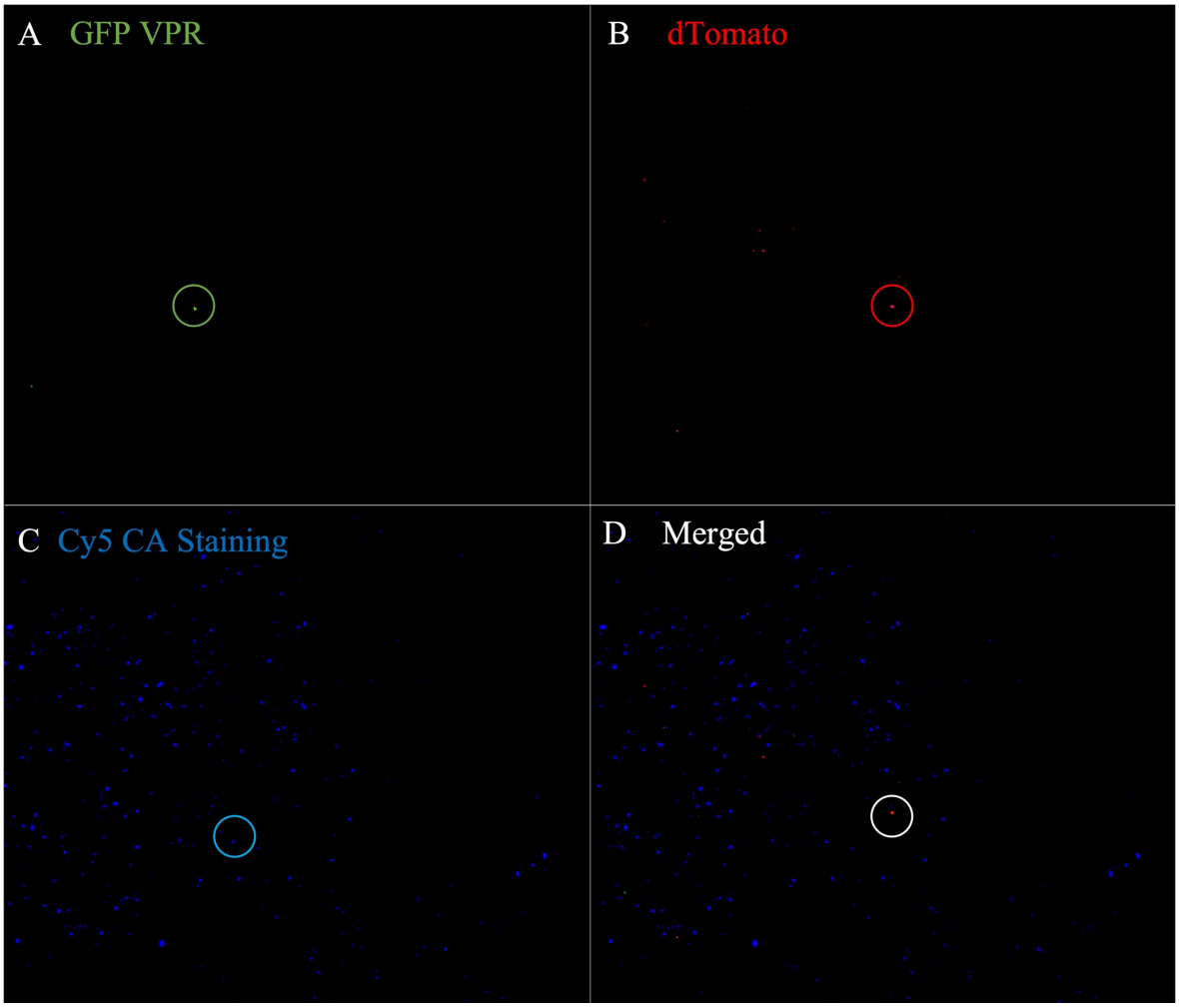

FIG 17 Representative *In Situ* Assay Image. The image shows the confocal microscopy of CHME3 cells infected with dual labeled virus and stained for CA. (A) GFP-Vpr labeling shows the location of fused and uncoated virions. Virions appear in the image as green pixels. (B) dTomato labeled virions show unfused virus. This is a control to ensure that only CA from fused virus is included in the uncoating analysis. (C) Cy5 antibody staining portrays where CA for each virion is located. (D) Overlay of all labeling and staining.

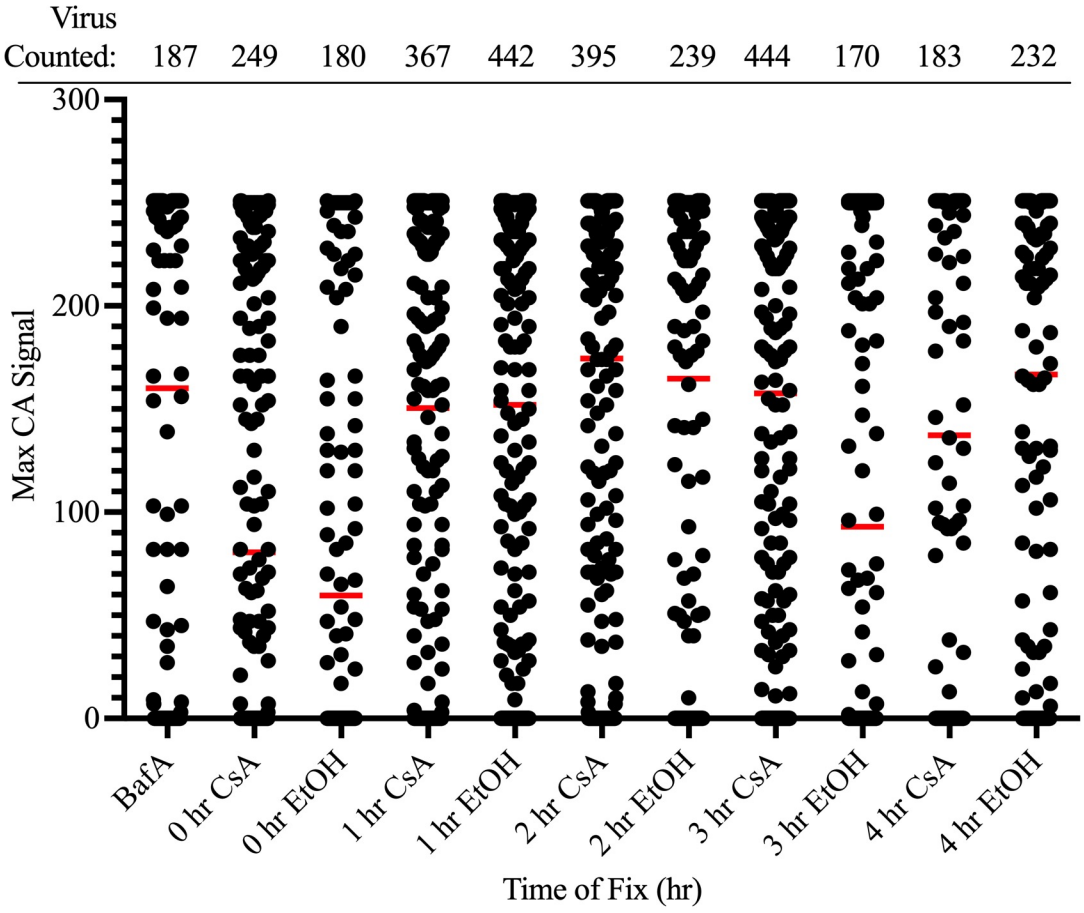

FIG 18 Scatterplot of Pooled *In Situ* Assay Data From Three Independent Experiments. Each dot represents one virion in each condition. The CA signal detection is represented on the Y axis and is Cy5 signal. The maximum signal is 251. The red bar is the average signal for each condition.

A

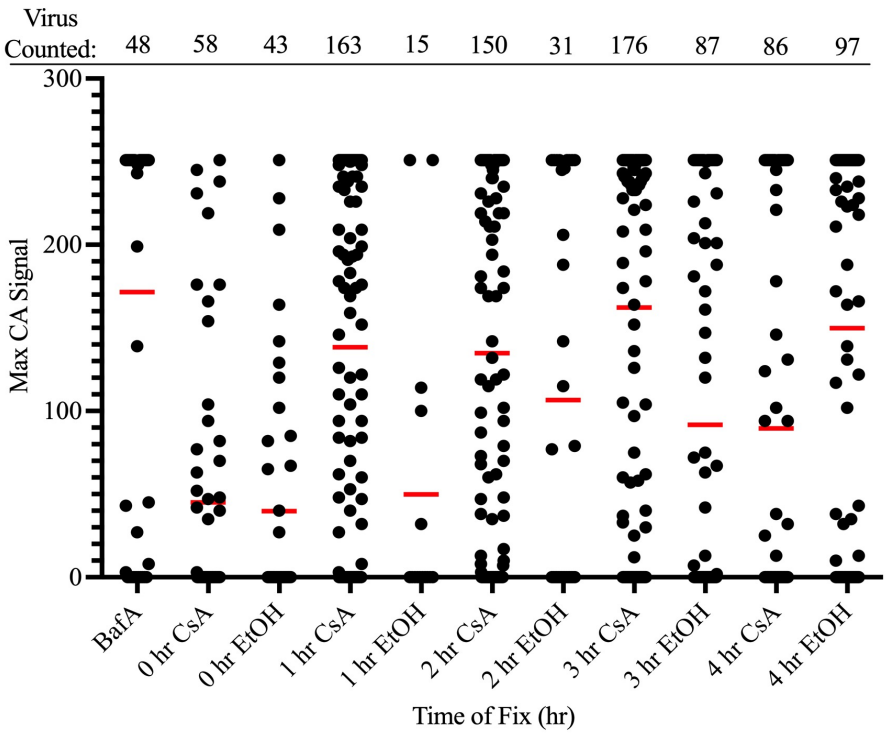

B

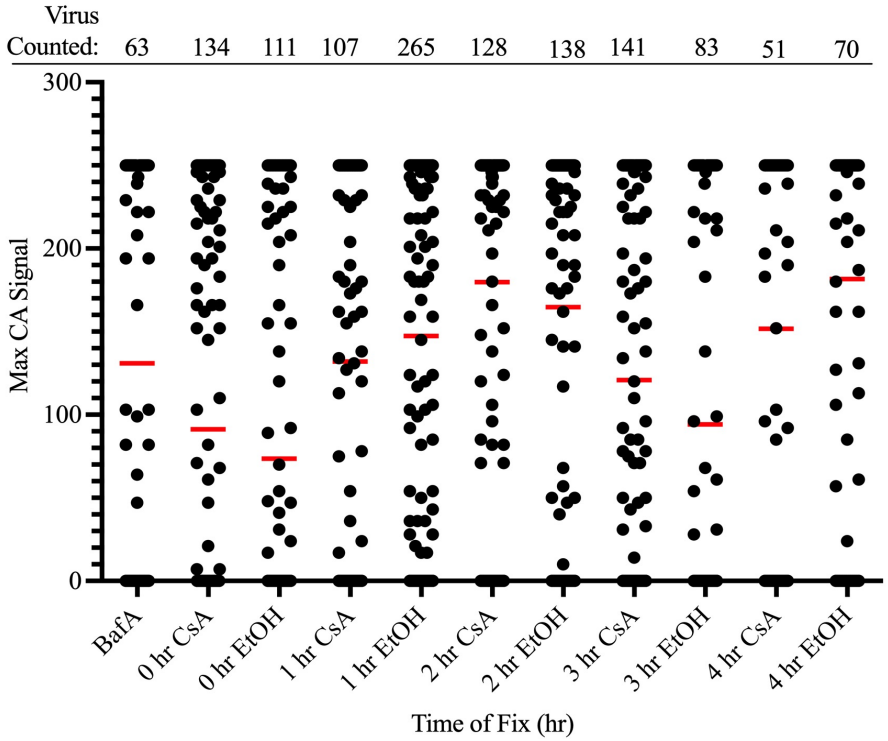

FIG 19 *In Situ* Uncoating Assay Maximum Cy5 Fluorescence. Continued with legend on the next page.

C

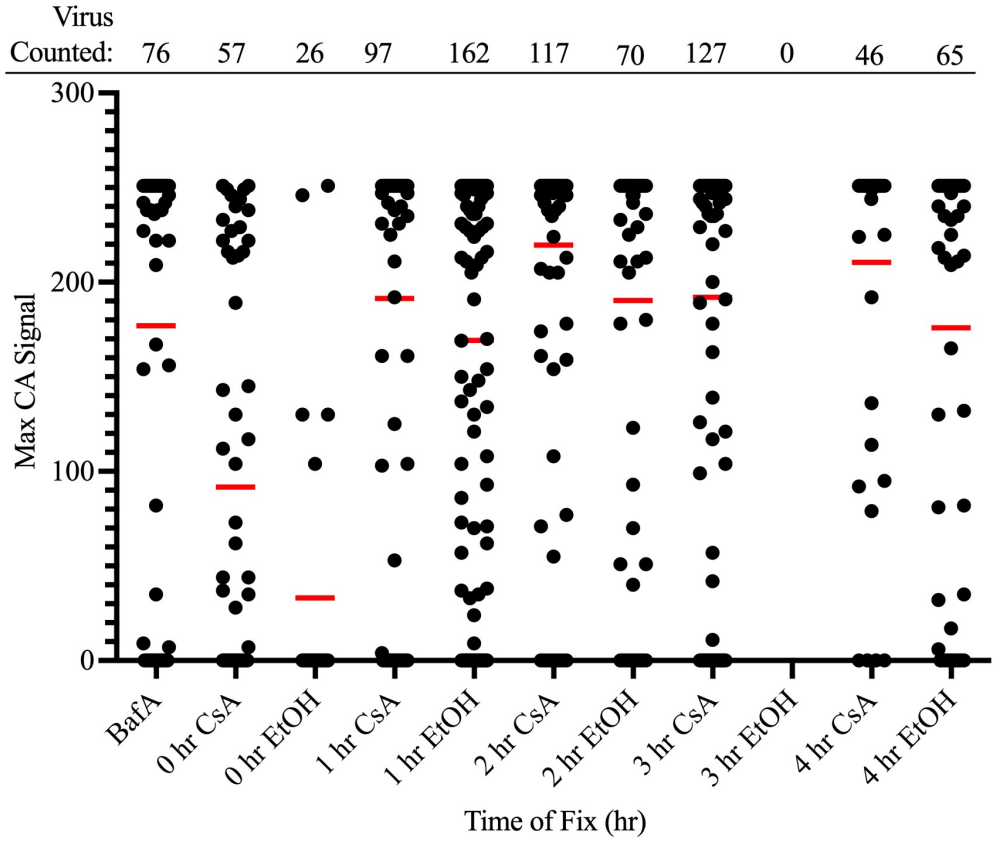

FIG 19 Continued *In Situ* Uncoating Assay Maximum Cy5 Fluorescence. Each scatterplot represents one assay. Cy5 signal intensity is represented as a scatterplot to show presence of capsid in each sample. The maximum threshold for the scatterplot is 251 CA signal. The red bar is the average signal for each sample. (A) June experiment. (B) February experiment. (C) March experiment.

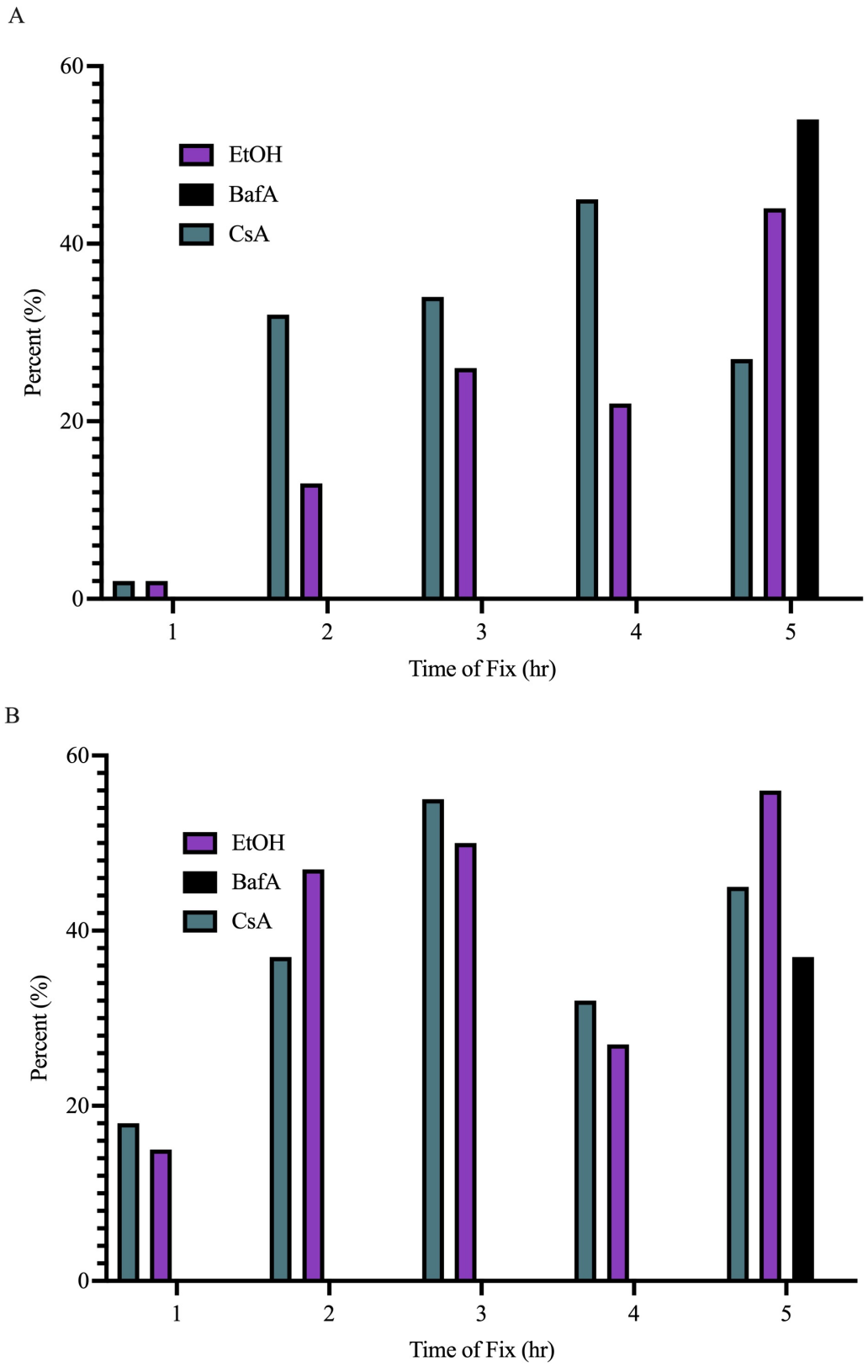

FIG 20 Percent Maximum Cy5 Signal. Continued with legend on the next page.

C

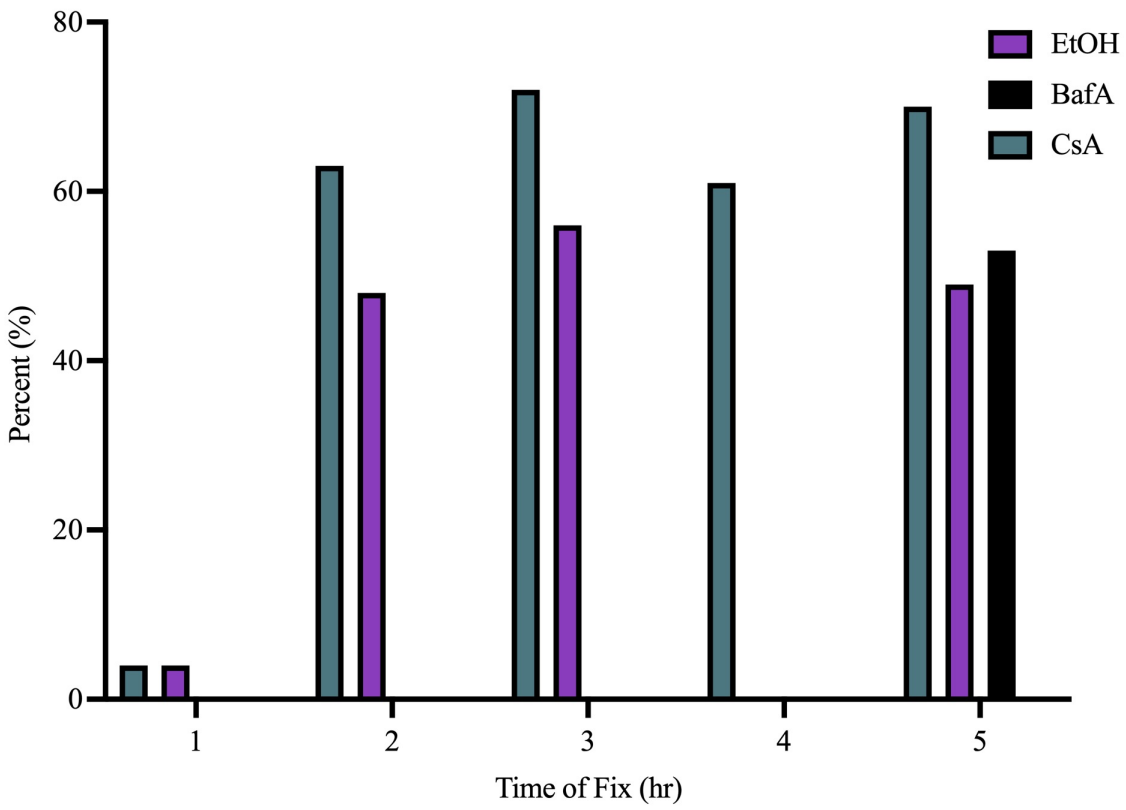

FIG 20 Continued Percent Maximum Cy5 Signal. Each graph represents one experiment and shows the percentage of virions reporting Cy5 signal at the maximum detection of 251. (A) June experiment. (B) February experiment. (C) March experiment.

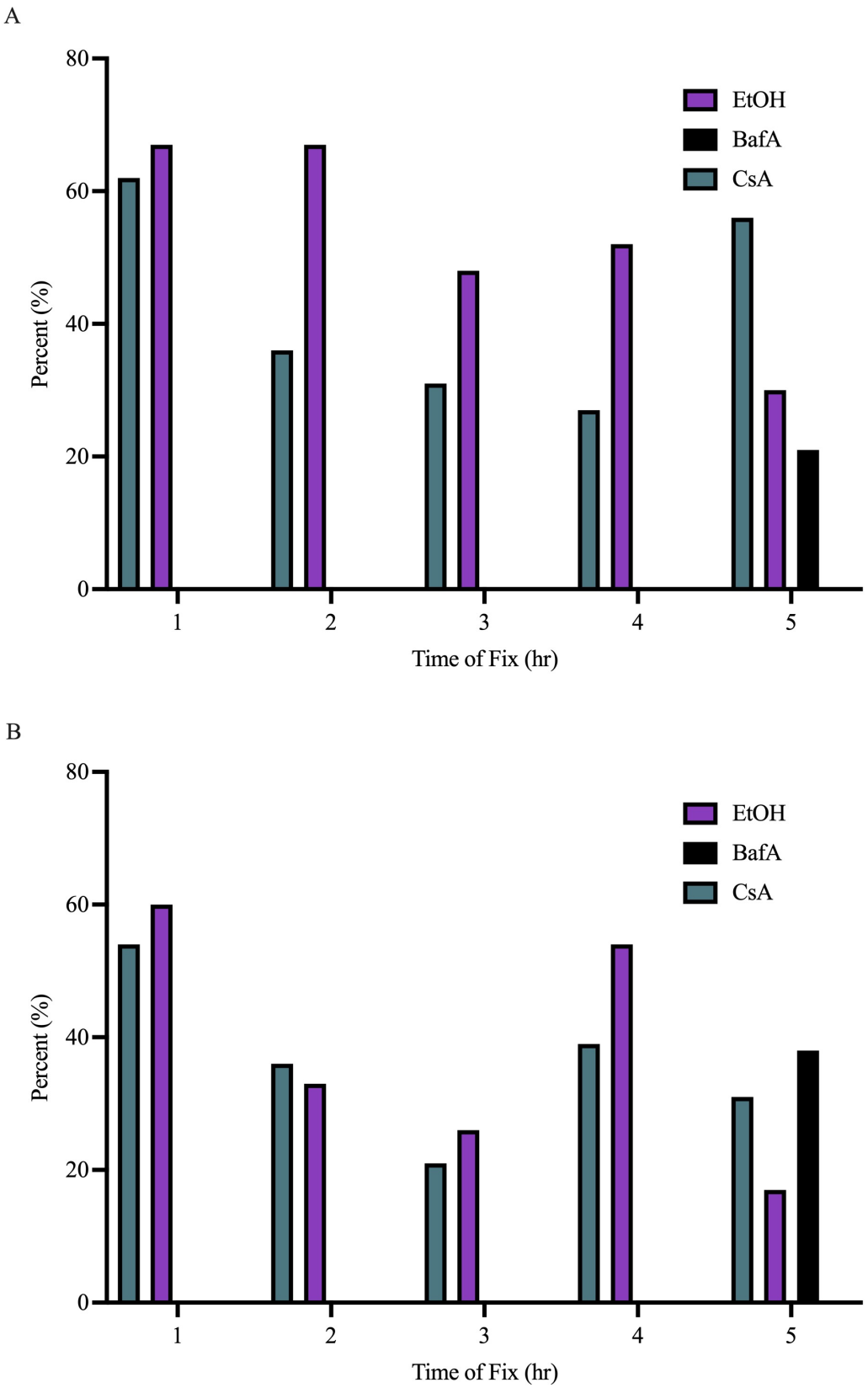

FIG 21 Percent Minimum Cy5 Signal. Continued with legend on the next page.

C

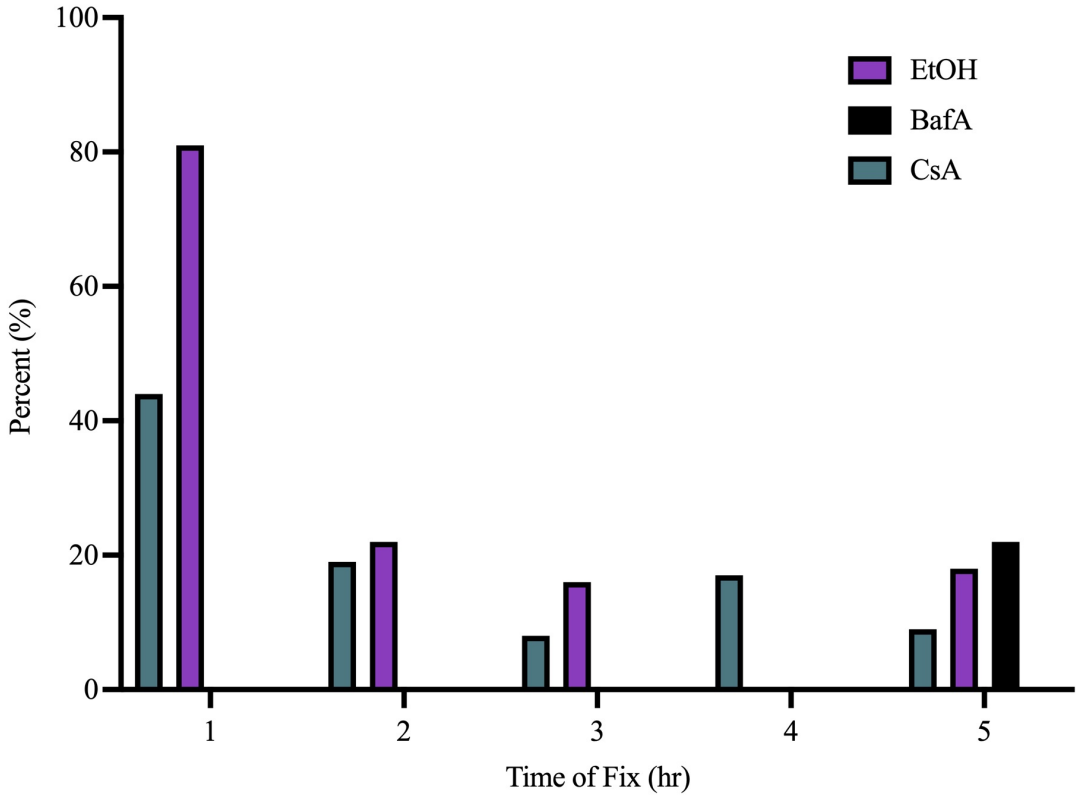

FIG 21 Continued Percent Minimum Cy5 Signal. Each graph represents one experiment and shows the percentage of virions reporting Cy5 signal at the minimum detection of 0. (A) June experiment. (B) February experiment. (C) March experiment.

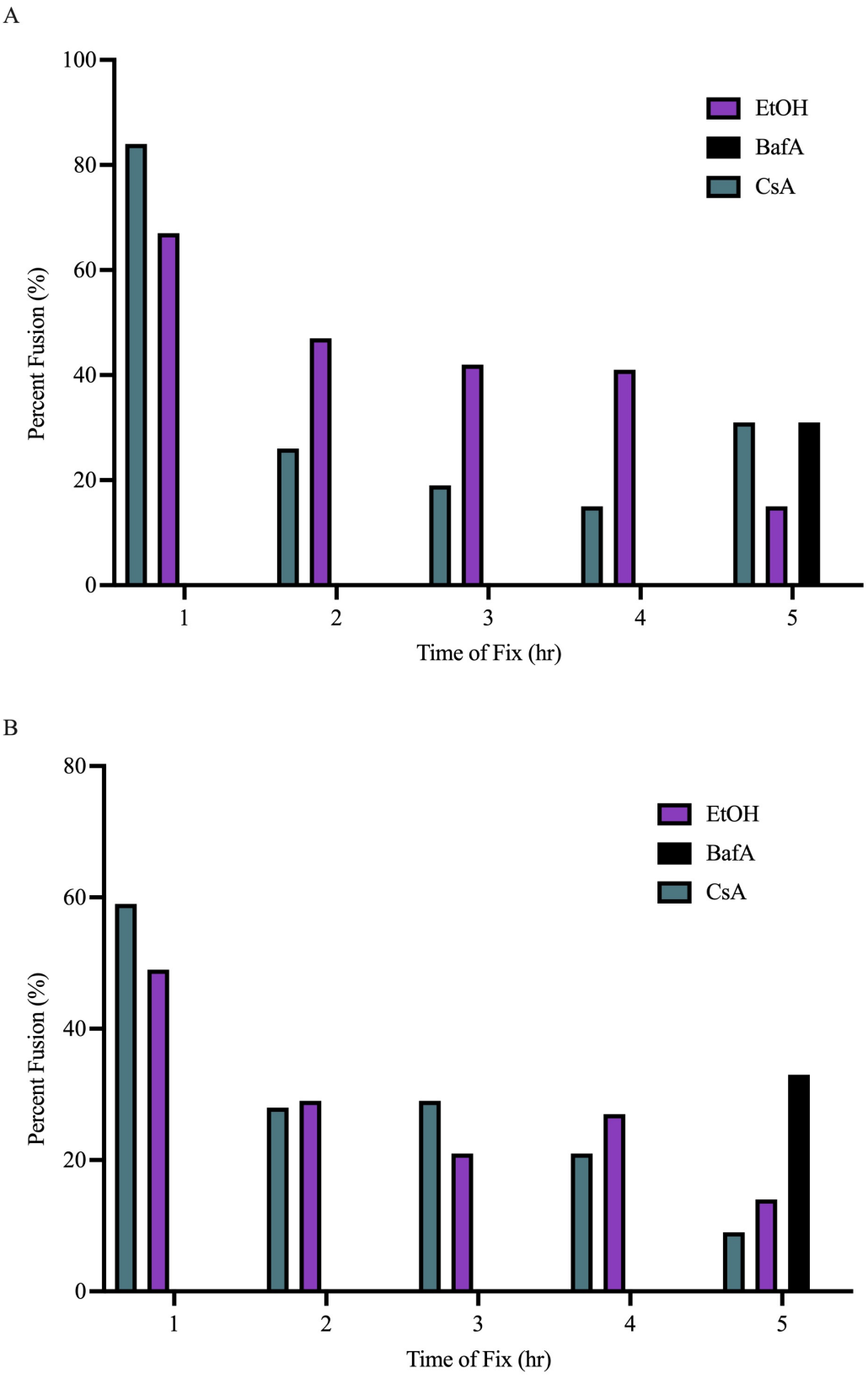

FIG 22 *In Situ* Assay Percent Viral Fusion. Continued with legend on the next page.

C

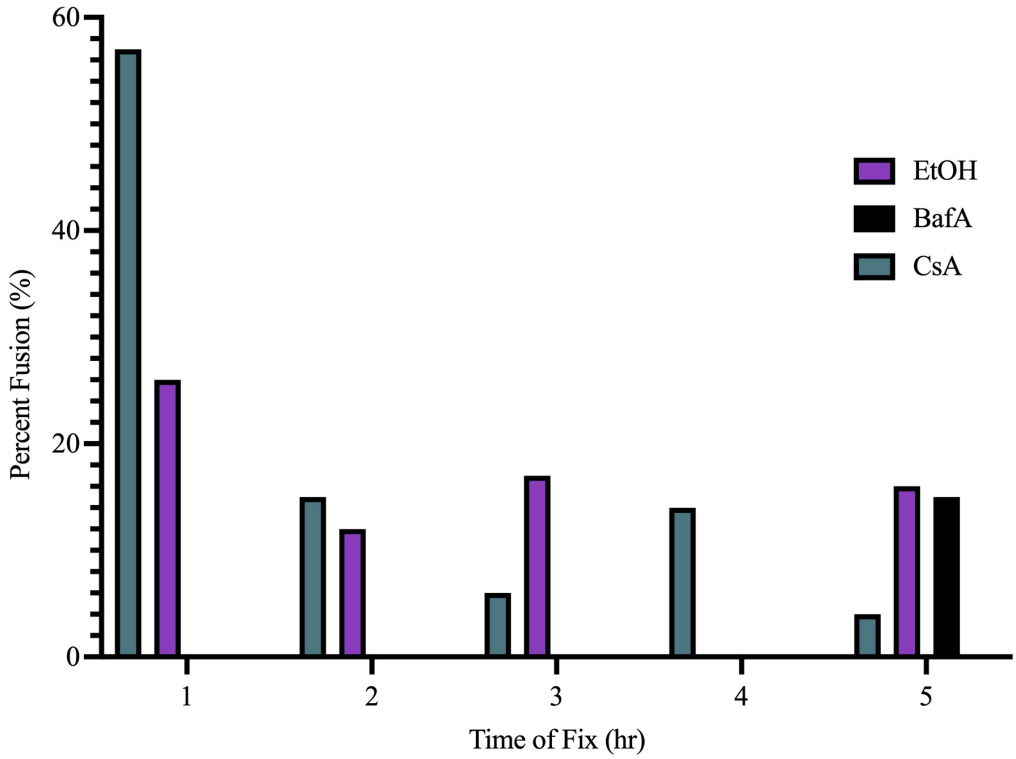

FIG 22 Continued *In Situ* Assay Percent Viral Fusion. Graph of percentage of virions fused at each time point for all conditions. BafA is the fusion inhibitor control. (A) June experiment. (B) February experiment. (C) March experiment.

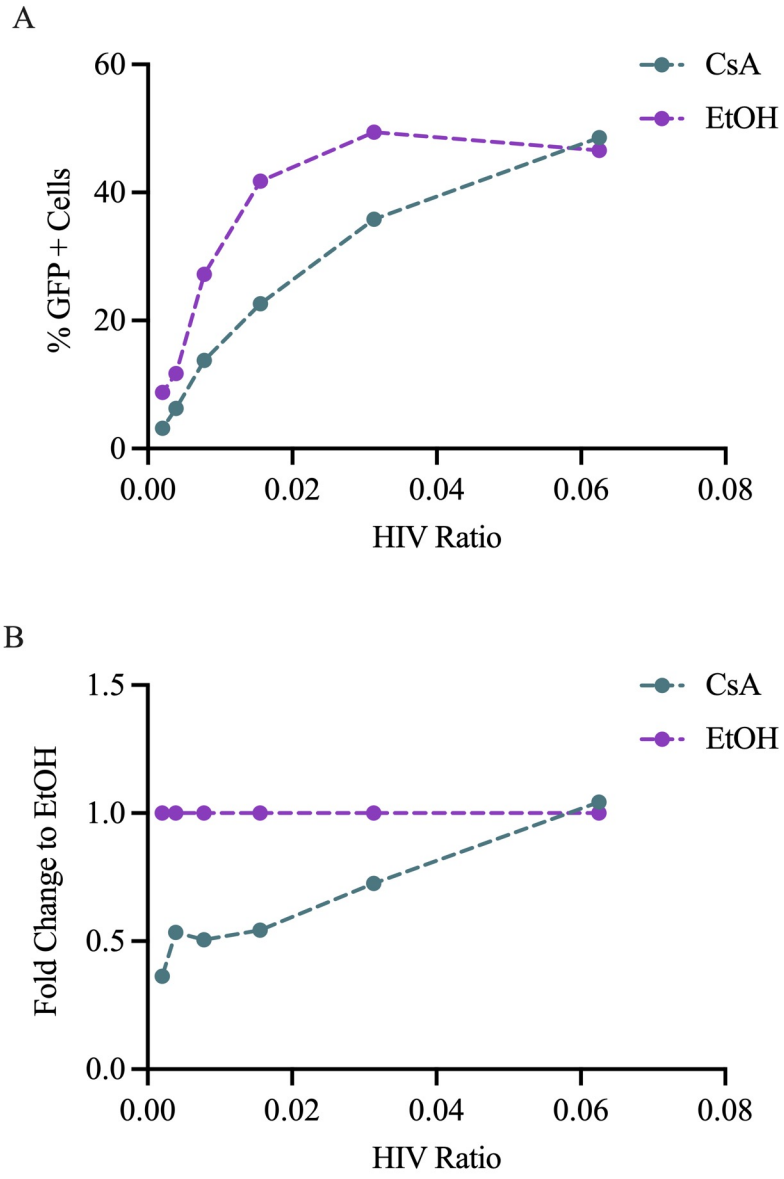

FIG 23 Effect of CsA Treatment in TRIM5α and NT4 Knockdown May Experiment
Continued with legend on the next page.

C

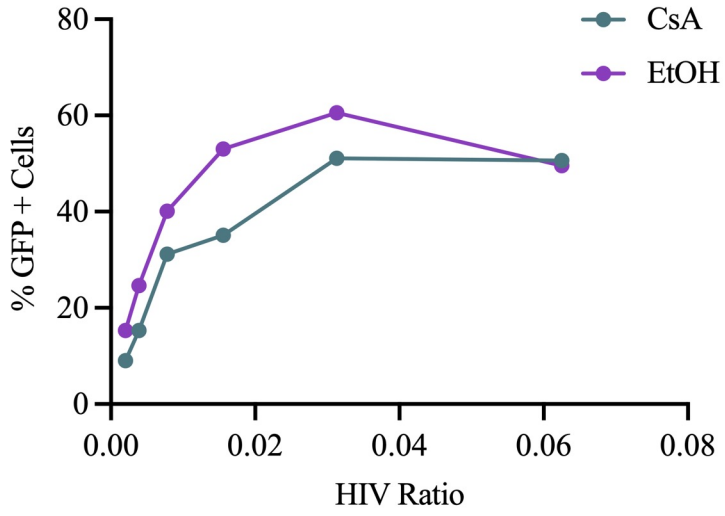

D

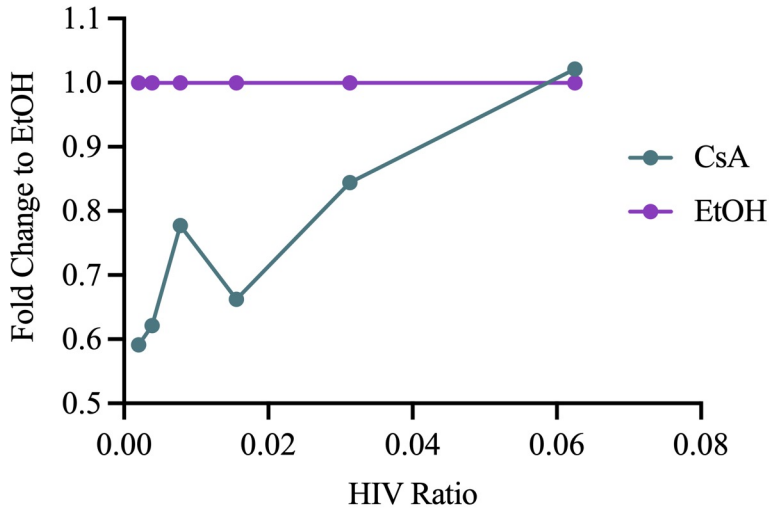

FIG 23 Continued Effect of CsA Treatment in TRIM5α and NT4 Knockdown May Experiment. (A) Raw data of NT4 knockdown cells treated with CsA or EtOH. Shows the percentage of infected cells. (B) Fold change of NT4 knockdown data normalized to EtOH. (C) Raw data of TRIM5α knockdown cells treated with CsA or EtOH. Shows the percentage of infected cells. (D) Fold change of TRIM5α knockdown data normalized to EtOH.

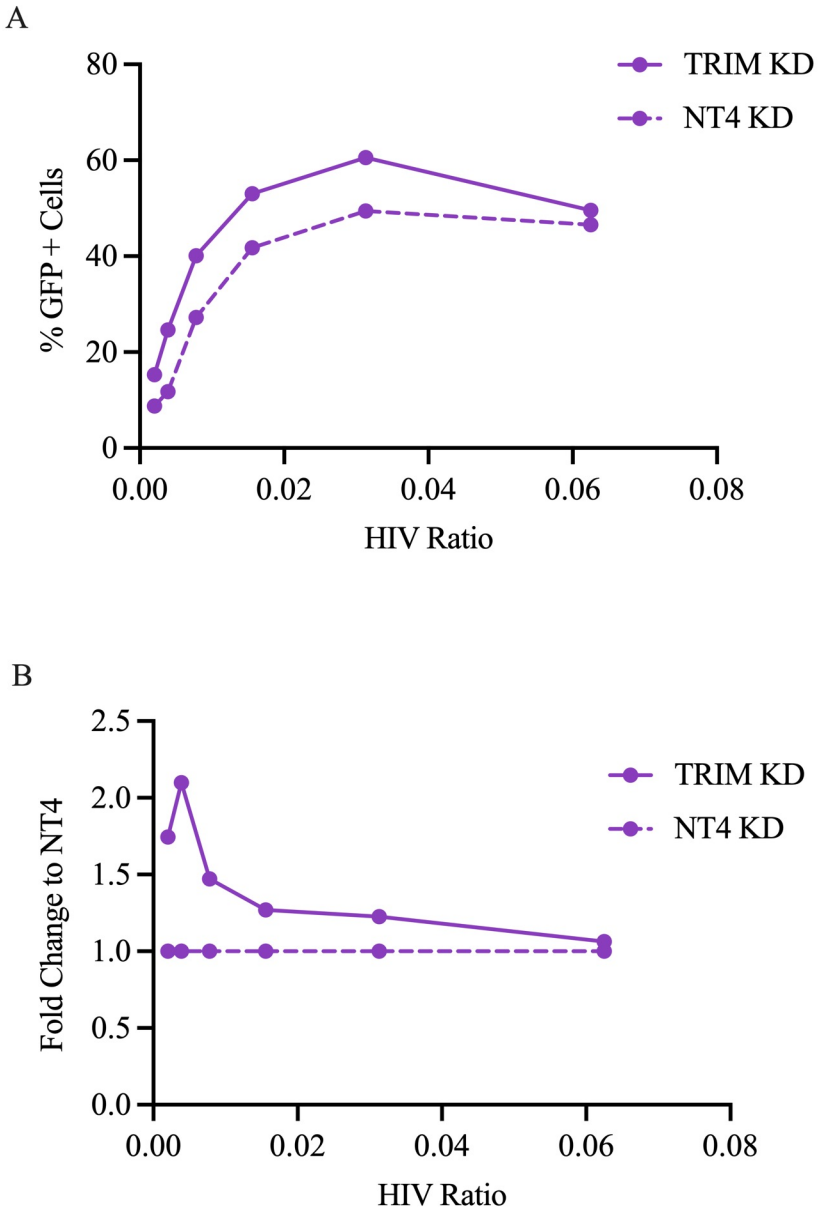

FIG 24 Effect of TRIM5α in EtOH and CsA Treated Cells May Experiment. Continued with legend on the next page.

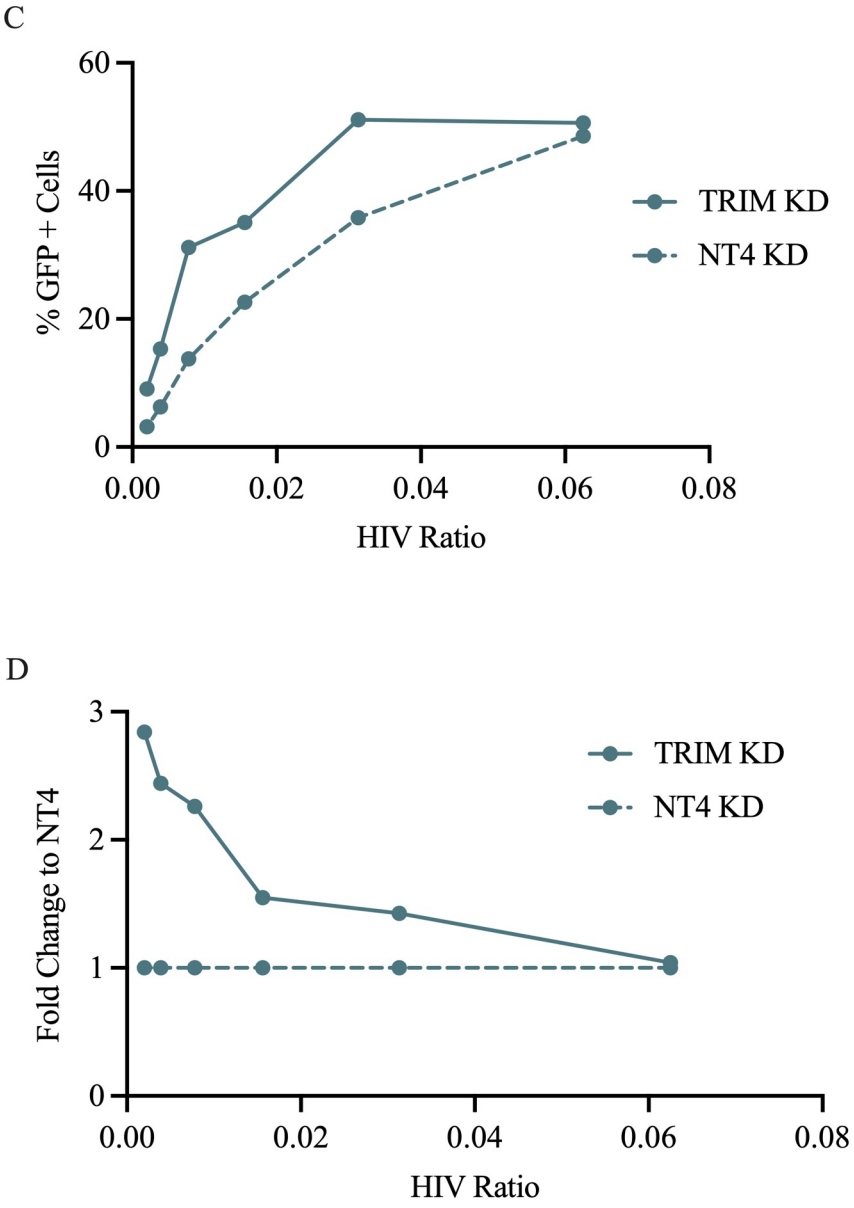

FIG 24 Continued Effect of TRIM5α in EtOH and CsA Treated Cells May Experiment. (A) Raw data of TRIM5α knockdown cells and NT4 knockdown cells treated with EtOH. Shows the percentage of infected cells. (B) Fold change of TRIM5α knockdown and NT4 knockdown cells treated with EtOH normalized to NT4. (C) Raw data of TRIM5α knockdown cells and NT4 knockdown cells treated with CsA. Shows the percentage of infected cells for each condition. (D) Fold change of TRIM5α knockdown cells and NT4 knockdown cells treated with CsA normalized to NT4.

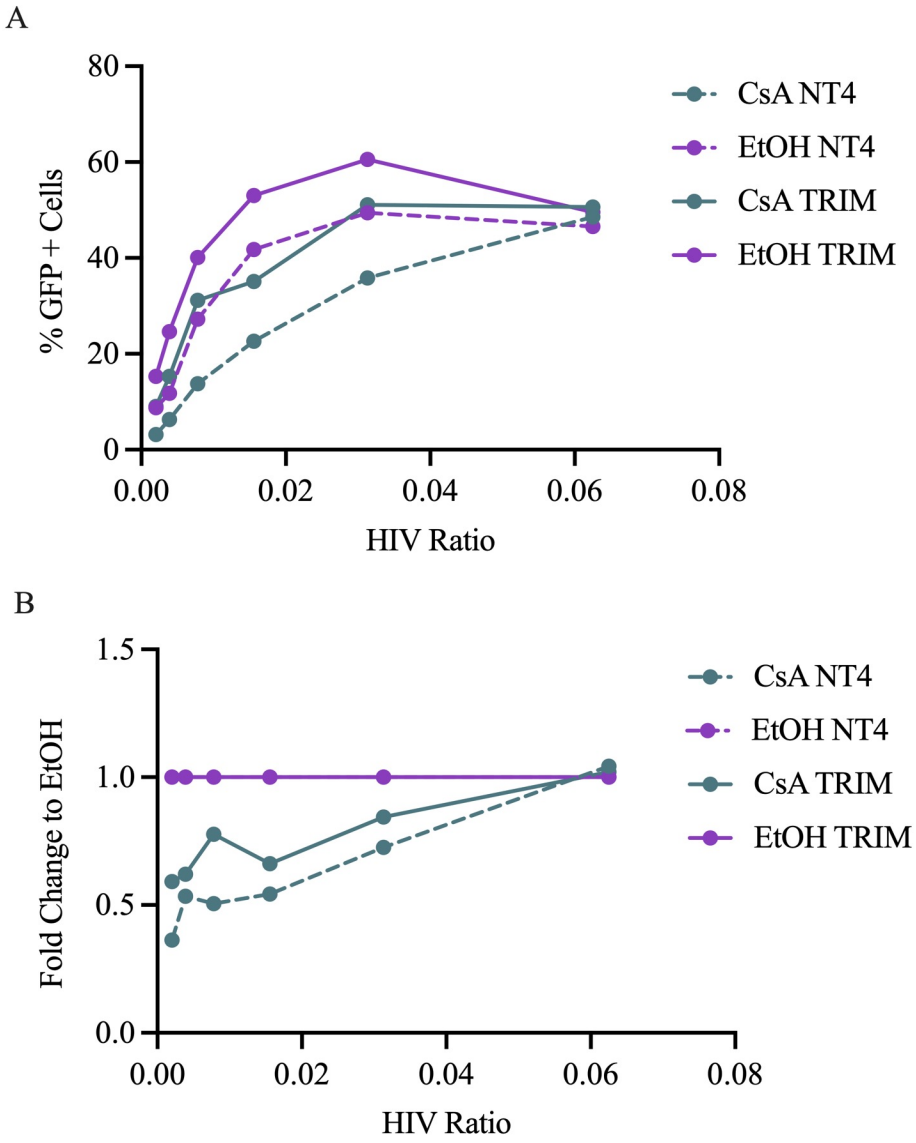

FIG 25 Effect of CypA in TRIM5α and NT4 KD Cells, May Experiment. (A) Raw data of TRIM5α and NT4 knockdown cells treated with CsA or EtOH. Percentage of infected cells is shown. (B) Data from figure (A) normalized to EtOH to show the fold change in infection.

A

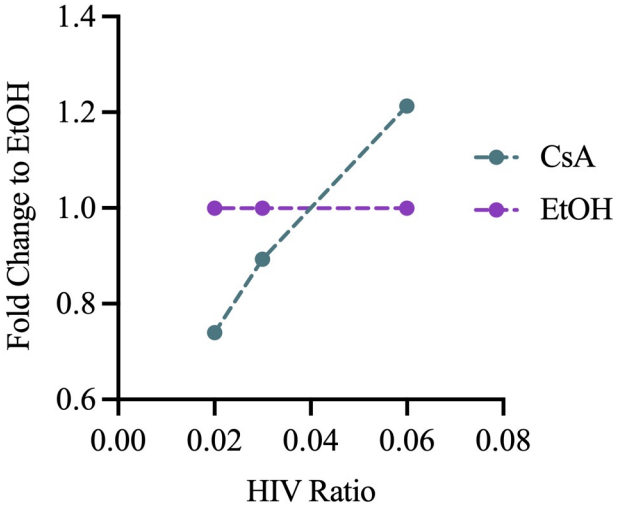

B

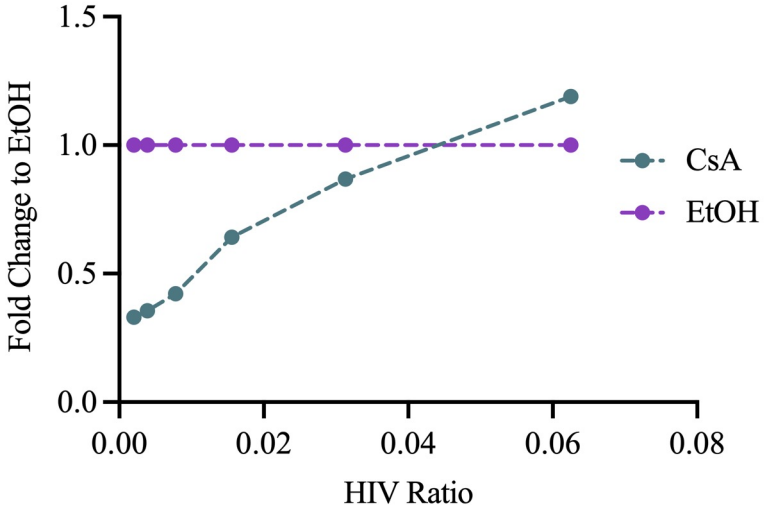

FIG 26 Effect of CsA Treatment on TRIM5α and NT4 Knockdown Cells in March and June Experiments. Continued with legend on the next page.

C

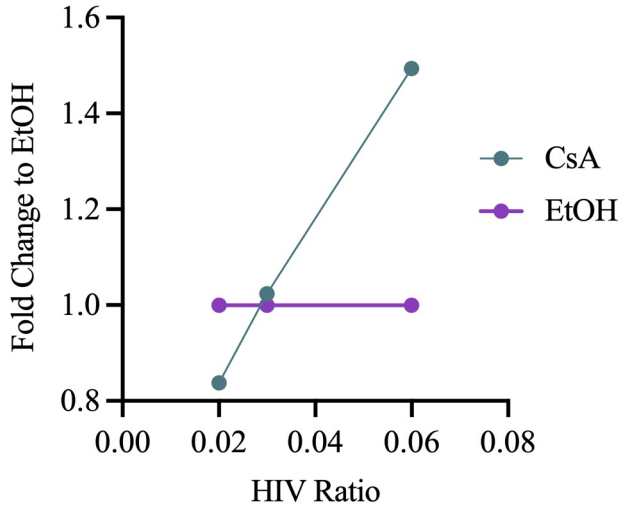

D

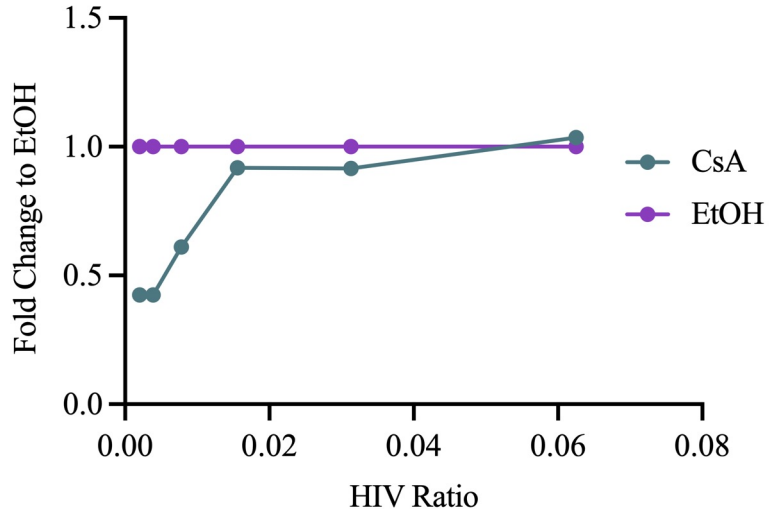

FIG 26 Continued Effect of CsA Treatment on TRIM5α and NT4 Knockdown Cells in March and June Experiments. (A) March experiment, fold change of NT4 knockdown data in CsA and EtOH treated cells normalized to EtOH. (B) June experiment, fold change of NT4 knockdown data in CsA and EtOH treated cells normalized to EtOH. (C) March experiment, fold change of TRIM5α knockdown data in CsA and EtOH treated cells normalized to EtOH. (D) June experiment, fold change of TRIM5α knockdown data in CsA and EtOH treated cells normalized to EtOH.

A

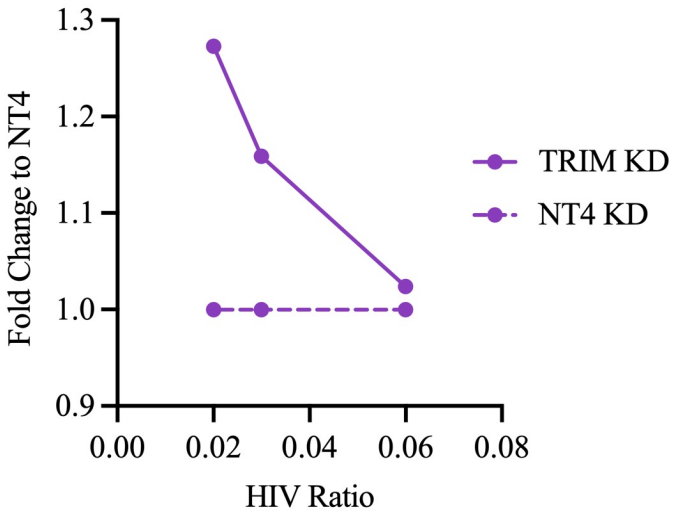

B

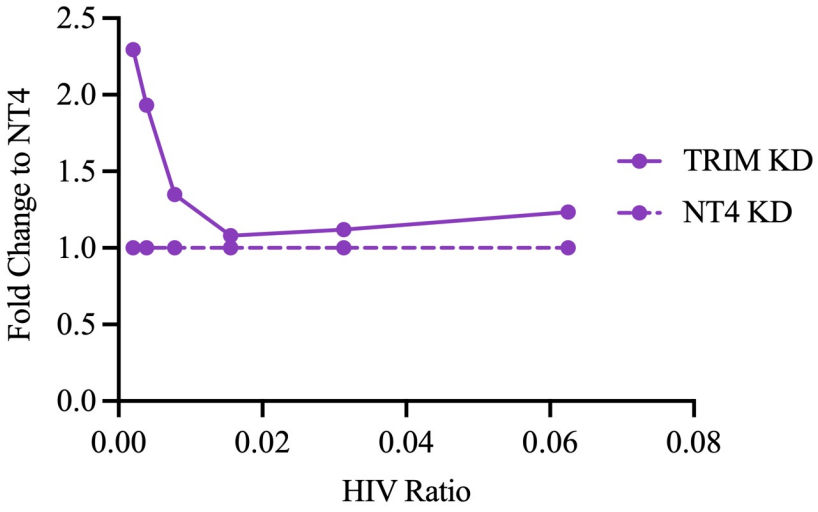

FIG 27 Effect of TRIM5α Knockdown in CsA or EtOH treated cells, March and June Experiments. Continued with legend on the next page.

C

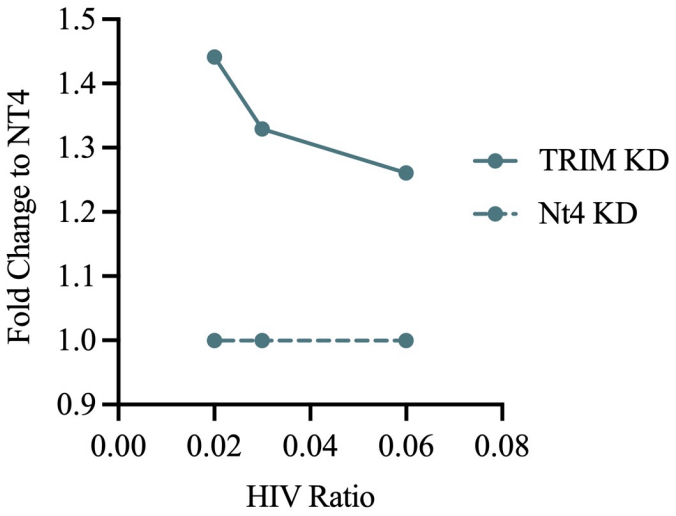

D

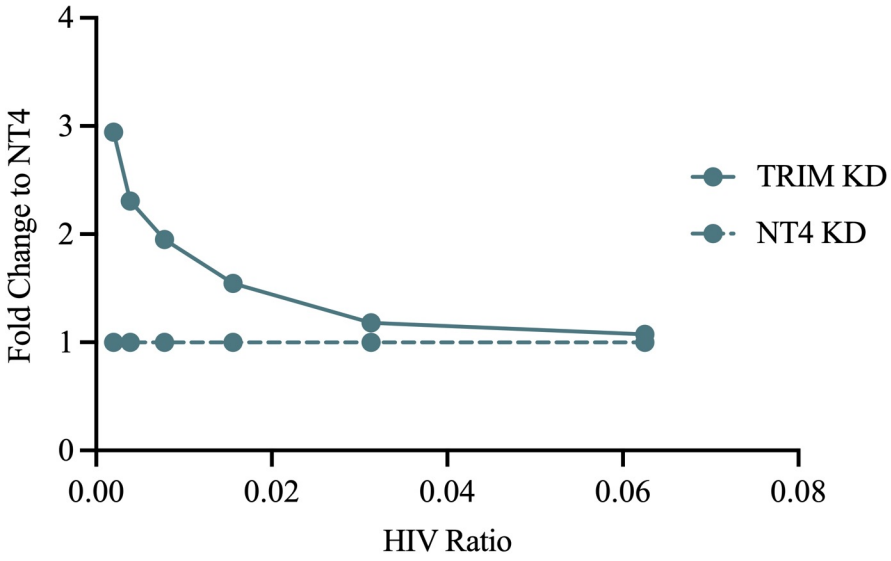

FIG 27 Continued Effect of TRIM5α Knockdown in CsA or EtOH treated cells, March and June Experiments. (A) March experiment, fold change of TRIM5α knockdown and NT4 knockdown cells treated with EtOH, normalized to NT4 to show the fold change in infection. (B) June experiment, fold change of TRIM5α knockdown and NT4 knockdown cells treated with EtOH, normalized to NT4 to show the fold change in infection. (C) March experiment, fold change of TRIM5α knockdown and NT4 knockdown cells treated with CsA, normalized to NT4 to show the fold change in infection. (D) June experiment, fold change of TRIM5α knockdown and NT4 knockdown cells treated with CsA, normalized to NT4 to show the fold change in infection.

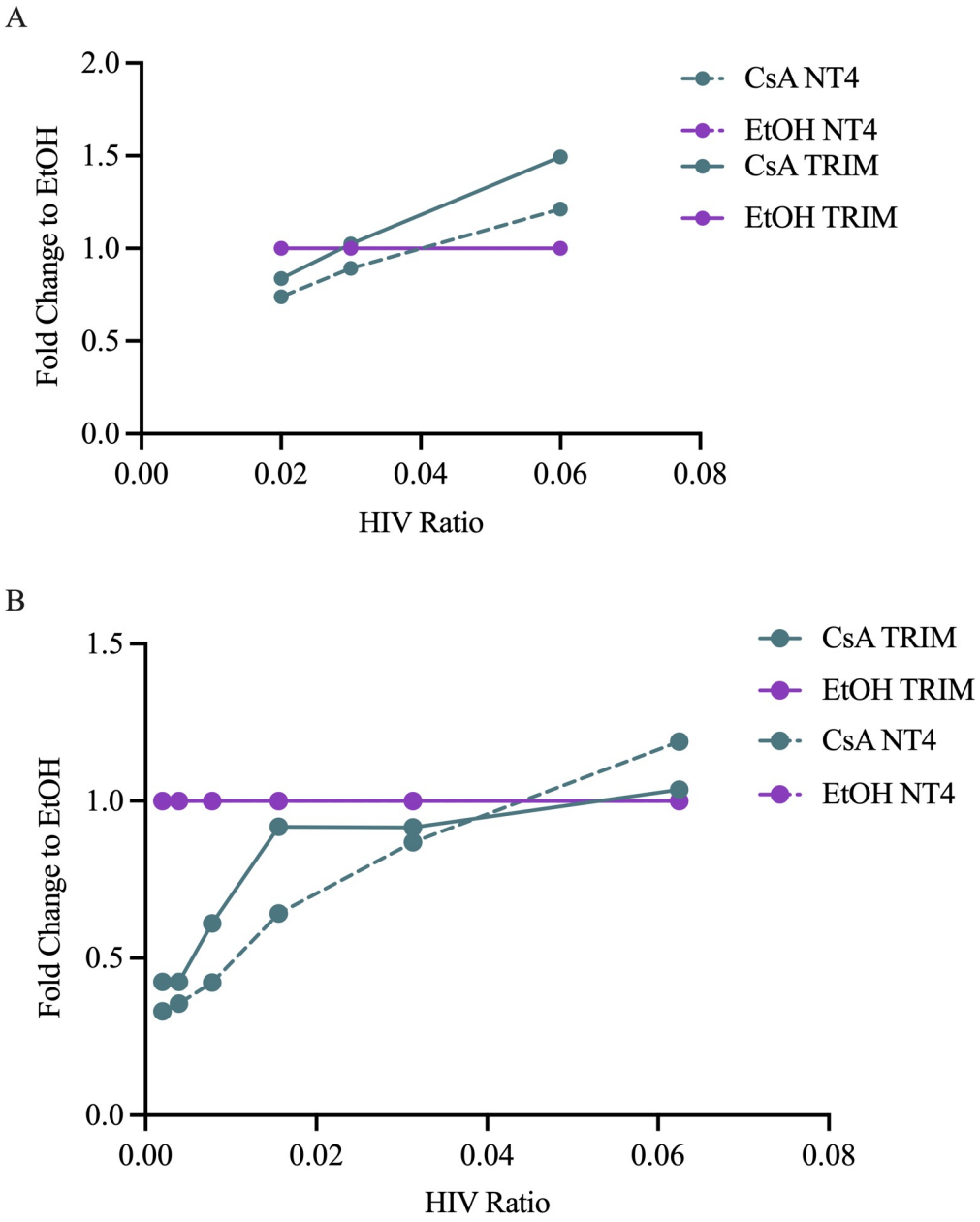

FIG 28 Effect of CsA in TRIM5α and NT4 Knockdown Cells, March and June Experiments. (A) March data normalized to EtOH to show the fold change in infection in NT4 and TRIM5α knockdown cells treated with CsA or EtOH. (B) June data normalized to EtOH to show the fold change in infection in NT4 and TRIM5α knockdown cells treated with CsA or EtOH.

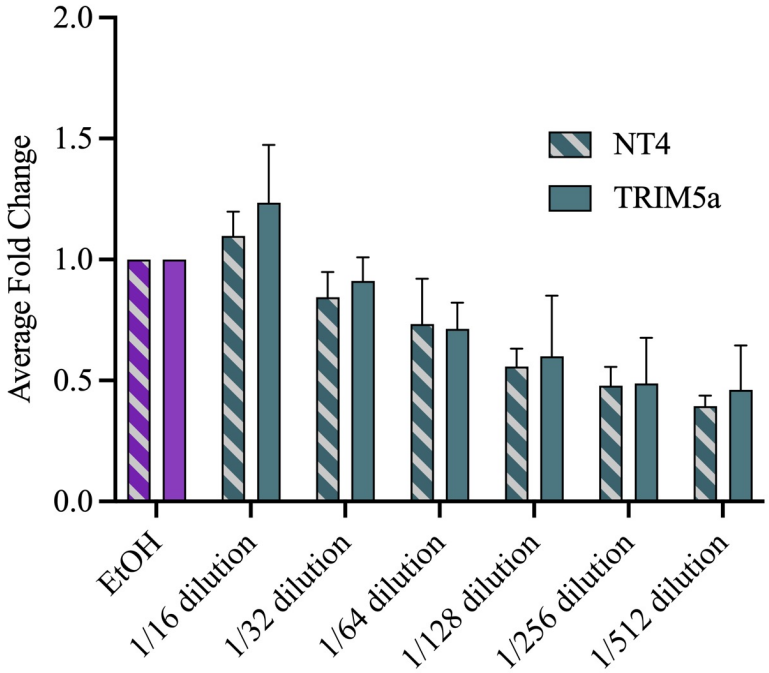

FIG 29 Average Fold Change of the Effect of CsA for Pooled Data. The bar graph shows the average fold change of infection for all experiments. The purple bars are cells treated with EtOH and the blue bars are cells treated with CsA. The dilutions 1/16 to 1/64 are averaged from 3 experiments. Dilutions 1/128 to 1/512 are averaged from 2 experiments. Error bars denote standard error among 3 experiments for dilutions 1/16 to 1/64 and 2 experiments for dilutions 1/128 to 1/512.

DISCUSSION

Blocking CypA-CA Interactions Inhibits HIV-1 Capsid Uncoating

HIV-1 uncoating is affected based on the presence and absence of CypA binding. Use of the *in situ* uncoating assay demonstrated that removing CypA-CA interactions by treatment with CsA increased the amount of CA present compared to treatment of EtOH (Fig. 18). This indicates a change in the amount of HIV-1 capsid uncoating.

When comparing the Cy5 antibody staining for the virus on glass assays completed with dual labeled virus, there was an unexpectedly low amount of fluorescence detected for the second round of stocks produced (Fig. 16). Stocks A, B, and C all had less than 20% Cy5 signal detected. This is almost certainly because of improper CA antibody staining and not due to a lack of CA. The focus of the virus on glass assay is the dTomato labeling to ensure that the cells producing the virus were successfully transfected with the four plasmids used. For all stocks made, there was 75% or more dTomato staining, indicating that all stocks had the proper fluorescent tags because at least 75% of virus labeled with GFP also had the proper dTomato membrane label.

The data produced from the *in situ* uncoating assay experiments indicates that CypA is assisting with HIV-1 uncoating. The average amount of Cy5 signal for each condition is corelated with the amount of uncoating present. The less CA detected in each sample, the more uncoating was present at that time and condition. When pooling the data, there is more uncoating present in the EtOH treatments where CypA is able to bind to CA compared to the CsA treatments for 2-, and 3- hours post infection (Fig. 18 and Table 5). The average Cy5 signal for the pooled 1-hour data is almost the same, 150.5 and 152.1 for CsA and EtOH treatments

respectively. At the 4-hour time point, the pooled data and independent experiments, showed an unexpected result of more uncoating when the interaction between CypA and CA is blocked.

The microscope used had a maximum signal detection of 251 and a minimum signal detection of 0. When the percent of virions at the maximum detection was calculated, it was found that overall, a higher percentage of timepoints treated with CsA were at the maximum when compared to EtOH. This may mean that the average for the CsA samples may be higher than currently calculated. If up to 72% of virions are at the top signal, it is possible that the amount of CA signal far exceeds the detection limit of the microscope. On the other hand, there was overall more EtOH samples at the minimum signal detection of 0. This means that there was no CA detected for the virion analyzed. At the most, up to nearly 80% of virions counted in the EtOH 0-hour sample in the March experiment were at 0. Therefore, there may be even more CA present in the CsA samples and less in the EtOH samples which further supports the hypothesis that CypA-CA interactions assist with uncoating.

For the average amount of Cy5 signal, there was a consistent switch between CsA and EtOH between 3- and 4- hours post infection for all three experiments. All experiments had more Cy5 fluorescence for CsA compared to EtOH at the 3-hour time points and this swapped at 4-hours for both June and February experiments. The 3-hour EtOH coverslip for the March experiment data was lost, so it is unknown whether or not this change occurred in this experiment as well. The change in the amount of CA present in the 4-hour samples may be due to a population of virus starting to fuse with the cell membrane. It is also possible that CsA treatment was depleted by 4-hours post infection. The warm media that the cells were treated with after spinoculation did not contain CsA or EtOH. The half-life of CsA for this experiment is

not known, so it may be that the drug is no longer associated with CypA at this time point. This could change the CA fluorescence detected between 3- and 4- hours post infection.

When comparing the average CA signal for each condition, the number of virions counted must be taken into consideration. Though analysis was still conducted, it may not be reasonable to compare results for 1-hour samples in the June experiment because there were only 15 virions detected for EtOH and 163 virions detected for CsA (Fig. 18). Since the coverslip was broken multiple times, the surface area for imaging was greatly decreased. There was less Cy5 fluorescence detected for EtOH compared to CsA for these samples, but since the EtOH sample contained less than 1% of the virus detected for CsA, the results are not reliable.

For all *in situ* assay experiments, there were coverslips that reported fusion lower than the BafA control. The BafA sample was used to show background fusion detection when dual labeled virus fusion is inhibited. Due to the nature of the assay, it is entirely possible that dTomato labeling was lost during experimentation. During the primary antibody staining, each coverslip is treated with a permeabilization solution that perforates the cell membrane to allow the antibody to enter the cells. This solution also permeates the viral membrane and causes loss of dTomato labeling. It is also possible that the detected virus never contained the dTomato label. When producing dual labeled virus, 293T cells are transfected with four different plasmids. It is unrealistic that the cells would take up all four plasmids and that every virion produced would have both GFP and dTomato labeling. This is the reason for the virus on glass assay, to ensure the virus used has a high percentage of both GFP and dTomato labeling. Therefore, some experimental samples may have less fusion detected compared to the BafA control.

Previous Research on Interactions Between CypA and CA

Effecting uncoating is not the only role of CypA in the replication cycle of HIV-1. Previous research has found CypA to be involved in reverse transcription and nuclear import in microglial cells (80). Treatment with CsA resulted in a decrease of reverse transcription. There was a greater than 20% difference in reverse transcription completion between samples treated with CsA compared to EtOH. It was concluded that CypA-CA interactions assist with reverse transcription (80). To further analyze the role of CypA in HIV-1 early replication, nuclear import was investigated by evaluating the quantification of 2-LTR circles as an indicator of import. It was found that treatment with CsA produced a decrease of nuclear import compared to samples treated with EtOH. Though the decrease in nuclear import may be due to downstream effects caused by a decrease in reverse transcription, it was concluded that blocking CypA-CA interactions also decreased nuclear import (80). Finally, early investigations for the role of CypA-CA interactions in uncoating were defined. Though the differences between CsA and EtOH treated samples were not as distinct, the 1-hour time point did show more CA signal when CypA-CA interactions were inhibited (80). The initial experiments did not include a 3-hour time point, so the time point with the largest difference from this experiment cannot be compared.

Investigating the role of CypA in capsid uncoating in microglial cells has produced similar results to reverse transcription and nuclear import. Blocking the interaction between CypA and CA decreased uncoating. Since the exact model of uncoating has yet to be determined, it cannot be stated whether uncoating occurs simultaneously, before, or after reverse transcription (13). It may be possible that treatment with CsA inhibits uncoating and therefore decreases reverse transcription and nuclear import. If uncoating does not happen at the proper part of replication, this could inhibit reverse transcription and a decrease in viral cDNA would therefore

decrease nuclear import. Altogether, there is a decrease in early replication steps when CypA cannot bind to CA and whether this effects one specific step or multiple remains to be determined.

Models of Uncoating

There are currently three proposed models of uncoating: biphasic, nuclear pore complex (NPC), and nuclear uncoating. Though the data generated does not prove one model over another, it may support NPC and nuclear uncoating. The greatest difference in uncoating between CsA and EtOH treatments was between 2- and 3-hours post infection. Therefore, uncoating may be occurring more frequently at these time points compared to others because the effect of CsA would be greatest when the capsid is uncoating. It is probable that the capsid is closer to the nucleus than the point of fusion after multiple hours post infection, so the data does not support biphasic uncoating. In consideration of the data, it is likely that the capsid is uncoating at the nuclear pore, or once completely within the nucleus.

TRIM5α Restriction Is Blocked by CypA in Microglial Cells.

By knocking down TRIM5α in CHME3 microglial cells, HIV-1 infectivity increased compared to the NT4 knockdown control. In previous experiments, human TRIM5α restriction has been found to work in human cell lines when CypA cannot bind to the capsid (43, 62). It is believed that CypA binds to the capsid and blocks TRIM5α restriction, and a similar conclusion can be drawn from these siRNA knockdown experiments.

All experiments conducted produced similar trends when cells were treated with CsA and EtOH. For all dilutions except where the amount of virus was the highest, treatment with CsA

decreased infectivity (Fig. 23 and 26). This was an expected result, as it has been found in previous work with microglial cells (80). When analyzing the fold change, there was a greater difference between CsA and EtOH in the dilutions that contained less virus. In all experiments, an increase of infection was seen at the $1/16^{th}$ dilution, the dilution with the highest amount of virus, despite treatment with CsA. This is most likely due to too much virus. Treating the cells with high amounts of HIV can create false positives by overwhelming the cells. Too much virus can cause cells to become infected more than once and surpass the natural restriction of the cells by saturating restriction factors. Comparing CsA versus EtOH treatment in the other dilutions ensures that CsA still decreases infectivity in CHME3 cells at lower dilutions. Knocking down TRIM5α did not cause any unexpected changes in infectivity.

To see what effect TRIM5α knockdown had on infectivity and if this changed with the presence and absence of CsA, the data was normalized to NT4 to show the fold change in infectivity (Fig. 24 and 27). Overall data from all experiments shows that knocking down TRIM5α increased HIV-1 infectivity. This indicates that TRIM5α is able to restrict HIV infection in human microglial cells. Further, treatment with CsA caused an even greater difference, showing a change of 3-fold higher in the June experiment (Fig. 27D). TRIM5α is able to restrict HIV-1 infection in this cell line when cells are treated with EtOH or CsA. An increase of this effect on infectivity was found in all experiments when cells were treated with CsA. This indicates that CypA is blocking TRIM5α restriction and that blocking CypA-CA interactions allows for more restriction.

An interesting conclusion can be drawn from the effect of CsA in TRIM5α and NT4 knockdown results. The ability of CsA treatment to decrease infectivity in CHME3 microglial cells may be, in part, due to TRIM5α restriction. Treatment with CsA blocks the interaction

between CypA and CA, therefore allowing for TRIM5α restriction. By removing CypA, TRIM5α is able to bind to the capsid to disrupt proper uncoating kinetics within this human cell line. When analyzing the effect of CsA in TRIM5α and NT4 knockdown cells, there was a greater decrease of infectivity in the NT4 control. By decreasing TRIM5α expression in the cell, the effect of CsA was consistently decreased. This further supports the hypothesis that CypA is blocking TRIM5α restriction within human microglial cells.

Two previous experiments have detailed the relationship between CypA and TRIM5α in macrophages and lymphocytes (43, 62). Both experiments found that blocking CypA binding to CA decreases infectivity. In macrophages, knocking down TRIM5α rescued infectivity to just below the control of 100% infection (43). In lymphocytes, decreasing TRIM5α expression with CRISPR also rescued infectivity to the same as the control (62). In both cell types, the data indicates that blocking CypA-CA interactions allows for TRIM5α restriction. This restriction does not occur when CypA proteins are bound to the capsid. Similar results were produced when investigating the relationship between CypA and TRIM5α in microglial cells. With treatment of CsA, infectivity decreased compared to the control (Fig. 23 and 26). Unlike the other experiments, when TRIM5α was knocked down, infectivity was not fully rescued. Yet, there was a lesser decrease of infectivity, indicating that removing the restriction factor does increase infectivity. It can be concluded that there is a similar link between CypA and TRIM5α in microglial cells as there is in macrophages and lymphocytes. Since infectivity was not entirely rescued when TRIM5α was knocked down, CypA may be involved in other roles in HIV-1 replication.

Future Directions

There are follow up experiments that should be completed in order to learn more about the role of CypA in HIV-1 capsid uncoating. To begin, the *in situ* assay should be imaged on a microscope with a higher signal limit. Increasing the limit would determine the true average CA detection for each condition and avoid virions clustering at the top of the detection limit. From the results produced here, it can be expected that the averages for CsA treatments would be greater than what was found. It is also possible that there would be an even greater difference between CsA and EtOH because of this. Another experiment would be to use other methods to stop CypA from binding to CA. This ensures that the change in uncoating is due to CypA and not off target effects of CsA. An example would be to use the capsid mutant P90A. This capsid has a mutation in the CypA binding loop and blocks CypA association with CA. Using wildtype capsid and P90A in place of EtOH and CsA would determine whether or not CypA effects uncoating and if there are other factors involved. The expected results would be a decrease in capsid uncoating when CypA is not able to bind, similar to treatment with CsA. Last, it would be interesting to test the *in situ* uncoating assay in other cell types. Microglial cells and astrocytes make up the majority of the viral reservoir in the brain (86). Investigating the relationship between CypA and uncoating in astrocytes may reveal more information about HIV-1 replication in neural cell lines. I would expect the two cell lines to react to CsA treatment similarly because they are both a part of the immune system for the CNS.

To further investigate the interplay between CypA and TRIM5α, a knockdown experiment to decrease CypA expression would be useful. Knocking down CypA to see if the effect is similar to CsA treatment would ensure that the reason TRIM5α cannot restrict infection in human cell lines is due to CypA. Knocking down CypA in microglial cells could be

accomplished similar to the TRIM5α knockdown, with a siRNA to target CypA. If CypA is blocking TRIM5α, then the knockdown results should be similar to treatment with CsA. Therefore, it would be expected that decreasing CypA expression would decrease HIV-1 infectivity.

Another continuing experiment would be to calculate the primer efficiency for the TRIM5α primers. This would reveal what degree TRIM5α was knocked down. Knowing how much TRIM5α expression decreased in the cell can explain any differences between siRNA experiments. Low TRIM5α knockdown may also be why infectivity was not fully rescued when the restriction factor was knocked down. Since there was a difference in infectivity between experiments, it can be speculated that there is a difference in the amount of knockdown achieved for each experiment.

Since interplay between TRIM5α and CypA has been determined in microglial cells, I believe the next step is to investigate the protein death domain-associated protein 6 (Daxx). This protein is a chaperone protein involved in many mechanisms, including apoptosis and carcinogenesis. In a recent study, Daxx was found to form a complex with the HIV-1 capsid through interaction with CypA (87). Using immunoprecipitation, HIV-1 capsid revealed a complex formed by Daxx, CypA, TRIM5α, TRIM34, and TNPO3 (87). It is possible that Daxx is an important part of HIV-1 early replication, specifically uncoating. The interplay between Daxx and the other proteins was analyzed in HEK293T cells. Investigating this relationship in microglial cells may reveal more about the role of CypA in early replication. To research Daxx in microglial cells, the expression could be decreased using siRNA. Then, an *in situ* uncoating assay could be conducted on the knockdown cell lines. If Daxx is involved with CypA and uncoating, then decreasing expression should decrease the amount of uncoating. Using the same

knockdown cells, TRIM5α restriction could also be investigated. By conducting an infectivity assay using HIV-GFP, infectivity could be analyzed between Daxx, TRIM5α, and control knockdown conditions. If Daxx inhibits restriction, then knocking it down would decrease infectivity. Researching Daxx may be the key to characterizing the role of CypA in HIV-1 replication.

Conclusion

Overall, I found that CypA interacting with the HIV-1 capsid plays two roles in HIV replication: assisting with proper uncoating kinetics and blocking TRIM5α restriction. Removing the interaction between CypA-CA decreased capsid uncoating. Similarly, treatment with CsA allowed for TRIM5α capsid restriction and ultimately decreased infectivity of HIV-1. It is possible that the interaction between CyA and CA plays more than one role in HIV-1 infection and replication, as blocking the interaction has been found to effect uncoating, reverse transcription, and nuclear import (80). This research has characterized the role of CypA in the uncoating step of replication and shown that TRIM5α restriction occurs within microglial cells.

REFERENCES

1. Ellis R. 2020. Types and Strains of HIV. WebMD.

2. Fauci A. 1988. The human immunodeficiency virus: infectivity and mechanisms of pathogenesis. Science 239:617–622.

3. World Health Organization. 2021. HIV/AIDS. WHO.

4. Centers for Disease Control and Prevention. 2021. AIDS and Opportubistic Infections. CDC.

5. Lorin V, Danckaert A, Porrot F, Schwartz O, Afonso PV, Mouquet H. 2020. Antibody Neutralization of HIV-1 Crossing the Blood-Brain Barrier. mBio 11.

6. Banks WA, Freed EO, Wolf KM, Robinson SM, Franko M, Kumar VB. 2001. Transport of human immunodeficiency virus type 1 pseudoviruses across the blood-brain barrier: role of envelope proteins and adsorptive endocytosis. J Virol 75:4681–4691.

7. Eggers C, Arendt G, Hahn K, Husstedt IW, Maschke M, Neuen-Jacob E, Obermann M, Rosenkranz T, Schielke E, Straube E, German Association of Neuro-AIDS und Neuro-Infectiology (DGNANI). 2017. HIV-1-associated neurocognitive disorder: epidemiology, pathogenesis, diagnosis, and treatment. J Neurol 264:1715–1727.

8. Antinori A, Arendt G, Becker JT, Brew BJ, Byrd DA, Cherner M, Clifford DB, Cinque P, Epstein LG, Goodkin K, Gisslen M, Grant I, Heaton RK, Joseph J, Marder K, Marra CM, McArthur JC, Nunn M, Price RW, Pulliam L, Robertson KR, Sacktor N, Valcour V, Wojna VE. 2007. Updated research nosology for HIV-associated neurocognitive disorders. Neurology 69:1789–1799.

9. Pardons M, Baxter AE, Massanella M, Pagliuzza A, Fromentin R, Dufour C, Leyre L, Routy J-P, Kaufmann DE, Chomont N. 2019. Single-cell characterization and quantification of translation-competent viral reservoirs in treated and untreated HIV infection. PLoS Pathog 15:e1007619.

10. Nimmerjahn A, Kirchhoff F, Helmchen F. 2005. Resting microglial cells are highly dynamic surveillants of brain parenchyma in vivo. Science 308:1314–1318.

11. German Advisory Committee. 2016. Human Immunodeficiency Virus (HIV). Transfus Med Hemother 43:203–222.

12. Turner BG, Summers MF. 1999. Structural biology of HIV 1 1Edited by P. E. Wright. Journal of Molecular Biology 285:1–32.

13. Campbell E, Hope T. 2015. HIV-1 Capsid: The Multifaceted Key Player in HIV-1 infection. Nat Rev Microbiol 13:471–483.

14. Doms RW, Moore JP. 2000. HIV-1 Membrane Fusion. Journal of Cell Biology 151:F9–F14.

15. Hernandez LD, Hoffman LR, Wolfsberg TG, White JM. 1996. VIRUS-CELL AND CELL-CELL FUSION. Annu Rev Cell Dev Biol 12:627–661.

16. Chen B. 2019. Molecular Mechanism of HIV-1 Entry. Trends in Microbiology 27:878–891.

17. Lin M-H, Apolloni A, Cutillas V, Sivakumaran H, Martin S, Li D, Wei T, Wang R, Jin H, Spann K, Harrich D. 2015. A Mutant Tat Protein Inhibits HIV-1 Reverse Transcription by Targeting the Reverse Transcription Complex. J Virol 89:4827–4836.

18. Levin JG, Mitra M, Mascarenhas A, Musier-Forsyth K. 2010. Role of HIV-1 nucleocapsid protein in HIV-1 reverse transcription. RNA Biology 7:754–774.

19. 1997. Retroviruses. Cold Spring Harbor Laboratory Press, Plainview, NY.

20. Forshey BM, von Schwedler U, Sundquist WI, Aiken C. 2002. Formation of a human immunodeficiency virus type 1 core of optimal stability is crucial for viral replication. J Virol 76:5667–5677.

21. Yang W, Gelles J, Musser SM. 2004. Imaging of single-molecule translocation through nuclear pore complexes. Proceedings of the National Academy of Sciences 101:12887–12892.

22. Kelich JM, Ma J, Dong B, Wang Q, Chin M, Magura CM, Xiao W, Yang W. 2015. Super-resolution imaging of nuclear import of adeno-associated virus in live cells. Molecular Therapy - Methods & Clinical Development 2:15047.

23. Burdick RC, Delviks-Frankenberry KA, Chen J, Janaka SK, Sastri J, Hu W-S, Pathak VK. 2017. Dynamics and regulation of nuclear import and nuclear movements of HIV-1 complexes. PLoS Pathog 13:e1006570.

24. Craigie R, Bushman FD. 2012. HIV DNA Integration. Cold Spring Harbor Perspectives in Medicine 2:a006890–a006890.

25. Ren L, Wang HW, Xu Y, Feng Y, Zhang HF, Wang KH. 2016. Sequencing of Gag/Env association with HIV genotyping resolution and HIV-related epidemiologic studies of HIV in China. Genet Mol Res 15.

26. Roebuck KA, Saifuddin M. 1999. Regulation of HIV-1 transcription. Gene Expr 8:67–84.

27. Doria M, Neri F, Gallo A, Farace MG, Michienzi A. 2009. Editing of HIV-1 RNA by the double-stranded RNA deaminase ADAR1 stimulates viral infection. Nucleic Acids Research 37:5848–5858.

28. Guerrero S, Batisse J, Libre C, Bernacchi S, Marquet R, Paillart J-C. 2015. HIV-1 Replication and the Cellular Eukaryotic Translation Apparatus. Viruses 7:199–218.

29. Perales C, Carrasco L, González ME. 2005. Regulation of HIV-1 env mRNA translation by Rev protein. Biochimica et Biophysica Acta (BBA) - Molecular Cell Research 1743:169–175.

30. Maffucci T, Falasca M. 2020. Signalling Properties of Inositol Polyphosphates. Molecules 25:5281.

31. Freed EO. 2015. HIV-1 assembly, release and maturation. Nat Rev Microbiol 13:484–496.

32. Briggs JAG, Simon MN, Gross I, Kräusslich H-G, Fuller SD, Vogt VM, Johnson MC. 2004. The stoichiometry of Gag protein in HIV-1. Nat Struct Mol Biol 11:672–675.

33. Berthet-Colominas C. 1999. Head-to-tail dimers and interdomain flexibility revealed by the crystal structure of HIV-1 capsid protein (p24) complexed with a monoclonal antibody Fab. The EMBO Journal 18:1124–1136.

34. Mattei S, Glass B, Hagen WJH, Kräusslich H-G, Briggs JAG. 2016. The structure and flexibility of conical HIV-1 capsids determined within intact virions. Science 354:1434–1437.

35. Ganser-Pornillos BK, Cheng A, Yeager M. 2007. Structure of Full-Length HIV-1 CA: A Model for the Mature Capsid Lattice. Cell 131:70–79.

36. Lahaye X, Satoh T, Gentili M, Cerboni S, Conrad C, Hurbain I, El Marjou A, Lacabaratz C, Lelièvre J-D, Manel N. 2013. The Capsids of HIV-1 and HIV-2 Determine Immune Detection of the Viral cDNA by the Innate Sensor cGAS in Dendritic Cells. Immunity 39:1132–1142.

37. Rasaiyaah J, Tan CP, Fletcher AJ, Price AJ, Blondeau C, Hilditch L, Jacques DA, Selwood DL, James LC, Noursadeghi M, Towers GJ. 2013. HIV-1 evades innate immune recognition through specific cofactor recruitment. Nature 503:402–405.

38. Hulme AE, Perez O, Hope TJ. 2011. Complementary assays reveal a relationship between HIV-1 uncoating and reverse transcription. Proceedings of the National Academy of Sciences 108:9975–9980.

39. Burdick RC, Li C, Munshi M, Rawson JMO, Nagashima K, Hu W-S, Pathak VK. 2020. HIV-1 uncoats in the nucleus near sites of integration. Proc Natl Acad Sci USA 117:5486–5493.

40. Schaller T, Ocwieja KE, Rasaiyaah J, Price AJ, Brady TL, Roth SL, Hué S, Fletcher AJ, Lee K, KewalRamani VN, Noursadeghi M, Jenner RG, James LC, Bushman FD, Towers GJ. 2011. HIV-1 Capsid-Cyclophilin Interactions Determine Nuclear Import Pathway, Integration Targeting and Replication Efficiency. PLoS Pathog 7:e1002439.

41. Miller MD, Farnet CM, Bushman FD. 1997. Human immunodeficiency virus type 1 preintegration complexes: studies of organization and composition. J Virol 71:5382–5390.

42. Braaten D, Ansari H, Luban J. 1997. The hydrophobic pocket of cyclophilin is the binding site for the human immunodeficiency virus type 1 Gag polyprotein. J Virol 71:2107–2113.

43. Kim K, Dauphin A, Komurlu S, McCauley SM, Yurkovetskiy L, Carbone C, Diehl WE, Strambio-De-Castillia C, Campbell EM, Luban J. 2019. Cyclophilin A protects HIV-1 from restriction by human TRIM5α. Nat Microbiol 4:2044–2051.

44. Xu H, Franks T, Gibson G, Huber K, Rahm N, De Castillia CS, Luban J, Aiken C, Watkins S, Sluis-Cremer N, Ambrose Z. 2013. Evidence for biphasic uncoating during HIV-1 infection from a novel imaging assay. Retrovirology 10:70.

45. Arhel NJ, Souquere-Besse S, Munier S, Souque P, Guadagnini S, Rutherford S, Prévost M-C, Allen TD, Charneau P. 2007. HIV-1 DNA Flap formation promotes uncoating of the pre-integration complex at the nuclear pore. EMBO J 26:3025–3037.

46. Toccafondi E, Lener D, Negroni M. 2021. HIV-1 Capsid Core: A Bullet to the Heart of the Target Cell. Front Microbiol 12:652486.

47. Dharan A, Bachmann N, Talley S, Zwikelmaier V, Campbell EM. 2020. Nuclear pore blockade reveals that HIV-1 completes reverse transcription and uncoating in the nucleus. Nat Microbiol 5:1088–1095.

48. Briones MS, Dobard CW, Chow SA. 2010. Role of Human Immunodeficiency Virus Type 1 Integrase in Uncoating of the Viral Core. J Virol 84:5181–5190.

49. Ingram Z, Taylor M, Okland G, Martin R, Hulme AE. 2020. Characterization of HIV-1 uncoating in human microglial cell lines. Virol J 17:31.

50. Mamede JI, Cianci GC, Anderson MR, Hope TJ. 2017. Early cytoplasmic uncoating is associated with infectivity of HIV-1. Proc Natl Acad Sci USA 114:E7169–E7178.

51. Li W, Singh PK, Sowd GA, Bedwell GJ, Jang S, Achuthan V, Oleru AV, Wong D, Fadel HJ, Lee K, KewalRamani VN, Poeschla EM, Herschhorn A, Engelman AN. 2020. CPSF6-Dependent Targeting of Speckle-Associated Domains Distinguishes Primate from Nonprimate Lentiviral Integration. mBio 11.

52. De Iaco A, Luban J. 2011. Inhibition of HIV-1 infection by TNPO3 depletion is determined by capsid and detectable after viral cDNA enters the nucleus. Retrovirology 8:98.

53. Diaz-Griffero F. 2012. The Role of TNPO3 in HIV-1 Replication. Molecular Biology International 2012:1–6.

54. Cannon L, Vargas-Garcia CA, Jagarapu A, Piovoso MJ, Zurakowski R. 2018. HIV 2-LTR experiment design optimization. PLoS ONE 13:e0206700.

55. Ke HM, Zydowsky LD, Liu J, Walsh CT. 1991. Crystal structure of recombinant human T-cell cyclophilin A at 2.5 A resolution. Proc Natl Acad Sci U S A 88:9483–9487.

56. Fischer G, Wittmann-Liebold B, Lang K, Kiefhaber T, Schmid FX. 1989. Cyclophilin and peptidyl-prolyl cis-trans isomerase are probably identical proteins. Nature 337:476–478.

57. Chopard C, Tong PBV, Tóth P, Schatz M, Yezid H, Debaisieux S, Mettling C, Gross A, Pugnière M, Tu A, Strub J-M, Mesnard J-M, Vitale N, Beaumelle B. 2018. Cyclophilin A enables specific HIV-1 Tat palmitoylation and accumulation in uninfected cells. Nat Commun 9:2251.

58. Gamble TR, Vajdos FF, Yoo S, Worthylake DK, Houseweart M, Sundquist WI, Hill CP. 1996. Crystal Structure of Human Cyclophilin A Bound to the Amino-Terminal Domain of HIV-1 Capsid. Cell 87:1285–1294.

59. Liu C, Perilla JR, Ning J, Lu M, Hou G, Ramalho R, Himes BA, Zhao G, Bedwell GJ, Byeon I-J, Ahn J, Gronenborn AM, Prevelige PE, Rousso I, Aiken C, Polenova T, Schulten K, Zhang P. 2016. Cyclophilin A stabilizes the HIV-1 capsid through a novel non-canonical binding site. Nat Commun 7:10714.

60. Peng W, Shi J, Márquez CL, Lau D, Walsh J, Faysal KMR, Byeon CH, Byeon I-JL, Aiken C, Böcking T. 2019. Functional analysis of the secondary HIV-1 capsid binding site in the host protein cyclophilin A. Retrovirology 16:10.

61. Miles RJ, Kerridge C, Hilditch L, Monit C, Jacques DA, Towers GJ. 2020. MxB sensitivity of HIV-1 is determined by a highly variable and dynamic capsid surface. Elife 9:e56910.

62. Selyutina A, Persaud M, Simons LM, Bulnes-Ramos A, Buffone C, Martinez-Lopez A, Scoca V, Di Nunzio F, Hiatt J, Marson A, Krogan NJ, Hultquist JF, Diaz-Griffero F. 2020. Cyclophilin A Prevents HIV-1 Restriction in Lymphocytes by Blocking Human TRIM5α Binding to the Viral Core. Cell Reports 30:3766-3777.e6.

63. Sayah DM, Sokolskaja E, Berthoux L, Luban J. 2004. Cyclophilin A retrotransposition into TRIM5 explains owl monkey resistance to HIV-1. Nature 430:569–573.

64. Liu S, Asparuhova M, Brondani V, Ziekau I, Klimkait T, Schümperli D. 2004. Inhibition of HIV-1 multiplication by antisense U7 snRNAs and siRNAs targeting cyclophilin A. Nucleic Acids Res 32:3752–3759.

65. de Wilde AH, Zevenhoven-Dobbe JC, Beugeling C, Chatterji U, de Jong D, Gallay P, Szuhai K, Posthuma CC, Snijder EJ. 2018. Coronaviruses and arteriviruses display striking differences in their cyclophilin A-dependence during replication in cell culture. Virology 517:148–156.

66. Franke EK, Luban J. 1996. Inhibition of HIV-1 Replication by Cyclosporine A or Related Compounds Correlates with the Ability to Disrupt the Gag–Cyclophilin A Interaction. Virology 222:279–282.

67. Li Y, Kar AK, Sodroski J. 2009. Target cell type-dependent modulation of human immunodeficiency virus type 1 capsid disassembly by cyclophilin A. J Virol 83:10951–10962.

68. Berthoux L, Sebastian S, Sokolskaja E, Luban J. 2005. Cyclophilin A is required for TRIM5{alpha}-mediated resistance to HIV-1 in Old World monkey cells. Proc Natl Acad Sci U S A 102:14849–14853.

69. Towers GJ, Hatziioannou T, Cowan S, Goff SP, Luban J, Bieniasz PD. 2003. Cyclophilin A modulates the sensitivity of HIV-1 to host restriction factors. Nat Med 9:1138–1143.

70. Hatziioannou T, Perez-Caballero D, Yang A, Cowan S, Bieniasz PD. 2004. Retrovirus resistance factors Ref1 and Lv1 are species-specific variants of TRIM5. Proceedings of the National Academy of Sciences 101:10774–10779.

71. Hatziioannou T, Perez-Caballero D, Cowan S, Bieniasz PD. 2005. Cyclophilin Interactions with Incoming Human Immunodeficiency Virus Type 1 Capsids with Opposing Effects on Infectivity in Human Cells. J Virol 79:176–183.

72. Stremlau M, Owens CM, Perron MJ, Kiessling M, Autissier P, Sodroski J. 2004. The cytoplasmic body component TRIM5α restricts HIV-1 infection in Old World monkeys. Nature 427:848–853.

73. Ohkura S, Yap MW, Sheldon T, Stoye JP. 2006. All Three Variable Regions of the TRIM5α B30.2 Domain Can Contribute to the Specificity of Retrovirus Restriction. J Virol 80:8554–8565.

74. Diaz-Griffero F, Qin X, Hayashi F, Kigawa T, Finzi A, Sarnak Z, Lienlaf M, Yokoyama S, Sodroski J. 2009. A B-Box 2 Surface Patch Important for TRIM5α Self-Association, Capsid Binding Avidity, and Retrovirus Restriction. J Virol 83:10737–10751.

75. Yu A, Skorupka KA, Pak AJ, Ganser-Pornillos BK, Pornillos O, Voth GA. 2020. TRIM5α self-assembly and compartmentalization of the HIV-1 viral capsid. Nat Commun 11:1307.

76. Javanbakht H, Diaz-Griffero F, Stremlau M, Si Z, Sodroski J. 2005. The Contribution of RING and B-box 2 Domains to Retroviral Restriction Mediated by Monkey TRIM5α. Journal of Biological Chemistry 280:26933–26940.

77. Black LR, Aiken C. 2010. TRIM5α Disrupts the Structure of Assembled HIV-1 Capsid Complexes *In Vitro*. J Virol 84:6564–6569.

78. Stremlau M, Perron M, Lee M, Li Y, Song B, Javanbakht H, Diaz-Griffero F, Anderson DJ, Sundquist WI, Sodroski J. 2006. Specific recognition and accelerated uncoating of retroviral capsids by the TRIM5 restriction factor. Proceedings of the National Academy of Sciences 103:5514–5519.

79. Hofmann W, Schubert D, LaBonte J, Munson L, Gibson S, Scammell J, Ferrigno P, Sodroski J. 1999. Species-Specific, Postentry Barriers to Primate Immunodeficiency Virus Infection. J Virol 73:10020–10028.

80. Ingram Z. 2019. Cyclophilin A enhances HIV-1 Reverse Transcription in Human Microglial Cells. Missouri State University.

81. Janabi N, Peudenier S, Héron B, Ng KH, Tardieu M. 1995. Establishment of human microglial cell lines after transfection of primary cultures of embryonic microglial cells with the SV40 large T antigen. Neuroscience Letters 195:105–108.

82. Ingram Z, Matheney H, Wise E, Weatherford C, Hulme AE. 2021. Overlap Intensity: An ImageJ Macro for Analyzing the HIV-1 In Situ Uncoating Assay. Viruses 13:1604.

83. Yu D, Wang W, Yoder A, Spear M, Wu Y. 2009. The HIV Envelope but Not VSV Glycoprotein Is Capable of Mediating HIV Latent Infection of Resting CD4 T Cells. PLoS Pathog 5:e1000633.

84. Campbell EM, Perez O, Melar M, Hope TJ. 2007. Labeling HIV-1 virions with two fluorescent proteins allows identification of virions that have productively entered the target cell. Virology 360:286–293.

85. Muroi M, Shiragami N, Nagao K, Yamasaki M, Takatsuki A. 1994. Folimycin (concanamycin A) and Bafilomycin A_1, Inhibitors Specific for V-ATPase, Exert Similar but Distinct Effects on Intracellular Translocation and Processing of Glycoproteins. Bioscience, Biotechnology, and Biochemistry 58:425–427.

86. Ash MK, Al-Harthi L, Schneider JR. 2021. HIV in the Brain: Identifying Viral Reservoirs and Addressing the Challenges of an HIV Cure. Vaccines 9:867.

87. Maillet S, Fernandez J, Decourcelle M, El Koulali K, Blanchet FP, Arhel NJ, Maarifi G, Nisole S. 2020. Daxx Inhibits HIV-1 Reverse Transcription and Uncoating in a SUMO-Dependent Manner. Viruses 12:636.

APPENDICES

Appendix A: Research Compliance Certificates

July 18, 2022

RE: IBC protocols 2022-02.3 & 2022-02.4

Hello Emma Wise,

IBC protocols #2022-02.3 & 2022-02.4 entitled "Studies on the early steps of HIV-1 replication" for biohazards and rDNA, were continued projects and approved 2/24/2022 to 2/23/2024. You are an approved member to work with Dr. Amy Hulme, Ph.D. on these protocols.

Thank you and if you need anything in the future regarding these protocols, please contact me via email (johnnapedersen@missouristate.edu) or at 417-836-3737.

Sincerely,

Johnna Pedersen

OFFICE OF RESEARCH ADMINISTRATION
901 South National Avenue, Springfield, MO 65897 • Phone: 417-836-5972
www.missouristate.edu
An Equal Opportunity/Affirmative Action/Minority/Female/Veterans/Disability/Sexual Orientation/Gender Identity Employer and Institution

Missouri State
UNIVERSITY

July 18, 2022

RE: IBC protocols 2022-02.3 & 2022-02.4

Dear Graduate College,

Protocols #2022-02.3 & 2022-02.4 entitled "Studies on the early steps of HIV-1 replication" for biohazards and rDNA, are Institutional Biosafety Committee (IBC) reviewed protocols originating from 2016. These protocols have been consistently updated per IBC policy since 2016. The latest approvals were dated 2/24/2022 to 2/23/2024, submitted by Dr. Amy Hulme, Ph.D.

Thank you and if you need anything in the future regarding these protocols, please contact me via email (johnnapedersen@missouristate.edu) or at 417-836-3737.

Sincerely,

Johnna Pedersen

OFFICE OF RESEARCH ADMINISTRATION
901 South National Avenue, Springfield, MO 65897 • Phone: 417-836-5972
www.missouristate.edu
An Equal Opportunity/Affirmative Action/Minority/Female/Veterans/Disability/Sexual Orientation/Gender Identity Employer and Institution

CITI PROGRAM

Completion Date 20-Oct-2019
Expiration Date 19-Oct-2021
Record ID 33856083

This is to certify that:

Emma Wise

Has completed the following CITI Program course:

Not valid for renewal of certification through CME.

Biosafety and Biosecurity (BSS)
(Curriculum Group)
Basic Biosafety Course
(Course Learner Group)
1 - Basic Course
(Stage)

Under requirements set by:

Missouri State University

CITI
Collaborative Institutional Training Initiative

Verify at www.citiprogram.org/verify/?w699d53c8-db16-487b-b645-2fc9766648b7-33856083

CITI PROGRAM

Completion Date 19-Jan-2022
Expiration Date 19-Jan-2024
Record ID 46748680

This is to certify that:

Emma Wise

Has completed the following CITI Program course:

Not valid for renewal of certification through CME.

Biosafety and Biosecurity (BSS)
(Curriculum Group)
Basic Biosafety Course
(Course Learner Group)
1 - Basic Course
(Stage)

Under requirements set by:

Missouri State University

CITI
Collaborative Institutional Training Initiative

Verify at www.citiprogram.org/verify/?wff0bd034-0e7f-4528-aa65-098f9cd1a393-46748680

Appendix B: TRIM5α Primer Efficiency

Primer efficiency calculation is an important part of knockdown quantification because it indicates the performance of the primers. High performance primers have an efficiency around 90% to 110%. This number indicates how much amplification is occurring in each qPCR cycle and is used to determine the amount of RNA expression has been knocked down in a sample using the Pfaffl method.

To begin the process of calculating TRIM5α primer efficiency, total RNA was isolated from CHME3 microglial cells. Next, a reverse transcription reaction was completed with the RNA to make complimentary DNA (cDNA). To start testing the primers, 3 sets of forward and reverse primers were selected: A, C and E. A PCR reaction was conducted with each primer set to amplify the cDNA. To visualize the PCR results, the products were run on a 3% gel for gel electrophoresis (Fig. A1). Primers A and C were selected for further experiments because the bands produced indicated a large amount of sample. The brighter bands indicate that the primers are amplifying the target. Primer set E did show some amplification, but there were also bands in the -RT and water controls.

Next, primer sets A and C were used to amplify the cDNA again, this time with the goal of cloning the PCR product into a plasmid. The PCR products from primers A and C underwent a PCR cleanup to purify the DNA, then a ligation reaction to insert the PCR product into the pGem-Teasy plasmid. HB101 competent E. coli was transfected with the ligation reactions and plated onto LB-Amp plates. Bacteria grew on the plates but resembled a lawn more than individual colonies for both plasmid sets. Despite this, five colonies were picked from each plate and grown in cultures, for a total of ten samples. Each culture underwent miniprep purification, to isolate the plasmid from the samples. To check if the insert was in the isolated plasmids, an

EcoR1 restriction digest was completed using the miniprep DNA. To see the results of the digest, samples were run out on a gel (Fig. A2). For all ten samples, there was no insert present in any of the plasmids. The cleaned up PCR reactions for A and C primers were run on PCR to check for insert and it was not present in either sample (Fig. A3).

To begin the process again, new PCR products were produced using the A and C primer sets. The products went through a PCR clean up reaction to purify the DNA with a new PCR cleanup kit. Using the purified products from A and C primers, a ligation reaction was done with the pGem-Teasy plasmid again. Competent HB101 cells were transfected with the ligations. The transfected E. coli was grown up on new LB-Amp plates and single colonies were grown for each sample. For both A and C transfections, six colonies were selected and gown in individual cultures. After growing overnight, the twelve total samples underwent miniprep purification to isolate the cloned plasmids.

The isolated plasmids went through an EcoR1 restriction digest to locate the insert within the cloned plasmids. The samples were run on a gel to visualize the results and no insert was found in the twelve samples (Fig. A4). In an attempt to find insert, the purified miniprep DNA was run through PCR using A and C primers. After running the PCR products out on a gel, faint bands were seen and miniprep samples A1, A3, C1, and C3 were selected moving forward (Fig. A5). The HB101 cultures that produced the selected miniprep samples were streaked out onto LB-Amp plates to produce more colonies. From the A3 plate, four colonies were selected and grown in cultures. As before, the cultures were purified using a miniprep kit.

To begin developing the qPCR, the total RNA was run with primer sets A and C. The conditions ran were samples with reverse transcriptase, without reverse transcriptase, and a no template control for each primer set (Table A1). Moving forward, primer set A was selected

because there was amplification at 18 cycles. C was not selected because the miniprep PCR showed two bands, one of which may be off target amplification. Next, qPCR was conducted with a serial dilution using the A3 miniprep DNA. The serial dilution was from 10^7 to 10^1 and a water control. The results from this qPCR had mostly background amplification, with the lowest cycle number being 31.62 from the no template control (Table A2). All Ct values for experimental samples exceeded that of the negative control (Table A2). The entire 10^7 triplicate set reported a Ct value of 0, showing that there may have been no target in the sample at all. Since only background was produced, the A3 stock, 10^7 sample, and water were run on PCR using primer set A to look for the insert. The PCR products were run out on a gel and there was insert in the A3 stock, but not in the 10^7 sample.

Moving forward, the A3 stock was used to make a new dilution series and the miniprep stock was used as the 10^7 sample. This new dilution series was also 10^7 to 10^1. The results from the qPCR run with the new dilution series had some amplification in the 10^6, 10^5, and 10^4 samples. The amplification was low, with Ct values of 24, 27, and 31 for 10^6, 10^5, and 10^4 respectively, but it was better than the previous qPCR results (Table 3). For the next qPCR, dilutions were added in between the samples with amplification to make $10^{5.5}$ and $10^{4.5}$. This dilution series was run on qPCR four separate times, but an acceptable primer efficiency curve was not able to be calculated (Fig. A6). To accept the primer efficiency, the line of the graph must fit the positive trend line to produce an R^2 value of 0.99 or above. This indicates that the primers are effectively replicating the target and doubling the target each cycle. If the R^2 is below 0.99, then the primers are not acceptable (Fig. A6).

In an attempt to try again, another culture of the A3 cloned plasmid was purified, this time with a maxiprep kit. But when the sample was digested with EcoR1, no insert was present

once again (Fig. A7). The same result was produced when the maxiprep A3 DNA was amplified through PCR and run out on a gel using the A primers (Fig. A8). In a final effort to calculate primer efficiency, qPCR was conducted on a serial dilution of cDNA. The total RNA isolated from CHME3 microglial cells was processed through a reverse transcription reaction to produce total cDNA. The cDNA was amplified using PCR and the A primer set. Some PCR product was observed, so a serial dilution was set up for qPCR (Fig. A9). The cDNA dilution ranged from 10^5 to 10^1. The results from this final qPCR using primer set A showed mostly background once again. The samples were run in triplicate, and the amplification was different for each trio of Ct values (Table A4). For example, the 10^3 dilution reported amplification at cycles 42, 31, and 28 (Table A4). These numbers were essentially the same as the water and negative controls, which had Ct values ranging from 27 to 41 (Table A4). Ultimately, the primer efficiency for the TRIM5α primer set was not able to be calculated.

TABLE A1 qRT-PCR Ct values

Samples	Ct values
A +RT	18.62
A -RT	32.09
A nontarget control	38.05
Blank	N/A
Blank	N/A
C + RT	16.82
C -RT	30.93
C nontarget control	32.44

TABLE A2 qPCR for 10^7 to 10^1.

Samples	Ct values
10^7	0
10^7	0
10^7	0
10^6	41.8
10^6	33.37
10^6	41.27
10^5	0
10^5	33.7
10^5	34.41
10^4	35.19
10^4	32.48
10^4	36.12
10^3	0
10^3	0
10^3	35.85
10^2	37.27
10^2	34.56
10^2	35.26
10^1	34.33
10^1	34.02
10^1	35.21
NTC	0
NTC	31.62
NTC	33.47

TABLE A3 qPCR A3 Serial Dilution

Samples	Ct values
10^7	0
10^7	0
10^7	0
10^6	24.74
10^6	24.71
10^6	24.69
10^5	27.9
10^5	27.91
10^5	28.06
10^4	31.42
10^4	31.62
10^4	31.74
10^3	34.08
10^3	35.02
10^3	34.96
10^2	35.01
10^2	36
10^2	36.04
10^1	39.28
10^1	35.68
10^1	34.29
NTC	34.86
NTC	34.53
NTC	33.99

TABLE A4 qPCR on cDNA Serial Dilution

Samples	Ct values
10^6	23.70
10^6	28.20
10^6	24.38
10^5	29.69
10^5	31.35
10^5	33.11
10^4	38.12
10^4	31.33
10^4	30.73
10^3	42.19
10^3	31.54
10^3	28.13
10^2	37.40
10^2	35.86
10^2	28.18
10^1	35.56
10^1	31.18
10^1	28.50
-RT	35.80
-RT	41.59
-RT	28.39
H_2O	38.66
H_2O	30.94
H_2O	27.98

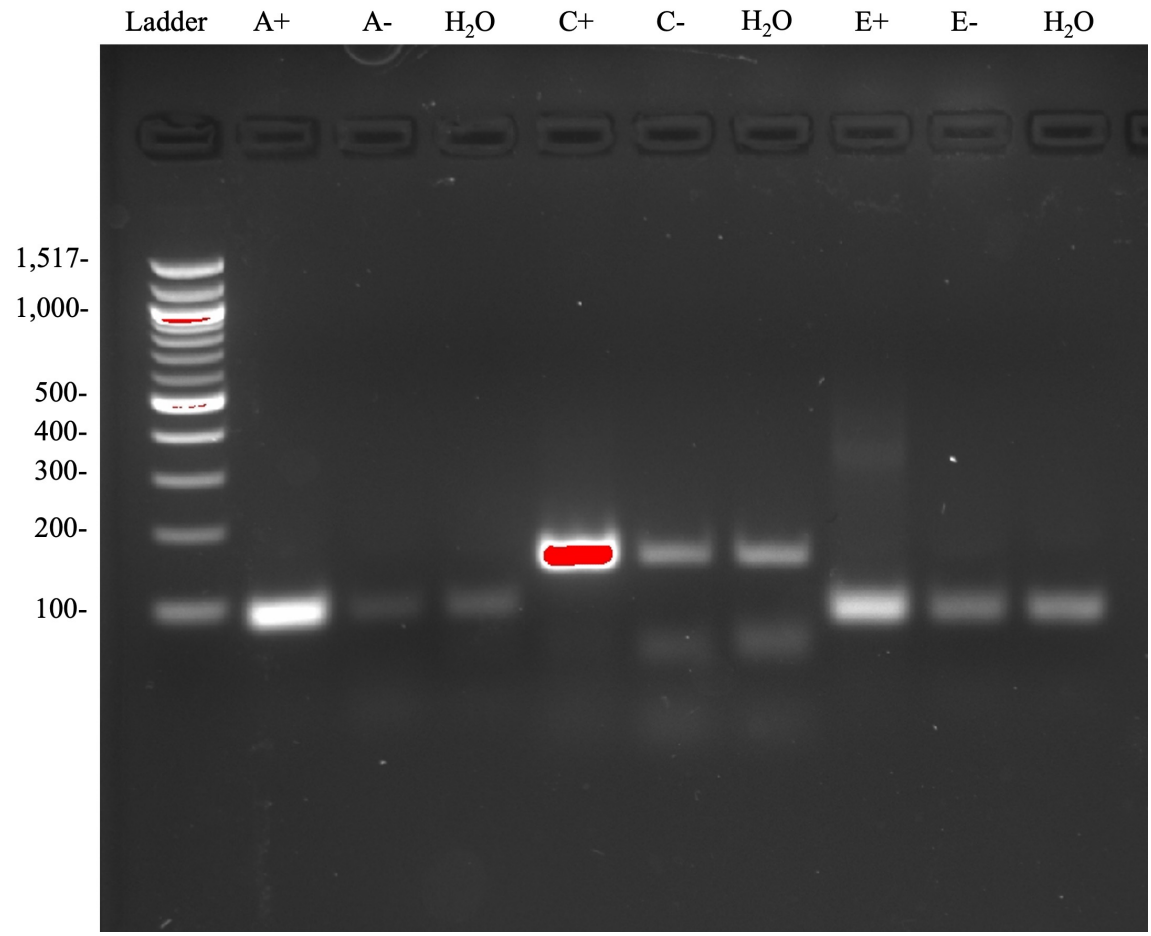

FIG A1 Testing Primer Amplification. PCR results on gel electrophoresis. Three primer sets, A, C, and E were tested on total RNA. Plus, reactions contained reverse transcriptase, minus did not have reverse transcriptase and H2O samples had no template. Cropped to show relevant lanes.

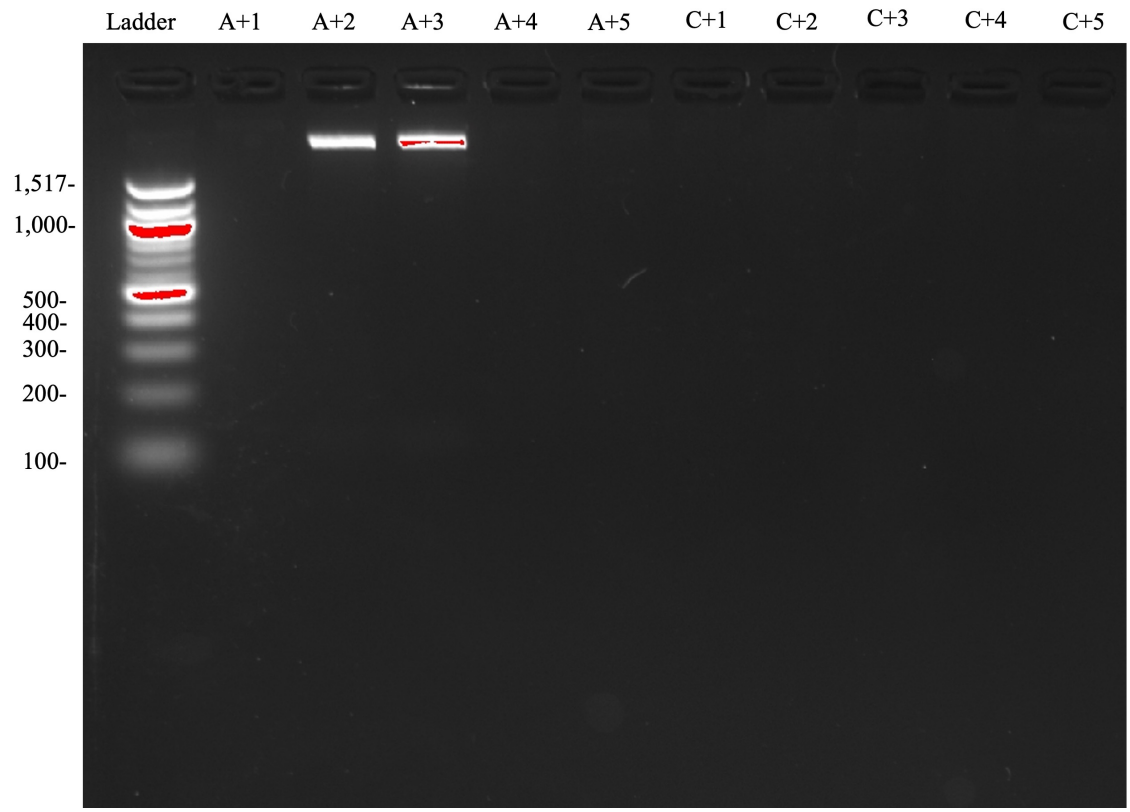

FIG A2 Miniprep Samples EcoR1 Digest. Restriction digest results on gel electrophoresis. Ten total samples of purified DNA for primer sets A and C. Gel has been cropped to only show lanes with samples.

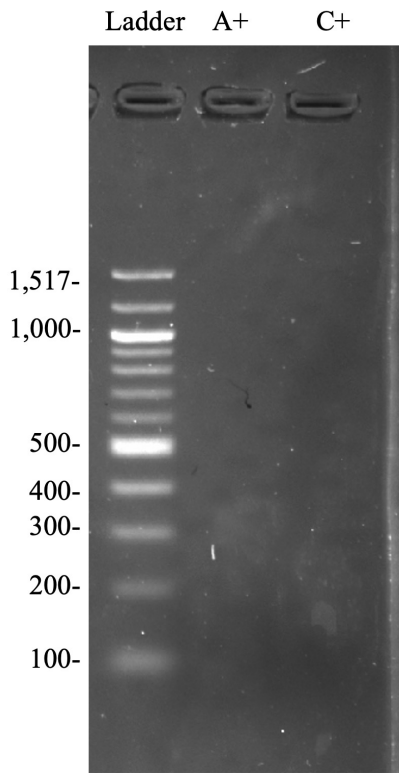

FIG A3 Insert for Cloning into pGem-Teasy Plasmid with A and C Primers. The plus indicates the reverse transcription reaction. The gel has been cropped to show relevant lanes.

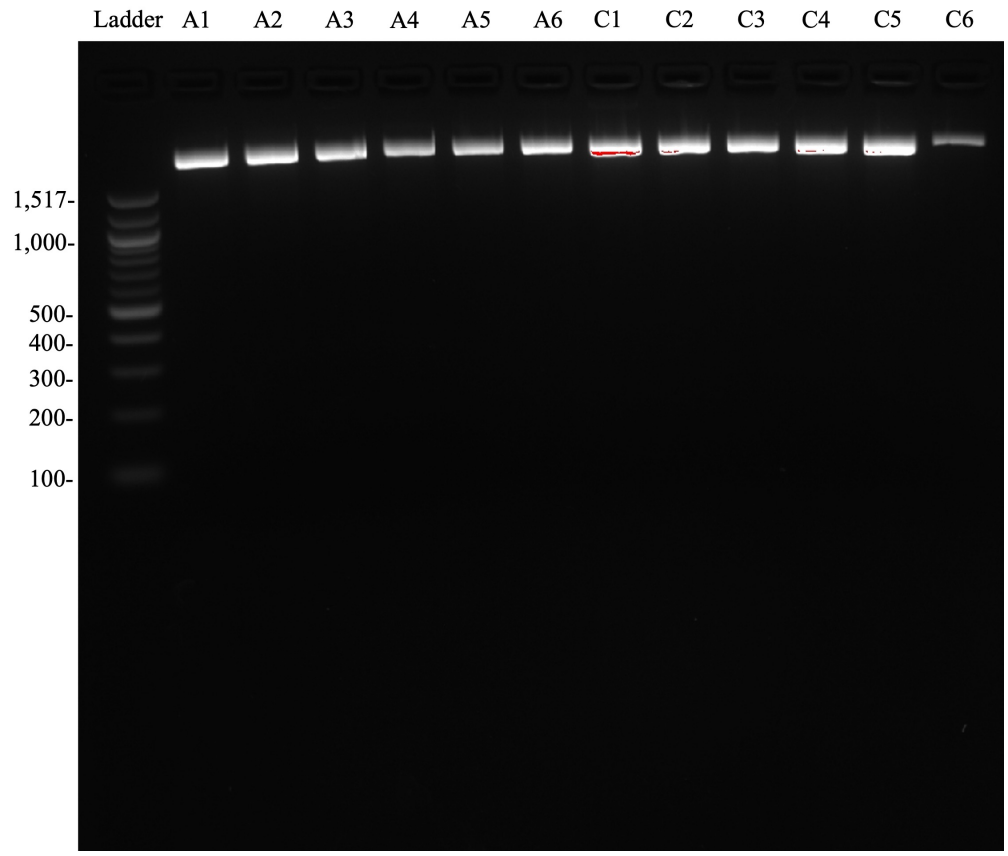

FIG A4 Restriction Digest for A 1-6 and C 1-6 Miniprep. EcoR1 restriction digest reaction for twelve different miniprep samples. A indicates the A primer set and C is the C primer set. Gel has been cropped.

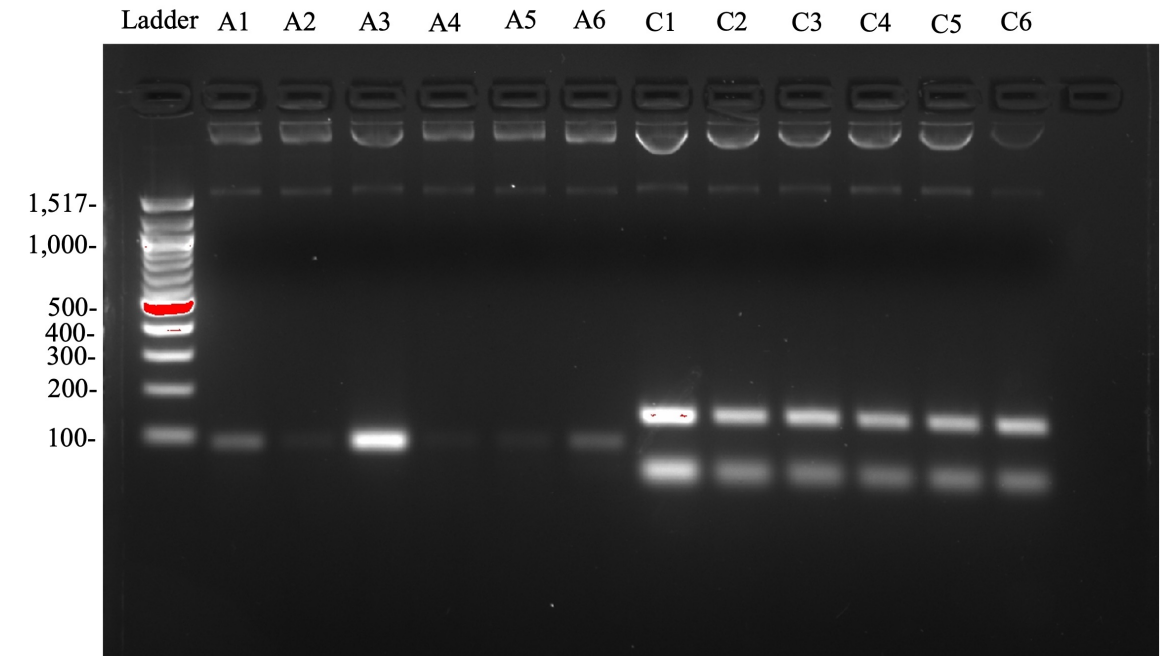

FIG A5 PCR Reaction on Minipreps. PCR with miniprep DNA for A 1-6 and C 1-6.

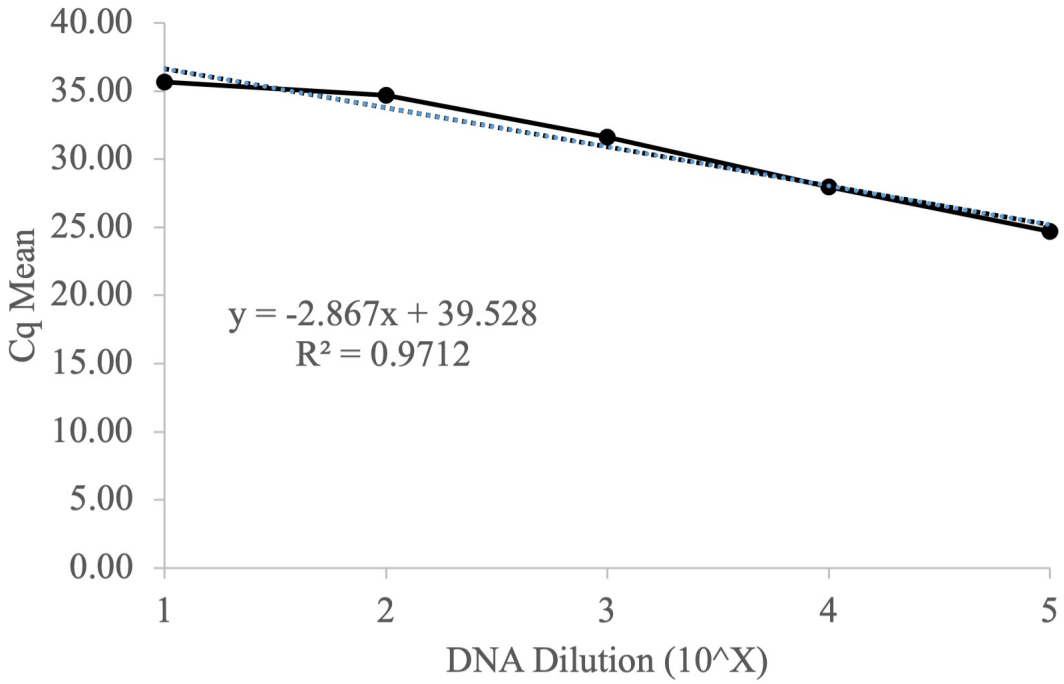

FIG A6 Attempted Primer Efficiency Curve. This curve was produced from the qPCR with the dilution series 10^5, $10^{4.5}$, 10^4, $10^{3.5}$, 10^3.

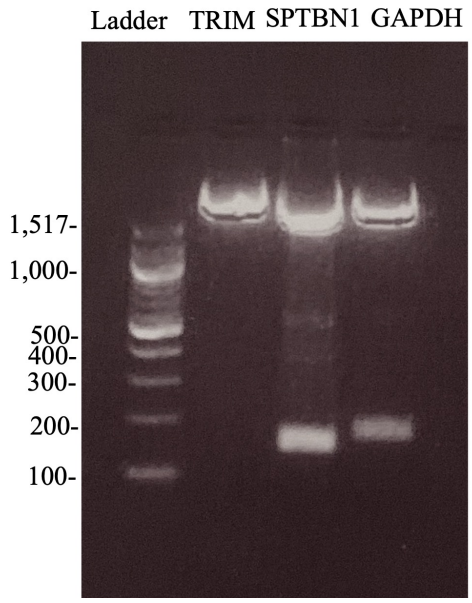

FIG A7 EcoR1 Restriction Digest. Digest results for maxiprep samples TRIM, SPTBN1, and GAPDH.

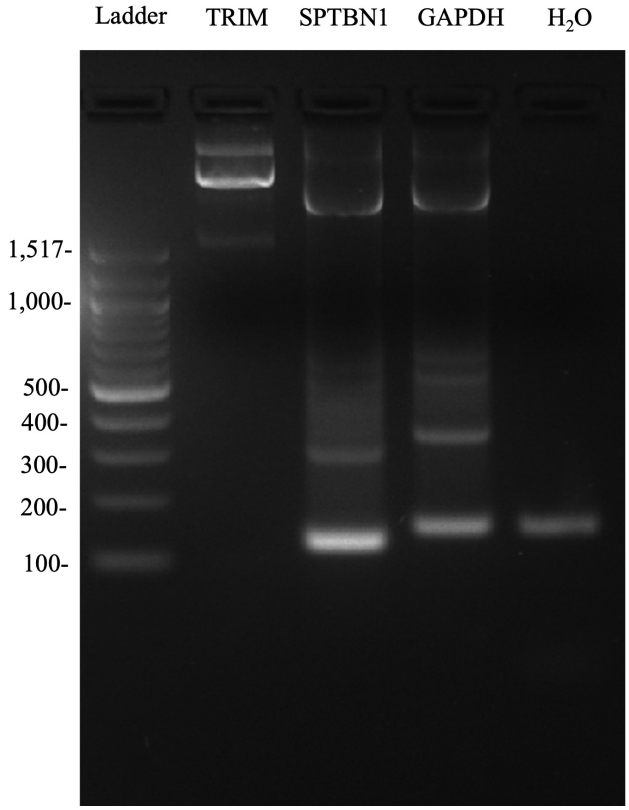

FIG A8 PCR on Maxiprep. Maxiprep on cloned A3 sample. Remaining lanes are PCR for maxiprep clones for SPTBN1 and GAPDH. Gel is cropped.

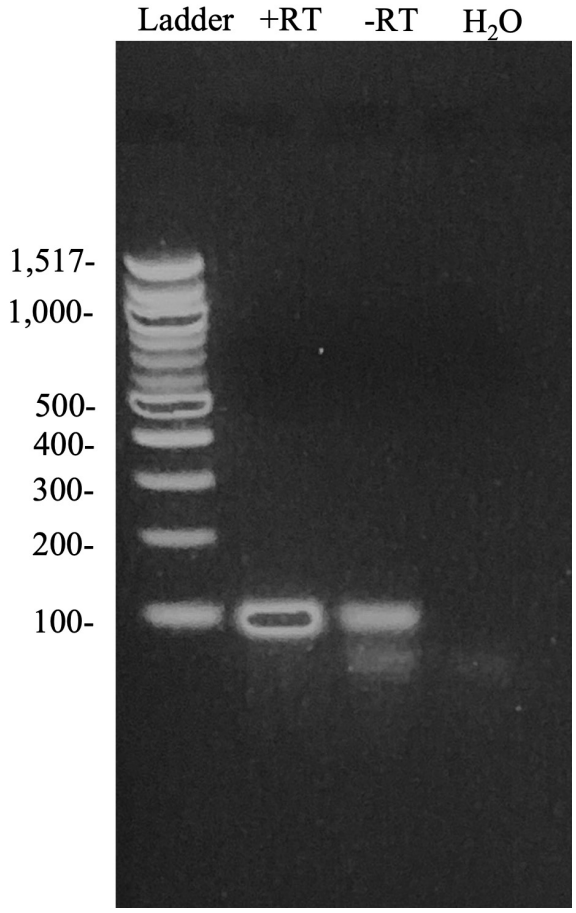

FIG A9 Reverse Transcription Reaction on Total RNA. +RT indicates presence of reverse transcriptase. -RT had no reverse transcriptase.